STUDIES RELATIVE TO THE β-DISINTEGRATION OF SOME HEAVY ELEMENTS, USING A MAGNETIC SPECTROMETER OF HIGH COLLECTING POWER.

THESIS

submitted by

IAN L. FAIRWEATHER, B.Sc.

for the degree of

DOCTOR OF PHILOSOPHY

University of Edinburgh

November 1958.

CONTENTS.

Chapter 4.

THE PREPARATION AND MOUNTING OF SOURCES.

Chapter 5.

THE DETERMINATION OF THE DETECTION EFFICIENCY USING THE β-SPECTRUM of SULPHUR-35.

Chapter 6.

THE β-SPECTRUM OF IRIDIUM-192.

Chapter 7.

THE DISINTEGRATION SCHEME OF IRIDIUM-192.

Chapter 8.

THE β-SPECTRUM OF NEPTUNIUM-239.

Chapter 9.

THE DISINTEGRATION SCHEME OF NEPTUNIUM-239.

Chapter 10.

THE ADAPTATION OF THE SPECTROMETER FOR COINCIDENCE MEASUREMENTS.

Chapter 1.

INTRODUCTION.

1. General.

In recent years the improved methods of nuclear spectroscopy have provided an increasing body of information about the modes of disintegration of both naturally occurring and artificially produced radio-elements. This has led to the development of nuclear models which are capable of interpreting the nuclear data in terms of the properties of the nuclear structure with some success. Spins and parities are assigned to nuclear energy levels, and selection rules have been formulated by which the observed decay properties can be explained fairly consistently. The properties of the nuclear levels can be established from a variety of measurements. In β- and γ-ray spectroscopy these include the relative intensities and high energy end-points of the partial components of the β-spectrum, determined by the method of Fermi analysis from the continuous spectrum produced in the β-decay of a parent nucleus, and the intensities, lifetimes and multipole nature of subsequent γ-transitions between higher and lower lying energy levels in the daughter nucleus. These γ-transitions give rise to internal conversion electrons which are superimposed as mono-energetic lines on the continuous

β-spectrum. The internal conversion electrons are formed through the interaction of a γ-ray of energy E_γ with an electron of the K, L, ... -shell of the product nucleus. The energy E_β of the electrons emitted from the shell is given by $E_\beta = E_\gamma - E_K'$ (or E_L', ...), where E_K' (or E_L', ...) is the binding energy of the K, L, ... -shell electrons in the product atom. It is customary to speak of the conversion of the γ-rays although it is now recognised that the electron emission is a competitive decay process resulting from the mutual interaction of the overlapping nuclear and electronic wave functions. The relative conversion efficiencies for γ-rays in the different shells or sub-shells and the ratio of conversion electrons to photon de-excitations (the conversion coefficients) in an atom depend, along with their lifetimes, on the energy and multipole nature of the radiation. The absolute intensities of the conversion lines, together with theoretically or experimentally determined conversion coefficients, permit the total intensities of γ-transitions to be calculated relative to the total number of β-transitions. The energies and intensities of the β- and γ-transitions in conjunction with γ-ray studies may then form the basis of a complete disintegration scheme, while measurements of the coincidence of β- and γ-transitions may be made to

decide conclusively between possible level schemes.

The present investigations on the electron spectrum of heavy radio-elements were undertaken with a magnetic spectrometer and provide information on the energies and intensities of β-transitions and internally converted γ-transitions. The spectrometer has recently been equipped with a γ-ray detector which, with the possibility of making β-γ coincidence measurements, will extend its capabilities in future studies.

The spectrometer was designed by Richardson (1, 2) and the performance has been investigated and described by Braid and Richardson (3). A description of the spectrometer is given in Chapter 3 but those features that distinguish it from conventional β-particle spectrometers will be mentioned here, together with those properties that determine the type of radio-element that can be most profitably investigated.

2. β-ray spectrometers.

2.1. Fixed-field and fixed-geometry types of spectrometer.

Magnetic spectrometers may be divided into two groups; fixed-field and fixed-geometry spectrometers.

In instruments of the fixed-field type the strength and shape of the field are held constant.

The β-particles are separated into a momentum spectrum which may be recorded by an electron sensitive photographic plate or scanned by moving the detector slit so as to receive the separate elements of the spectrum in turn. The earliest magnetic β-spectrometer to employ focusing as well as deflection of the electrons was of the fixed-field type and was due to Danysz (4) who in 1912 employed the so-called semi-circular principle of focusing in a uniform magnetic field.

In a fixed-geometry spectrometer the positions of the detector and the defining slits are fixed. The path of the β-particles through the field depends on the field shape, but is independent of the intensity of the field which is varied to change the momentum of the electron-sheaf passing through the defining slits to reach the detector.

2.2. Resolving power and collecting power.

The choice of fixed-field or fixed-geometry for a spectrometer type in general implies a choice between high resolving power and high collecting power as the primary characteristic of the instrument's performance.

The resolving power is the reciprocal of the resolution where the resolution is defined in terms of the ratio of the "half width" of the resolved momentum interval to the average momentum of the interval. It

is a measure of the precision with which particles of differing momenta can be distinguished and is measured in terms of the full width at half peak height of the shape of an internal conversion line, as recorded by the instrument.

The collecting power, or transmission, is defined as the proportion of all particles leaving the source in the 4π solid angle that can be focused at the detector.

The requirements of high resolving power, that is a small value of the relative line width defined above, and high collecting power, that is large effective solid angle, are to a large extent conflicting so that a compromise must be accepted in the design of a spectrometer.

2.3. The characteristics of the fixed-field spectrometer.

In the fixed-field semi-circular focusing spectrometer a very high resolving power can be attained by using a very narrow beam of electrons. This entails a reduction in the collecting power, which is already limited in that, without additional space focusing, only rays with small inclinations to the median plane can be accepted. This type of spectrometer can be used to make absolute measurements of the energies of conversion lines. If a photographic plate is used as

detector the whole spectrum can be recorded with high resolution at one exposure, and the low collecting power is no great disadvantage. If the detection is ~~by means of a moving~~ through a movable slit the resolution must be reduced to give a higher solid angle thus producing statistically satisfactory counting rates without an excessively high source activity.

2.4. The characteristics of the fixed-geometry spectrometer.

The fixed-geometry type of spectrometer allows a much larger solid angle for electron collection than is usual in the semi-circular spectrometer. The field and slit system is usually axially symetric to the source-detector axis and accepts an electron sheaf which is a hollow cone. The use of such a field as a magnetic lens system permits a high solid angle for transmission, but for energy discrimination the paraxial rays cannot be used and the consequent introduction of spherical aberration entails a low resolving power for such an instrument. There are many applications where a loss in resolving power is acceptable if a high collecting power can be obtained. The study of the shape of the continuous electron spectrum arising from the β-decay of a radio-element is itself of great value and in many cases does not require high resolution. The high energy portion of the spectrum is

often of low intensity so that an instrument with high collecting power is necessary for its detection if the shape of the spectrum is not to be distorted by the use of thick layers of active material to give a satisfactory counting rate.

3. The spheroidal field β-spectrometer.

3.1. The design of the spectrometer.

The β-spectrometer used in the present investigation is of the fixed-geometry type with an axially symmetric magnetic field. Like all magnetic lens spectrometers it can be expected to be used to best advantage when adjusted for high collecting power with moderate resolution. Richardson (1) showed that a prolate spheroidal field has the property that rays in the meridional plane will experience double focusing, the first cross-over being at a ring near the mid-plane and the second at a ring close to the axis and placed symmetrically to the object with respect to the mid-plane. The spherical aberration present in the first focal ring, where an annular slit is located, is reduced at the second focal ring which comprises the detector slit. Richardson showed that, if the chosen electron sheaf makes a large angle with the axis, it is possible with such a field to focus electrons from a large solid angle with a resolving power comparable

with that of a conventional semi-circular spectrometer.

3.2. The performance of the spectrometer.

The performance of the spectrometer was investigated by Braid (5), and although it proved possible to obtain a resolution of less than 1% this only allowed a collecting power of 1.4%. If adjusted for high collecting power the spectrometer had a ~~resolving power~~ resolution of 2% with a collecting power of 6%. The spectrometer is obviously employed to best advantage when use is made of its inherently high collecting power and the present investigation has been undertaken with the spectrometer adjusted accordingly.

A ~~resolving power~~ resolution of 2% is only obtained provided the diameter of the flat disc source, mounted coaxially to the field, is not greater than 2-3 mm., which restricts the possible source strength.

There is an upper limit of 1.5 Mev to the energy of the electrons that can be focused by the spectrometer, set by the heating of the coils and the saturation of the cores. The use of a scintillation counter as detector leads to a loss of efficiency in the detection of low energy electrons; this is discussed in Chapter 5.

4. The choice of radio-elements suitable for investigation with the spectrometer.

The choice of a suitable radio-element for investigation is determined by several factors. The source material must be obtainable in a suitable form and with a high degree of purity. It is desirable that the half-life should not be shorter than a few days and that the initial specific activity of the material permits a source to be used which is not more than a few millimetres in diameter and is as thin as possible while still giving a peak counting rate that is several orders of magnitude higher than the background rate. The high energy end-point must be less than 1.5 Mev.

The resolving power and collecting power of the instrument are best suited to the study of electron or positron emitters, which have high energy partial β-spectra of low intensity. The absolute intensities of conversion lines may be measured providing that the available resolution is sufficient to separate them from neighbouring lines.

The two heavy radio-elements chosen for investigation were the β^--emitters Ir^{192} and Np^{239}. The results of investigations prior to the present work are discussed in Chapter 2.

Chapter 2.

PREVIOUS INVESTIGATIONS OF Ir^{192} AND Np^{239} β-DECAY.

1. Iridium-192.

Ir^{192} is a product of neutron capture in natural Ir^{191}. It decays with a 74.5 day half-life by emission to Pt^{192} but there is also some K capture decay (4%) to Os^{192}. The γ-rays produced in the decay have been extensively studied but the β-spectrum has not received so much attention. Mandeville and Scherb (6) reported a beta end-point of 560 kev from Feather analysis of the absorption in Al while Goodman and Pool (7) reported an end-point of 590 kev. Wiedenbeck and Chu (8) reported the beta end-point as 680 kev from coincidence studies using absorber techniques.

The first investigation of the electron spectrum with a magnetic spectrometer was by Levy (9) who gave a value for the high energy end-point of 670 kev. This was supported by Shpinel and Forafontov (10) who found the end-point to be 660 kev, and by Johns and Nablo (11) who reported a 672 kev end-point. The earlier work assumed that the spectrum was simple but the γ-ray work threw doubt on this interpretation and Bashilov et al. (12) reported a complex β-spectrum

with end-points at 670, 570 and 240 kev. Unpublished results of Kyles and Campbell (13) of this department are quoted by Pringle et al. (14) indicating the existence of five partial β-components. The results of Bashilov and Kyles are shown in Table 1.

The γ-ray energies of Ir^{192} decay have been accurately measured by several workers using various methods. Curved crystal spectrometers have been used by Muller et al. (15), Ryde and Andersson (16) and by Baggerly et al. (17). The γ-ray energies have been deduced from the internal conversion line energies by Cork et al. (18), and Grard et al. (19) while the external conversion lines have been studied by Johns and Nablo (11). A comparison with the energies of the γ-rays from the levels of Pt^{192} observed by Ewan and Thompson (20) in the electron capture decay of Au^{192} enables the Ir^{192} decay γ-rays to be assigned between the Pt^{192} and Os^{192} nuclei. γ-γ angular correlation experiments are reported by Taylor and Pringle (21).

A disintegration scheme was suggested by Cork (18) and a further scheme was proposed by Muller (15). The discovery of five high energy γ-rays by Pringle and his collaborators (14) together with γ-γ coincidence measurements showed Cork's scheme to be substantially correct. The existence of these γ-rays was later confirmed by Johns and by Baggerly. Unpublished β-β

Table 1.

	1st partial kev	2nd partial kev	3rd partial kev	4th partial kev	5th partial kev
Bashilov et al.		840 (< 0.4%)	670 (44%)	540 (40%)	240 (16%)
Kyles and Campbell	1175 (0.5%)	849 (2%)	701 (32.5%)	568 (45%)	281 (20%)

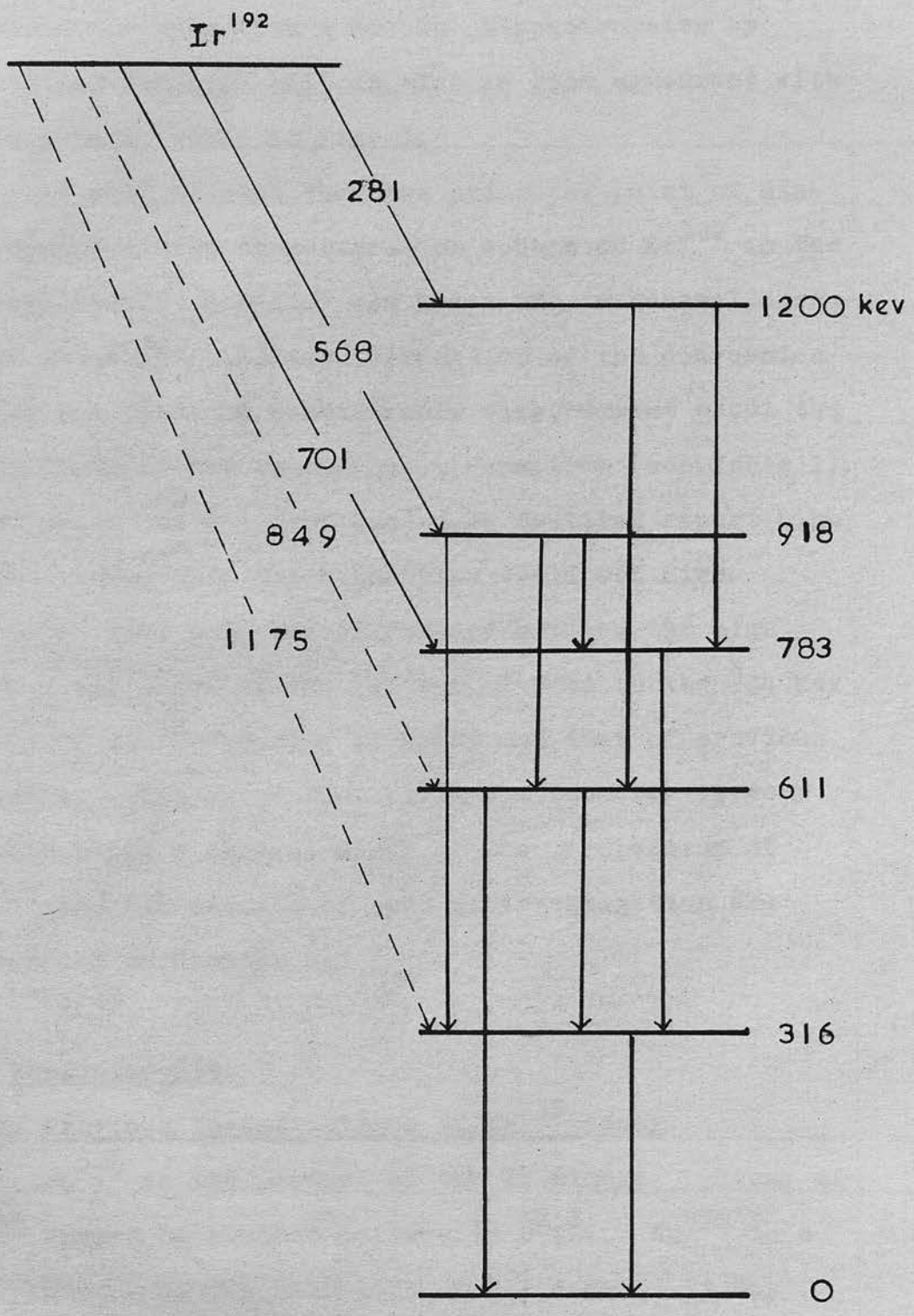

Figure 1. Energy levels proposed by Cork for Pt^{192} following β-emission from Ir^{192} showing the β-components of Kyles.

coincidence work with a double β-spectrometer by Kyles and Campbell (13) is also in good agreement with this scheme, shown in Fig. 1.

It will be seen that the principal point of disagreement in the disintegration scheme of Ir^{192} is the β-spectrum. Bashilov and Kyles are in general agreement about the absolute intensities of the conversion lines but there is considerable disagreement about the components of the continuous β-spectrum (see Table 1). Both Kyles and a worker quoted by Bashilov report high energy components which Bashilov could not find. There is also a 30 kev difference between the high energy end-point of the 700 kev β-feed to the 784 kev level in Pt^{192} reported by Kyles and that of previous workers. The spheroidal field spectrometer is very suitable for a careful study of the β-spectrum of Ir^{192} and the results of such an investigation are presented in Chapter 6.

2. Neptunium-239.

2.1. Previous investigations of Np^{239} decay.

Np^{239} is the product of the 23 minute β-decay of U^{239} formed by neutron capture in U^{238}. Np^{239} is a β^--emitter with a half-life of 2.3 days. It was first separated chemically by McMillan and Abelson (22) in 1940 and its radiations were investigated by

absorption methods in 1941 by Feather (23) who showed that the β-spectrum was complex.

The conversion electron spectrum was examined photographically with a semi-circular spectrograph by Philipp, Riedhammer and Wiedmann (24) in 1944. They identified conversion lines of γ-rays of 209, 226 and 278 kev. The first measurement with a magnetic spectrograph with Geiger counter detector was by H. Slatis in 1947 (25). Fermi analysis of the spectrum showed the presence of four components with end-points at 288, 403, 676 and 1179 kev. Slatis identified conversion lines corresponding to γ-rays of 57, 61, 67 206, 227 and 275 kev. The suggested decay scheme had levels at 275, 502, 708, 775, 836 and 893 kev for the Pu^{239} nucleus.

In 1951 Graham and Bell (26), using a double spectrometer, found no radiations in coincidence with their highest energy β-feed with 705 kev end-point. They further demonstrated that the 210, 226 and 275 kev γ-rays originated at a common level at 276 kev, which is metastable with a lifetime of 1.1×10^{-9} sec., and is populated by a β-feed of 435 kev end-point.

Other measurements on the β-spectrum of Np^{239} were reported by Tomlinson, Fulbright and Howland (27) in 1951 and by Freedman, Wagner, Engelkemeir, Huizenga and Magnusson (28) in 1953. A disintegration scheme

was proposed by Fulbright (29) and is shown in Fig. 2. Engelkemeir and Magnusson (30) showed that the 384 kev level, populated by a 343 kev β-feed, is metastable with a lifetime of 193 mμsec.; it is de-excited by 61 and 106 kev electric dipole transitions.

Pu^{239} is also formed by the α-decay of Cm^{243}. Asaro, Thomson and Perlman (31) showed that 80% of the α-transitions populate the 278 kev level of Pu^{239}. Just prior to the start of the present investigation two detailed studies of the electrons in Np^{239} decay were published.

Baranov and Shlyagin (32) using a magnetic spectrometer of 0.3% ~~resolving power~~ resolution measured the continuous spectrum and the conversion electron spectrum. Their values for the end-points of the partial spectra are in good agreement with the values of Freedman et al. They also reported a low energy β-component with end-point at 70 kev and intensity 22% of the total spectrum. The possible existence of low energy components had been mentioned by Tomlinson et al. (27).

Baranov and Shlyagin's results led them to propose additional levels in the decay scheme at 228, 382 and 656 kev shown dotted in Fig. 2.

Hollander, Smith and Mihelich (33) reported work on the conversion electron spectrum of Np^{239} using a moderately high resolution semi-circular magnetic

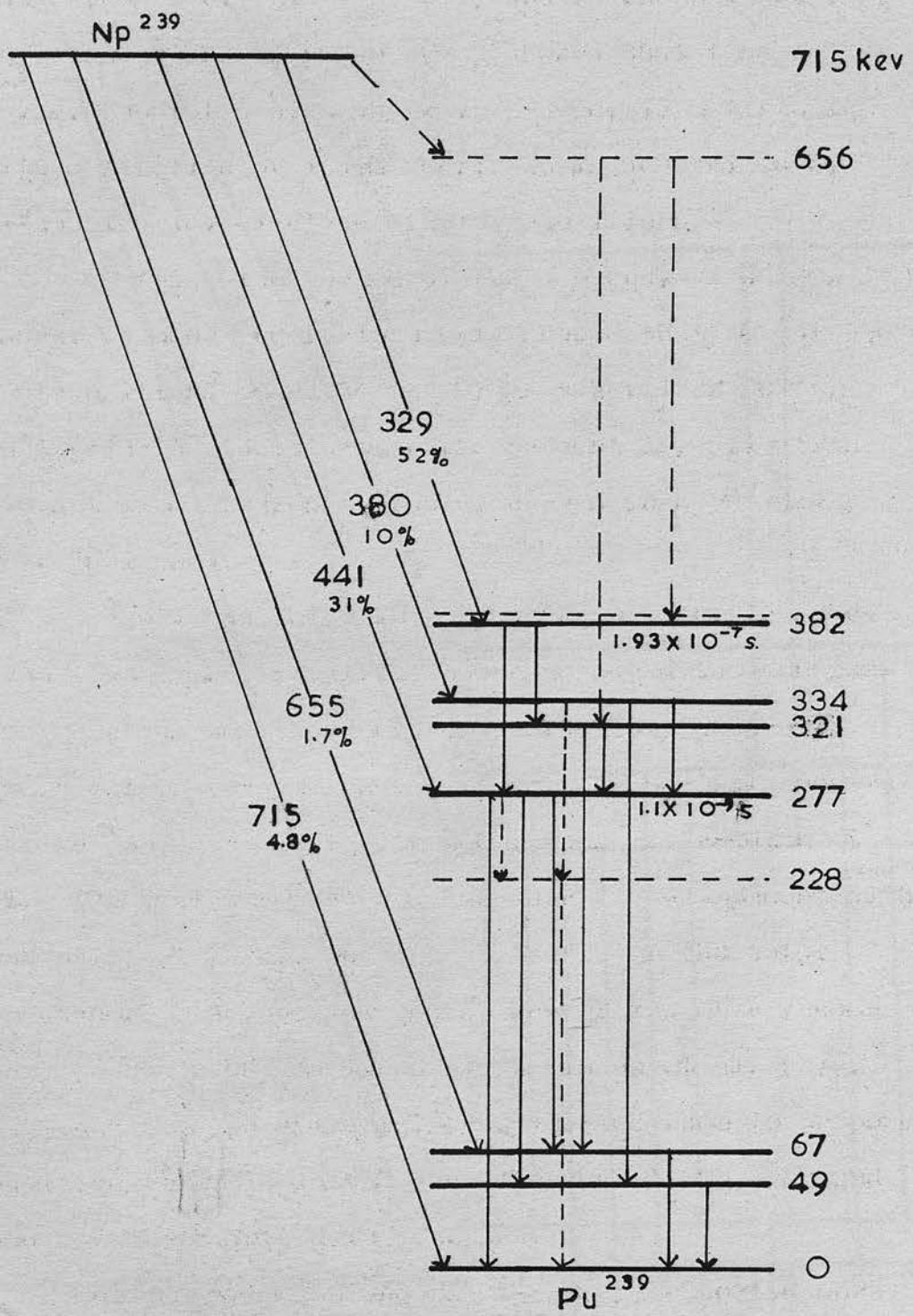

Figure 2. Decay scheme for Np^{239} proposed by Fulbright. (Additional levels suggested by Baranov and Shlyagin are shown dashed).

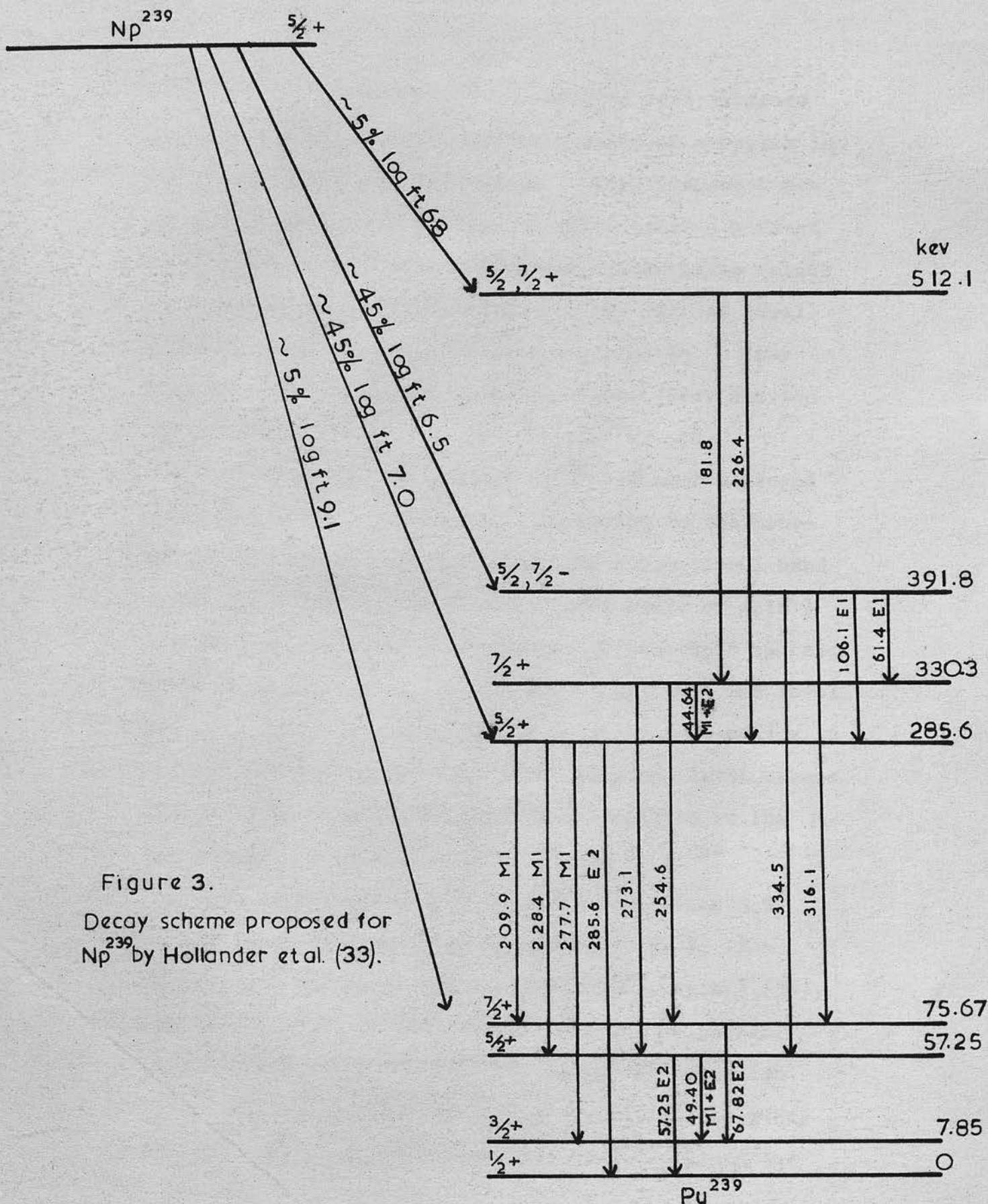

Figure 3.

Decay scheme proposed for Np^{239} by Hollander et al. (33).

spectrograph. Accurate line energies were obtained for 80 conversion lines and the transition energies in Pu^{239} were precisely determined. They propose a new level scheme for Pu^{239} (Fig. 3) which assumes a first excited state at 8 kev, ~~subsequent~~ higher levels being raised by this amount. The existence of the 512 kev level was demonstrated by coincidence experiments. They suggest that the ground state and first three excited states form a rotational band in Pu^{239}.

The ground state spin of Pu^{239} has been measured by Bleaney et al. (34) as $\frac{1}{2}$. According to the Bohr-Mottelson unified nuclear model (35) a rotational band in an odd A nucleus based on a ground state of spin $\frac{1}{2}$ should exhibit anomalous spacing. If the spin sequence $\frac{1}{2}, \frac{3}{2}, \frac{5}{2}, \frac{7}{2}$ is assumed, with even parity, then the level sequence 0, 8, 57 and 75 kev is in close agreement with the theoretical prediction. The proposed level scheme still leaves unexplained the low intensities of the β-transitions to these low-lying levels of Pu^{239}.

The ground state spin of Np^{239} was measured by Conway and McLaughlin (36) and found to be $\frac{1}{2}$; β-transitions to the ground state of Pu^{239}, spin $\frac{1}{2}$ (34), should therefore be allowed ($\Delta I = 0$, no), or possibly first forbidden ($\Delta I = 0$, yes), by normal selection rules and strongly favoured over transitions to other levels. Bohr and Mottelson (35) have explained the

apparent hindrance of some β-transitions, in the case of strongly deformed nuclei, as due to the violation of the K-selection rules, K being the component of I (the total nuclear angular momentum)along the axis of symmetry of the nucleus and a constant of the motion. In the nuclear ground state $K = \Lambda$, where Λ is the component of the total particle angular momentum along the symmetry axis. The K-selection rules forbid transitions for which $\Delta K > L$, the multipolarity. In the present case if the ground state spins of Np^{239} and Pu^{239} are both $\frac{1}{2}$, then $\Delta K = 0$ and the β-transitions cannot be K-forbidden so that the apparent hindrance is unexplained.

During the present investigations work has been published by several authors on the level scheme of Pu^{239}. Their results will not be discussed at this stage. Newton, Rose and Milsted (37) have studied the γ-rays ~~produced~~ emitted in the α-decay of Cm^{243} to Pu^{239}. Newton (38) has proposed independently a level scheme similar to that of Hollander from Coulomb excitation studies of Pu^{239}. Smith, Gibson and Hollander (39) have published details of the conversion electrons produced in Am^{239} electron capture decay. Hollander (40) has discussed the proposed level scheme for Pu^{239} in terms of the asymptotic selection rules, assuming a value of $\frac{5}{2}$ for the spin of Np^{239}. A recent measure-

Table 2.

	1st partial kev	2nd partial kev	3rd partial kev	4th partial kev	5th partial kev
Graham and Bell 1951		705 (7%)	435 (46%)		301 (47%)
Tomlinson et al. 1951	715	654	440		330 (38%)
Freedman et al. 1953	715 (4.8%)	655 (1.7%)	441 (31%)	380 (10%)	329 (52%)
Baranov and Shlyagin 1956	(723 +	655)(7%)	439 (21%)	382 (27%)	327 (45%)

ment of the Np^{239} ground state spin by Abraham et al. (41) confirmed the previous value of $\frac{1}{2}$.

2.2. The present investigation of Np^{239}.

While the end-point energies of the partial β-spectra of Np^{239} are quite well agreed, the relative intensities assigned by different workers show considerable differences. The end-points and intensities quoted in recent reports are shown in Table 2.

It will be seen that there is general agreement that the two highest components ~~only~~ total only about 7% of the spectrum. There is also some agreement that the 330 kev β-feed is $\sim$ 45%. However Engelkemeir and Magnusson (30) have estimated from coincidence studies that the intensity of this β-component is only about 20% of the whole spectrum.

In view of the considerable interest and conflicting evidence in the disintegration of Np^{239} it was decided to proceed with the present investigation. The spheroidal field spectrometer is well suited to the study of the β-spectrum of Np^{239}. The five principal beta end-points lie above the region where the many conversion lines are superimposed upon the continuous spectrum. The moderate resolution of the instrument is therefore of secondary importance whilst the high collecting power permits the relatively weak high

energy end-points to be examined in detail, and their intensities of the corresponding partial spectra to be determined with some precision.

Chapter 3.

THE SPHEROIDAL FIELD β-SPECTROMETER.

1. Introduction.

The general properties of the present β-spectrometer have been mentioned in Chapter 1, where its performance was discussed. Details of its design, construction and preliminary performance have been published (1, 2, 3) so it is only necessary to describe here the more important features of the instrument.

2. Theory of the spectrometer.

Magnetic lens spectrometers employing an axially symmetric field permit focusing of rays in three dimensions but introduce some spherical aberration. For a narrow angle sheaf of mono-energetic electrons emitted from a point source on the axis two focal lines are produced; a meridional and an axial line; the meridional line results in a circle or "ring focus". Conventional lens spectrometers use axial focusing, placing the detector at the disc of least confusion, although this means a reduction in resolving power.

A theoretical treatment by Richardson (1) showed that considerable improvement should be possible by employing meridional focusing and wide angles of emission in a spheroidal field. The trajectories of

rays from a point on the axis of an axially symmetric field may be described in terms of their motion in a meridional (y,z) plane and the rotation of this plane about the axis. The field chosen by Richardson has equipotentials which are hyperboloids of revolution while the orthogonal lines of force are a family of confocal ellipsoids. The field bears some resemblance to a cylindrical mirror. By numerical integration of relativistic equations of motion adjacent rays were shown to cross over at two meridional focal rings, one near the mid-plane and the other close to the axis and symmetrically placed to the object with respect to the mid-plane. The computed orbits are shown in Fig. 4 for the case when the meridional focus at the mid-plane is at radius of 0.9a, where 2a is the distance between the foci of the family of confocal ellipsoids. The axial co-ordinate of the point of origin of the rays is $z = -0.6a$. The rays are inclined at $\alpha = 74^{\circ}$ to 84° to the axis and give two meridional focal rings, one near the mid-plane and the other near the axis. Suitable defining slits are shown in the diagram. The annular slit B_1B_2 provides the main momentum selection since no rays are passed with lower momentum than that of the central ray which just reaches the slit (a "central ray" is one falling normally on the mid-plane). The baffle B_3B_4 excludes any rays of higher momentum

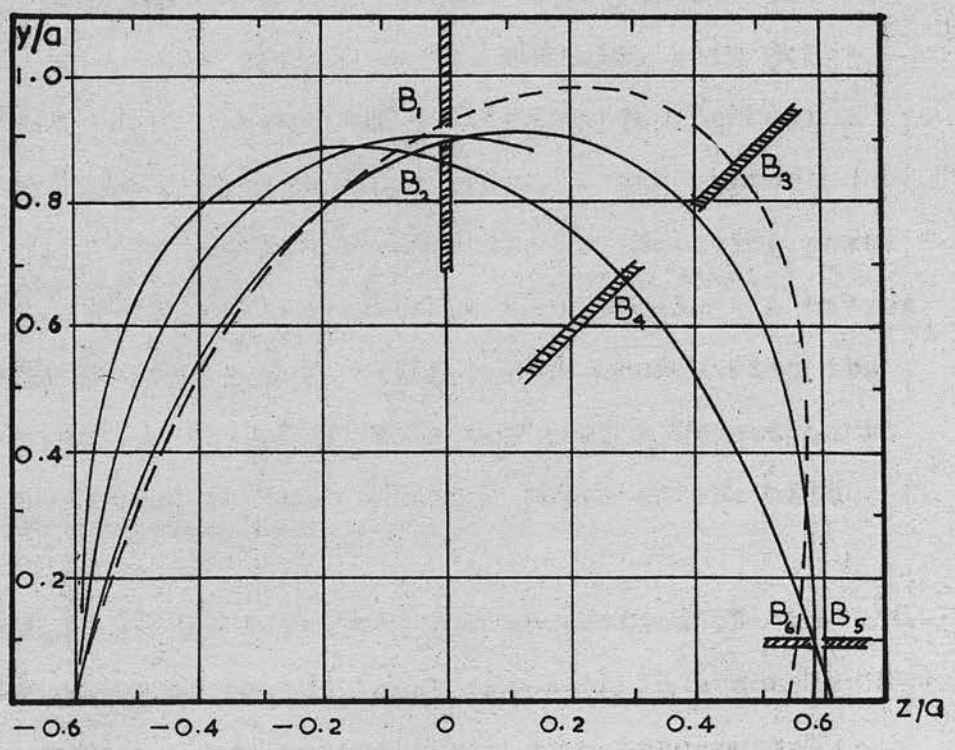

Figure 4. Trajectories of electrons in spheroidal field.

that pass through B_1B_2. A further slit B_5B_6 takes advantage of any chromatic aberration in the formation of the second focal line, rejecting some of the rays of neighbouring energy that reach this slit. The resolving power will depend on the defining slit B_1B_2 and baffles B_3B_4 as well as the chromatic aberration in the formation of the final image. The latter effect will not contribute much to the resolving power unless the width of the image is very small. A narrow image can be obtained by using a disc source with its plane normal to the axis, although with a reduction in the contribution to the resolving power of the slit B_1B_2.

Braid (5) has discussed the properties of the field in terms of second image focusing in a double lens. This analogy is obviously more fundamental than one involving reflection. He develops a simplified theory in terms of two separated ideal thin lenses which shows that compensation for spherical aberration is possible in such a system. The use of a wide-angle sheaf increases the collecting power but will also introduce some additional aberration. The resolution is shown to be proportional to at least the square power of the solid angle. The axial motion of the source and image are shown to be contracurrent.

3. Description of the spectrometer and accessories.

The instrument was designed by Richardson (2) with an interfocal distance of 2a = 20 cm. determined by the availability of the magnet coils and cores.

3.1. The magnet.

The pole-pieces for the magnet are approximately hyperboloids of revolution but because of the possibility of flux leakage to the frame their precise shape was determined by means of an electrolytic tank method. The end-plates are dodecagons of 4 ft. diameter 3 ft. apart to which the twelve flat 33 in. x 12 in. x $\frac{3}{4}$ in. side-plates are bolted. The symmetrically arranged side-plates which complete the magnetic circuit give a fair degree of axial symmetry and a barrel-like appearance (Plate 1); the two vertical plates are hinged to give access to the interior of the magnet. The 7 in. diameter cores are screwed to the end-plates to which are bolted end-discs to equalise the flux density. The pole-pieces are recessed and are drawn into close contact with the cores by bolts passing through a brass cradle which gives additional support. Screws passing through the upright plates of the cradle can be brought to bear against the pole-pieces making some fine adjustment of their position possible. A 1 in. rod was passed through the end-plate and cores and screwed into the pole-piece to draw them into good magnetic

contact. Two $\frac{1}{4}$ in. holes were bored through the pole-pieces to enable their axial symmetry to be tested; they were normally plugged by soft iron rods. The magnetising coils contain about 3,000 turns of d.c.c. copper wire of 13 Ω resistance. They were impregnated with glyptal resin and covered by a layer of empire cloth. To cool the coils a copper sheet, bearing on its outer surface water-cooling pipes, was bolted tightly round the coil. Current is supplied to the coils from a bank of fifty 2 volt accumulators. A stable current supply is obtained by connecting these in opposition to the D.C. mains and high currents may be drawn without loss in stability. The current through the coils is limited by the variable series resistance R_1 shown in the simplified circuit of Fig. 5. The charging resistance R_2 is adjusted so that only a small current is flowing through the batteries; a charging current rather than discharging gives greatest stability. The magnet coils are connected in parallel and the current flowing through one of them is measured by the ammeter A_1; a precise current measurement is obtained by measuring the potential difference across a 0.1 Ω standard resistance with a Tinsley vernier potentiometer. A stable current may be maintained provided the resistances R_1 and R_2 have been set to give a small current flow through the ammeter A_2 in the battery

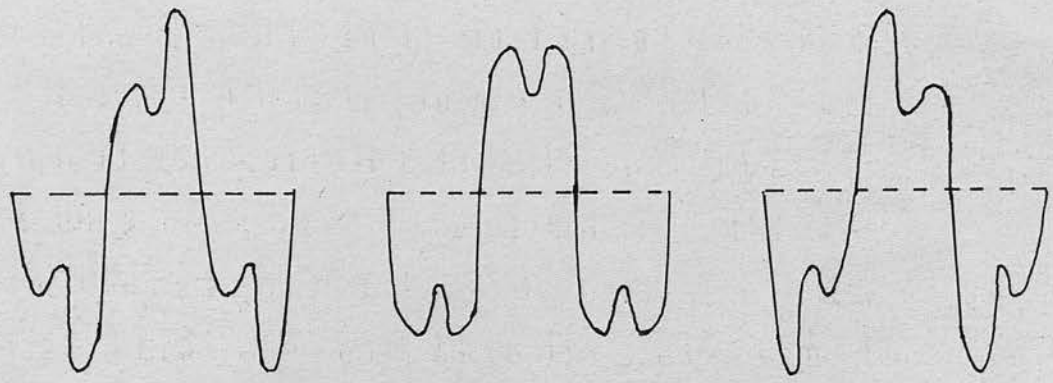

(a) I_H too large. (b) Balance point. (c) I_H too small.

Figure 6. Magnetic field measurement wave-forms.

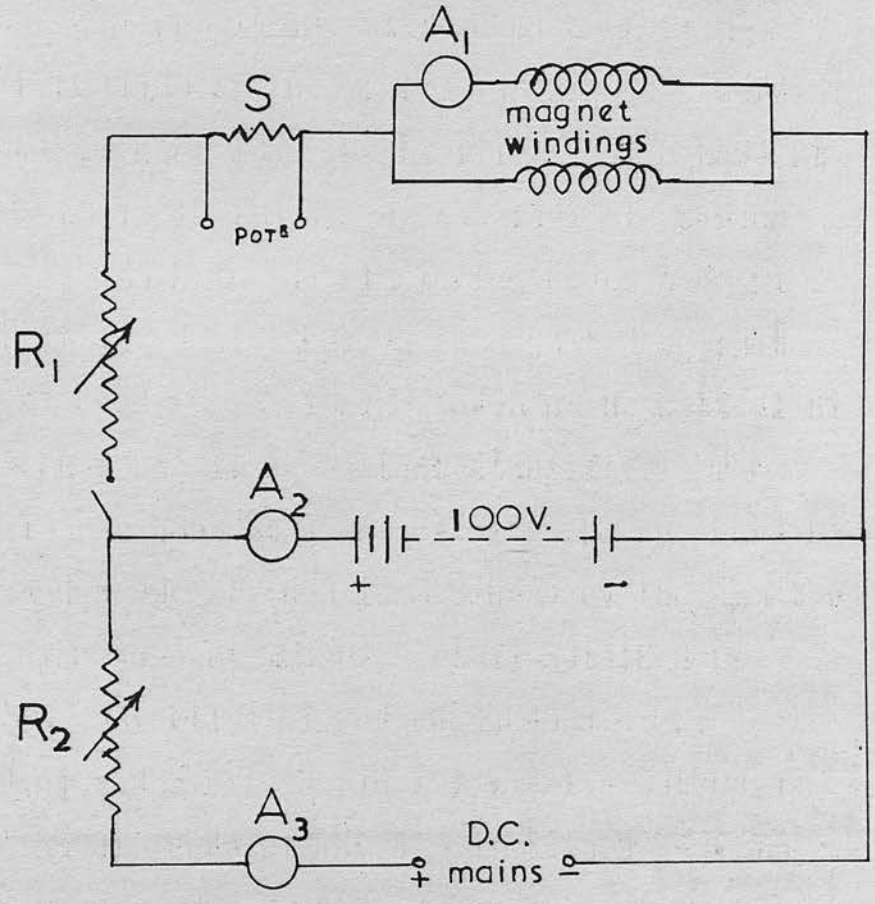

Figure 5. Spectrometer magnet circuit (simplified).

circuit.

3.2. The measurement of the field intensity.

It is not necessary to make absolute measurements of the field strength of a magnetic lens spectrometer provided that a parameter is available that is directly proportional to the intensity of the field. The instrument is then calibrated at leisure by means of the conversion lines of a β-emitter for which the $B\rho$ values have been measured by an absolute method. Braid (5) used the current I_M energising the magnet coils as a measure of field strength. The pole-pieces, made from high permeability steel, have a greater cross-sectional area than have the cores so that saturation will occur first in the cores without affecting the shape of the field. Braid found that the saturation of the cores only affected the linear relation between I_M and $B\rho$ in the region I_M = 5-7 amps. The remanence of the magnetic circuit gives an appreciable width to the B-H hysteresis plot and, to preserve his calibration, Braid took all his observations on the ascending branch of a standard hysteresis cycle, which was completed at the termination of a run.

Knight (42) designed and fitted an improved method of field measurement that is independent of the magnet current and saturation effects. A spinning coil method first suggested by Hedgran et al. (43) is used

to measure the field intensity at a fixed point in the field. Coils are mounted on a spinning shaft and generate alternating voltages proportional to the magnetic field intensity at the coils. In the present arrangement three coils are used, all mounted with their axes perpendicular to the shaft. One coil c_F is spinning at an arbitrary point just outside the spectrometer box, while a second coil c_H spins in the uniform field produced between two Helmholtz coils by a d.c. energising current I_H (the Helmholtz current). The "Helmholtz field" is uniform and its intensity is proportional to I_H. The soft iron magnet frame screens the coil c_F from the earth's field but it is necessary to compensate for the contribution to the Helmholtz field due to the earth's field. This is done by connecting a coil c_E identical to c_H, mounted on the shaft out of the Helmholtz field, with its voltage output in series opposition to c_H. The output from these two coils is connected in phase opposition to that from c_F. The resultant alternating voltage may be reduced to zero by adjusting the value of I_H, which is then proportional to the intensity of the field at the coil c_F, and is measured in the same manner as I_M. The position of the Helmholtz coils and the spinning shaft carrying the pick-up coils is shown in Plate 1. The Helmholtz coils have an outside

diameter of 9 in. and have 1770 turns, they are connected in parallel and are supplied by a 12 volt bank of accumulators, the current being controlled by a series rheostat. The three pick-up coils are wound on a $\frac{1}{4}$ in. diameter paxolin former $\frac{7}{8}$ in. long; c_H and c_E have 30,000 turns while c_F has 6200 turns. The shaft is driven at 1500 r.p.m. and is supported by ball bearings mounted in brass holders and at its upper end by a porous bronze bush. The resultant voltage from the three coils is transferred to two thin wire brushes pressed against slip rings. The 25 c/s alternating voltage is amplified by a factor of about 900 before being applied to the Y-plates of a cathode ray oscillograph. In practice complete balancing of the pick-up voltage is not possible as the non-uniformity of the spheroidal field introduces some harmonic components into the wave-form, the third harmonic being predominant. This harmonic is utilised to provide an easily recognisable wave pattern which can be adjusted to a standard position which is chosen as the arbitrary zero of the wave-form, see Fig. 6. The sensitivity of the spinning coil system is such that a change in I_H of 1 part in 800 produces a detectable unbalance in the zero wave-form.

It is convenient to preserve the correlation between the magnet current I_M and the Helmholtz current

I_H. The net residual field is arranged to be zero at c_F by applying such a reversed field that when removed the amplitude of the alternating voltage displayed on the oscilloscope is zero when there is no Helmholtz current.

3.3. The vacuum chamber.

The chamber, which contains the source, slit and detector system, is a 6 in. long brass cylinder, 10 in. in diameter, closed by two end discs. It stands on four levelling screws and is supported on two rails of a brass cradle. At one side of the chamber is a flat entrance door through which the brass slide passes in which the sources are mounted (see Plates 2 and 4). The massive lead block, which acts as a γ-ray shield, and the slit and baffle system are attached by a supporting frame to the wall of the chamber, see Fig. 7.

(1) The ring slit S_1, which corresponds to the slit B_1B_2 of Fig. 4, is located near the mid-plane. S_1 consists of eighteen 20° sectors and is variable in width while its radius can be varied between 9.0 and 9.4 cm. Paddle-shaped vanes bridge S_1 and are set at 30° to the plane of the annulus so as to be tangential to the computed helical electron trajectories; the vanes are clearly visible in Plate 3. β-particles of the wrong polarity are obstructed while lateral grooves

on the vanes prevent scattered electrons from passing through S_1. The main momentum selection takes place at this slit.

(2) The two ring baffles B_3B_4 of Fig. 4 comprise slit S_2. Particles passing obliquely through S_1 with momentum greater than that of the central ray selected by S_1 are prevented by S_2 from reaching the detector. Further ring baffles and the aluminium clad core are designed to trap scattered electrons. The vacuum chamber is lined with aluminium to reduce scattering.

(3) The second ring focus of the electron-sheaf is selected by a 1 cm. radius cylindrical slit S_3 mounted axially. This is slit B_5B_6 of Fig. 4. The particle detector is placed so as to record electrons passing through this slit.

The source holder is mounted in a 12 in. long brass slide which passes through a rubber seal in the entrance door of the chamber, see Plates 2 and 4. The source is positioned so as to be on the axis of the instrument and fine adjustment is possible in three dimensions. The axial adjustment is obtained by means of a screw passing through a vacuum seal to bear upon the slide.

The original detector was a Geiger-Muller counter with a cylindrical thin window situated to receive the electrons passing through S_3 but this has been replaced

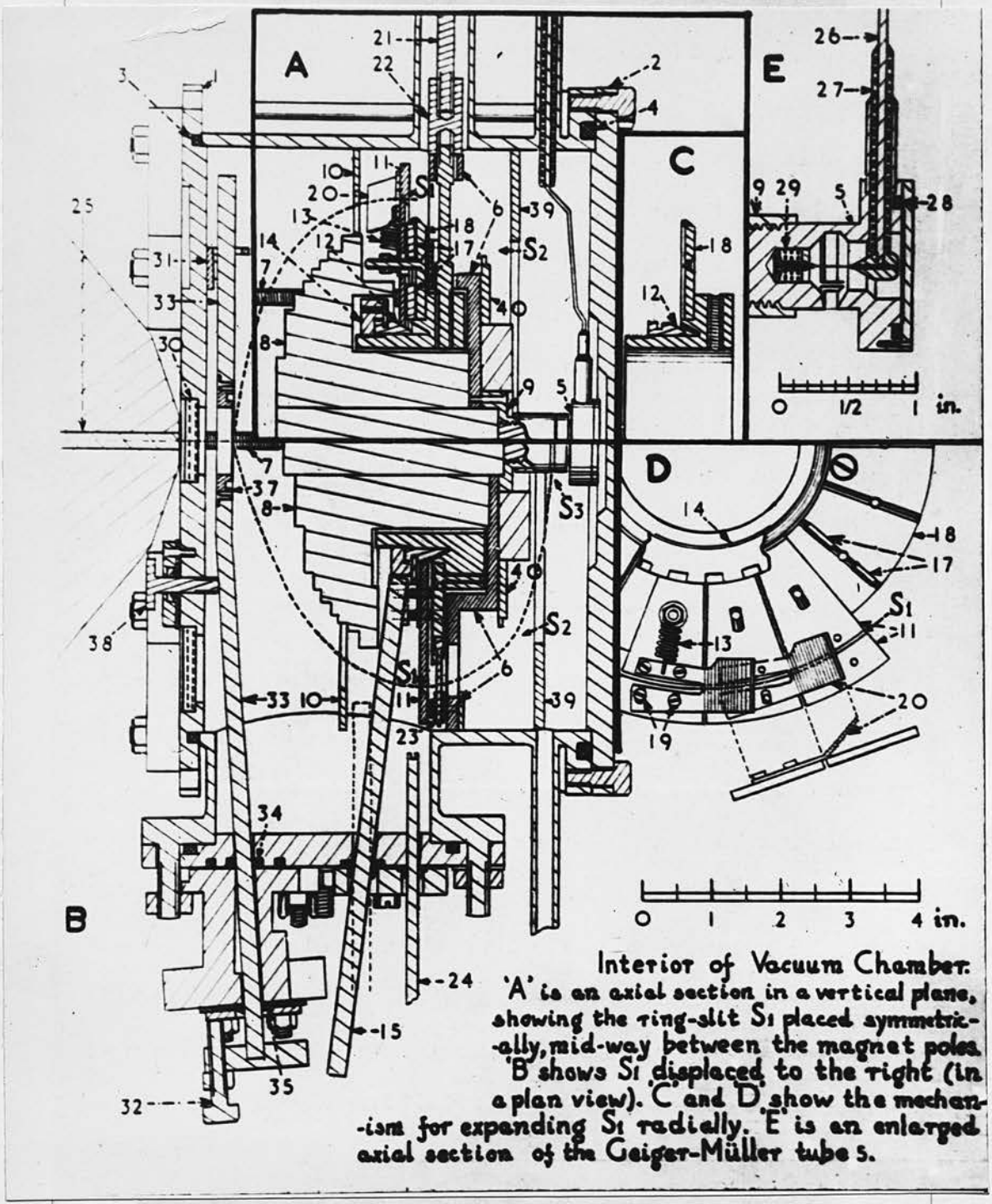

Interior of Vacuum Chamber.
'A' is an axial section in a vertical plane, showing the ring-slit S_1 placed symmetrically, mid-way between the magnet poles. 'B' shows S_1 displaced to the right (in a plan view). 'C' and 'D' show the mechanism for expanding S_1 radially. 'E' is an enlarged axial section of the Geiger-Müller tube 5.

Figure 7

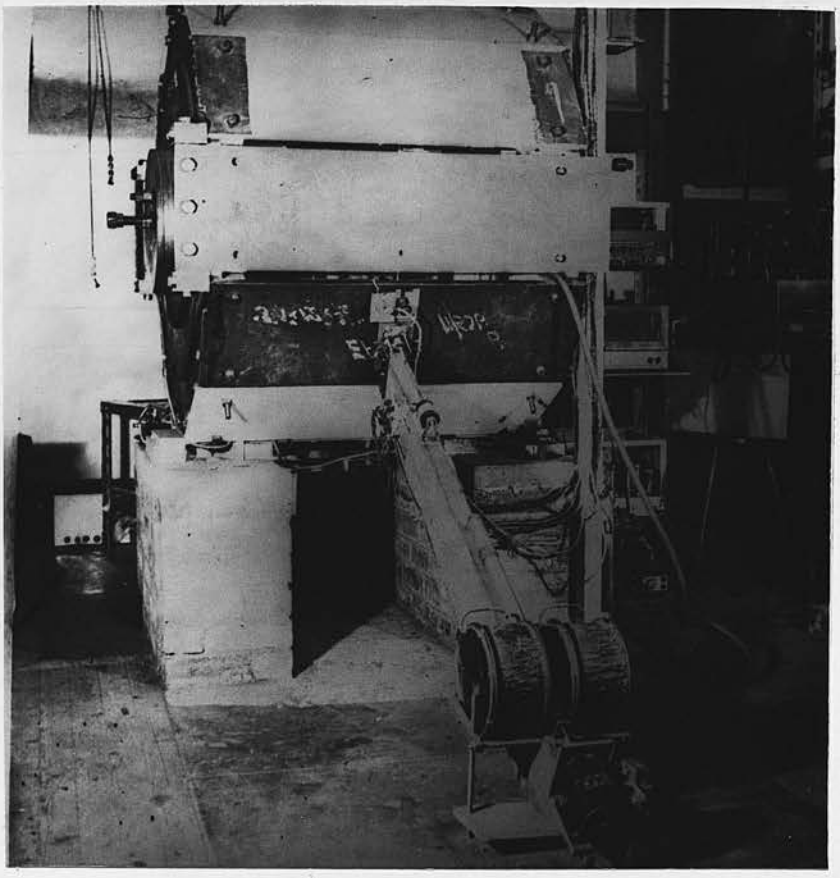

Plate 1.

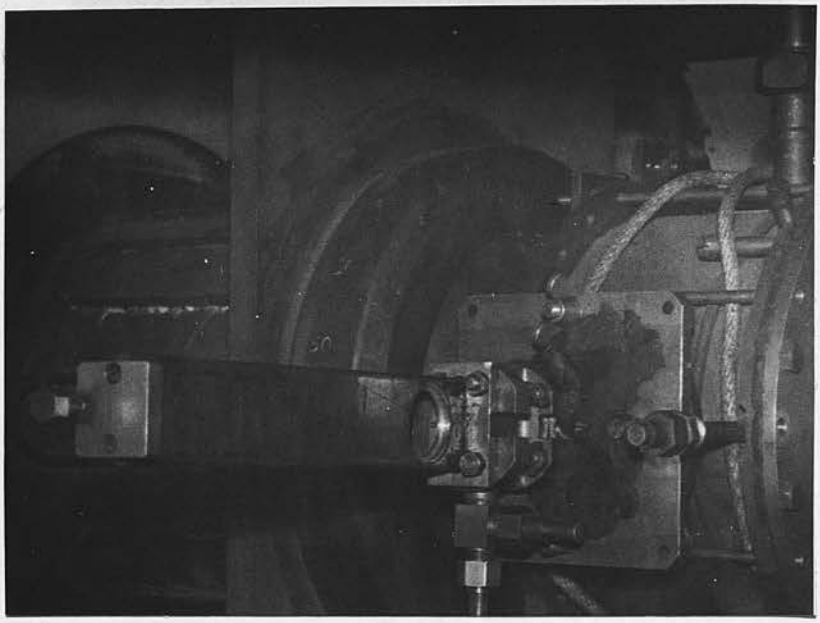

Plate 2

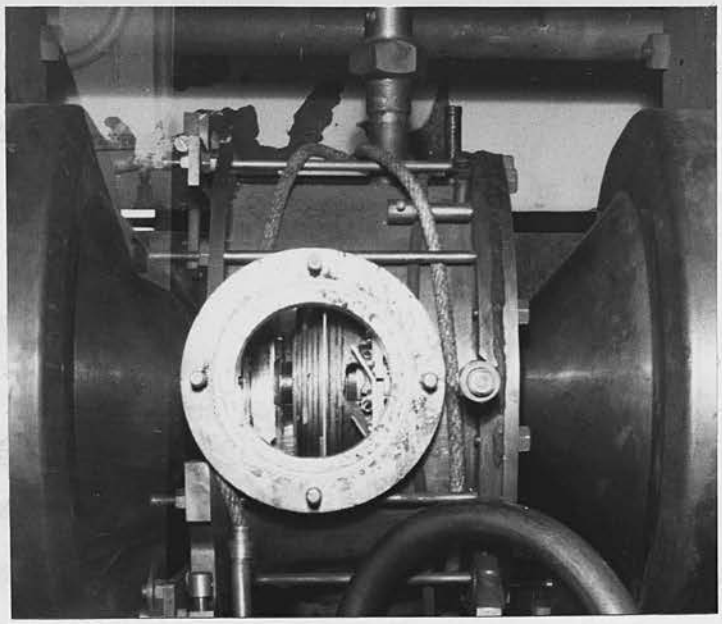

Plate 3.

Plate 4.

by a scintillation counter.

An oil diffusion pump hangs directly below the chamber and is backed by a rotary pump giving a normal vacuum of better than 10^{-4} cm. of mercury.

4. The scintillation counter detector.

The Geiger-Muller counter originally used as detector had a cylindrical window. Difficulty was experienced in obtaining a satisfactory thin window of the required shape and the use of a crystal detector was proposed by Knight (42). This has the added advantage of utilising the full azimuth angle for collection, since the window supports of the Geiger counter reduced the collection angle to 290°. Knight fitted a detector system comprising an annular crystal whose scintillations were internally reflected down a perspex rod light guide on to the photo-cathode of a photomultiplier. The crystal mounting, photomultiplier and cathode follower used by Knight were not found to be very satisfactory and have been changed; the present system is now described.

For the detection of electrons from an external source a plastic or organic scintillator is usually preferable; the decay time of such phosphors is $\sim 10^{-8}$ sec., which is much less than the microseconds dead time associated with the Geiger counter and opens up

the possibility of using the spectrometer for coincidence measurements. Anthracene has outstanding properties for an organic phosphor giving a large pulse height per Mev as well as having an emission spectrum peak at 4300A which matches the spectral sensitivity peak of the photomultiplier detector. Curran (44) reports that anthracene evaporates fairly readily in a vacuum but it has been used with success in the present work with little sign of evaporation. The crystal used is a 1.8 cm. diameter anthracene disc 4 mm. thick and attached by a white vaseline joint to a short length of perspex rod passing through a rubber seal in the end-disc of the vacuum chamber. The main light guide is a 20 in. long $\frac{7}{8}$ in. diameter perspex rod passing through the centre of the core to the photocathode of an EMI 6097B type photomultiplier, mounted on the axis outside the magnetic field. The perspex rods are highly polished and white vaseline is used to give good optical joints free of parasitic reflections; the main light guide is surrounded by, but not in contact with, a brass cylinder passing through the 1 in. hole in the core (see Fig. 7) and centrally through the pole-piece which has been drilled out for the purpose.

The photomultiplier is enclosed in a light-tight housing consisting of two interscrewed brass cylindrical flanges. The inner flange is attached

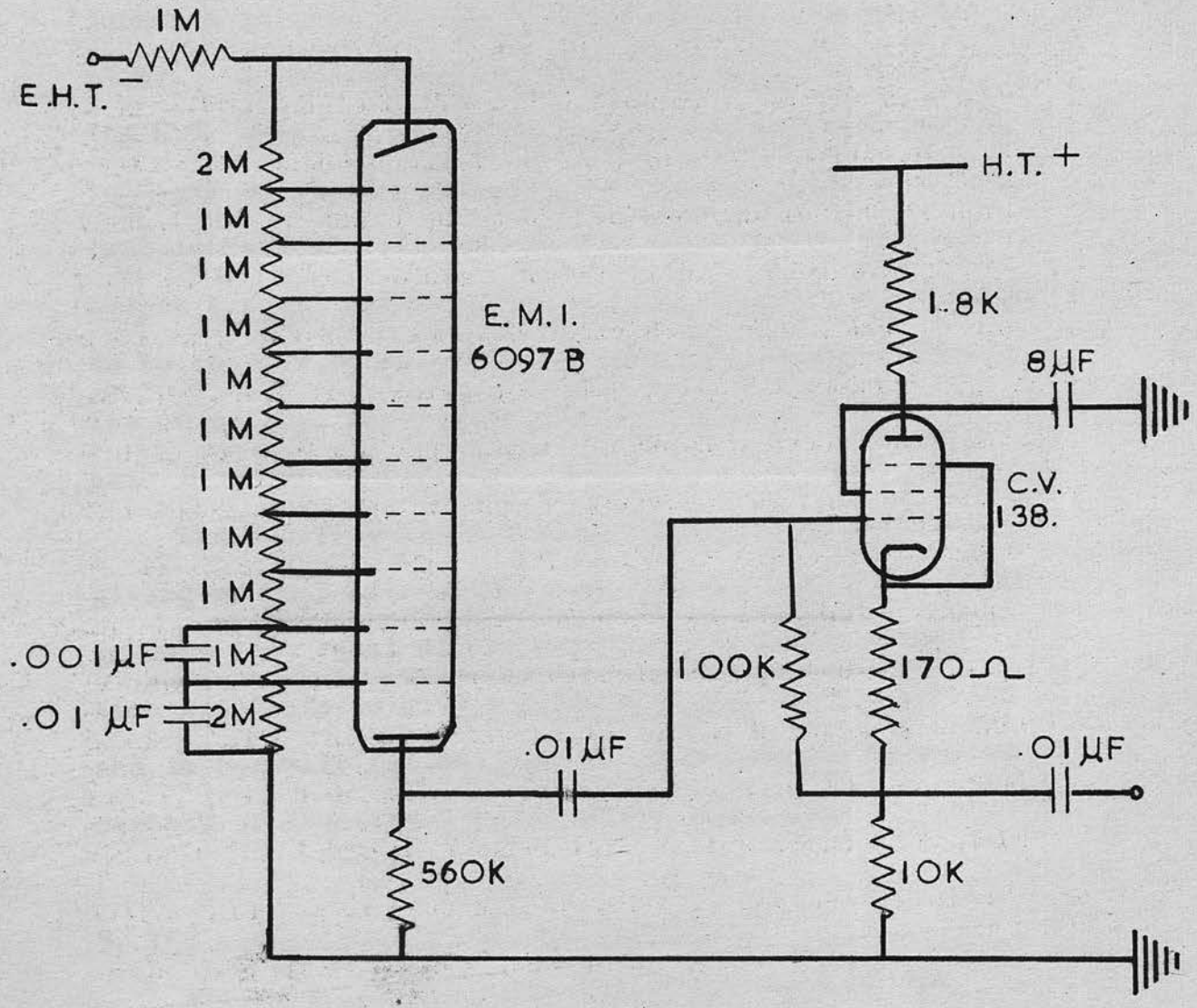

Figure 8. Photomultiplier and cathode follower circuits used in the electron detection system.

co-axially to the iron end-plate of the magnet. The outer flange supports the photomultiplier base by means of a spring seating, which allows the outer flange to be screwed safely on to the inner one until a good junction is made between perspex rod and photomultiplier. A box attached to the outer flange contains the H.T. input to the resistance chain determining the voltages at the dynodes, and the output circuit to the cathode follower pre-amplifier. The photomultiplier output circuit differentiation time constant is arranged to be about 1 μsec. which is very much greater than the 30 mμsec. decay time of the phosphor. The circuit is shown in Fig. 8.

The E.H.T. unit is a standard Dynatron 1033 unit giving up to 3 kilovolts. The Dynatron 1049 amplifier is used with equal differentiation and integrating time constants to give a maximum signal to noise ratio and is normally followed by two 1009 scalers in series capable of counting 5×10^4 pulses a second.

5. The performance of the spectrometer.

Braid (5) investigated the performance of the spectrometer when set firstly for high resolving power, and secondly for high collecting power. In the first case the resolution was 1% with a transmission of slightly greater than 1%. The second setting was found to give a better overall performance; a

resolution of 2% being possible with a collecting power of 6%, when normalised to full azimuthal angle. This setting has been maintained for the present investigation.

The position of slit S_1 is that shown in section B of Fig. 7, with the angle of emission of the sheaf 74°. S_1 is displaced towards the counter by 1 cm. from the mid-plane. The slit widths are S_1 = 1.7 mm., S_2 = 15 mm. and S_3 = 1.15 mm. With S_1 displaced from the mid-plane the spherical image of a disc object is produced with magnification slightly less than unity, so that sources of diameter larger than the width of the collecting slit S_3 may be used without serious loss in performance. The dependence of the resolution, R, and the solid angle, Ω (here corrected for full azimuth), on source diameter, d, was investigated by Braid, who showed that the solid angle decreases with increased diameter as shown in Table 3.

Table 3.

d mm.	$\frac{1}{3}$	1	2	3
R (%)	2	2	3	4
Ω (%)	5.2	5.0	4.7	4.0
L	0.45	3.9	14.6	28
L/R	0.22	2.0	4.8	7.0

The comparison of source diameter and solid angle is misleading, for the actual number of electrons reaching the detector is determined by the luminosity $L = \Omega \sigma$, where σ is the area of the source. In contrast to Ω, the luminosity can be seen from Table 3 to increase rapidly with the source diameter. A useful figure of merit for a spectrometer is the ratio of the luminosity to the resolution and in the present case this also increases with the source size.

6. The calibration of the spectrometer.

6.1. The instrumental line shape.

Lindstrom and Slatis (45) have observed the natural line width of two conversion lines in the spectrum of thorium B, using a very high resolution spectrometer. The line width normally measured by a spectrometer is many times the natural width and is instrumental in origin; it arises from the finite slit widths present which allow an electron-sheaf of appreciable angular width to be detected. Mono-energetic electrons are able to reach the detector as the momentum of the interval selected is varied over a small region and similarly the electrons detected at any one momentum setting vary in momentum over a finite interval. The observed line profile is unsymmetrical, see Fig. 9. The use of central rays in the second image focusing type

~~focusing~~ of ~~the~~ spectrometer gives a line-shape similar to that of the semi-circular instrument. Lawson and Tyler (46) have shown that the momentum of the centroid of the line profile is to a close approximation the true momentum of the conversion line. The transmission of the instrument is proportional to the momentum value selected so that all electron intensity measurements must be normalised by dividing by the mean momentum value of the interval. Fig. 9 shows the profile of the thorium F-line after the underlying continuous spectrum has been subtracted. The normalised electron count belonging to the conversion line is designated N and the momentum is expressed in terms of I, the Helmholtz current. The centroid is calculated from the plotted line by determining the area and the first moment of the line-shape about an arbitrary $I = I_o$ axis. The first moment is

$$\int_{I_{min}}^{I_{max}} N(I)(I_o - I)\,dI = (I_o - \bar{I}) \int_{I_{min}}^{I_{max}} N(I)\,dI$$

I_{min} and I_{max} are the values of I at the extremities of the line and $\bar{I}$ is the desired value of I, corresponding to the centroid of the line-shape. In practice the line-shape is divided into a number of strips of width ΔI, and the centroid is determined by numerical integration.

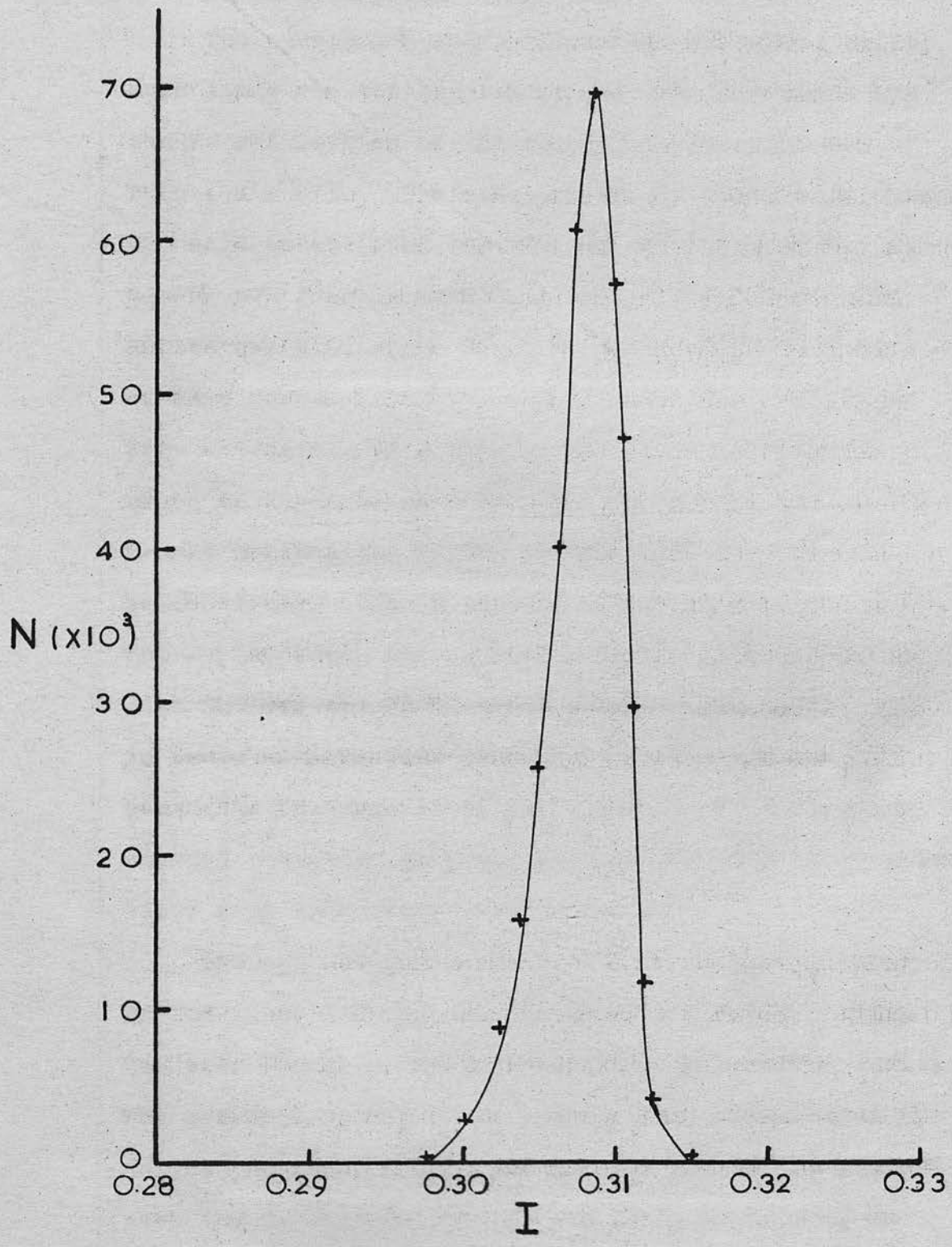

Figure 9 The instrumental line-shape of the F-line of Thorium B.

6.2. The calibration factor.

The conversion lines chosen as the normal reference lines for the calibration of the instrument are the F- and L-lines of the complex β-ray spectrum of Th(B + C + C"). The energies of the conversion lines are well established and sources of high specific activity are readily available in the form of thorium active deposit, which has a suitably short half-life of 10.6 hours. The $B\rho$ values have been determined very accurately by Siegbahn, Edvarson and Lindström (47) using an absolute method. They find for the thorium F- and L-lines $B\rho$ = 1388.44 and 2607.17 gauss-cm. respectively. The F-line is a conversion line of ThB $\longrightarrow$ ThC decay and is very intense; the weaker L-line follows the ThC" $\longrightarrow$ ThD decay. The positions, in terms of Helmholtz current I_H, of the peaks and centroids of these lines for a series of calibration sources are shown in Table 4, together with the resolutions with which they were detected.

The calibration gives the ratio of the I_H value of the line centroid and the known $B\rho$ value. This has been found to remain constant within narrow limits. The proportionality of I_H and $B\rho$ was demonstrated by Knight (42) for the range 0-500 kev and in the present work the calibration factor was found to hold up to 800 kev.

Table 4.

Line	Resolution %	I_H values		Calibration factor $I_H/B\rho$
		Peak	Centroid	
F	2.3	.3083	.3074	2.215
F	1.7	.3095	.3076	2.216
F	1.7	.3089	.3077	2.217
F	1.8	.3090	.3079	2.218
L	1.7	.5815	.5795	2.223
L	1.9	.5800	.5783	2.218

Chapter 4.

THE PREPARATION AND MOUNTING OF SOURCES.

1. Source size.

The focusing properties of the spheroidal field which determined the design of the spectrometer strictly apply only to the case of an axial point source. With the instrument adjusted for high collecting power this restriction is relaxed and a disc source of 1 mm. diameter gives a resolution of 2%. If the spectrometer size were increased the source diameter could be similarly increased. It has been pointed out in Chapter 3 §5 ~~4~~ that, although a finite diameter of the source reduces the solid angle of the spectrometer, nevertheless the luminosity increases rapidly with source diameter. In order to obtain the maximum possible counting rates the source size should never be smaller than is necessitated by the requirements imposed by a desired value of the resolution.

2. The effect of source and backing thickness.

The shape of the β-spectrum from a radioactive source may be seriously distorted if careful attention is not given to the thickness of the radioactive layer and to the nature and thickness of the supporting backing. Two processes occur which lead to distortion,

namely absorption and backscattering. In the case of an uncovered source absorption occurs only in the source material and effectively reduces the energy of the electrons passing through the layer, particularly in the case of low energy electrons which may be absorbed completely in a thick source layer. Backscattering occurs in a thick source layer or in the backing material that supports the active material. Electrons lose a comparatively large amount of energy in being backscattered and appear in the spectrum as an enhancement of the low energy region. Backscattering effects are roughly proportional to the thickness of the scatterer and depend strongly on the atomic number of the backing, hence it is usual to use aluminium or organic materials as source mountings. If an organic material is used as a backing it is necessary to provide a conducting path across the film to prevent the source becoming positively charged by continuous electron emission. Albert and Wu (48) have shown that source thicknesses of as little as 5 $\mu g/cm.^2$ cause a marked excess of electrons below 60 kev. The 74^o emission angle in the spheroidal field instrument increases the effective source thickness by a factor of 4, so it becomes of the utmost importance to use the thinnest sources and backings. Unfortunately the limitation in the source area means that, to give a specified counting rate, the

source thickness is determined by the specific activity of the source material. Sources should, however, be mounted on thin backings to minimise backscattering.

The effect of source and backing thickness on conversion lines must also be considered. All backscattered electrons are considerably reduced in energy and will no longer appear in the line. The effect of source absorption is to degrade the energies of the line electrons producing a slight shift in energy and an increased low energy tail. The effect of absorption on lines of different energy is illustrated in Fig. 10. The 390 kev line is nearly unaffected but the 130 kev line is shifted in energy and reduced in peak height, some electrons being degraded out of the line. The source was a 40 μg/cm.^{2} layer of Ir^{192} mounted on 0.2 mg/cm.^{2} Al leaf. The lines were measured with the source positioned normally and then reversed, so that the effect is due to absorption in 0.2 mg/cm.^{2} of aluminium. There is no appreciable change in the height of the underlying continuous spectrum, which suggests that backscattering in the aluminium is probably small at these energies.

3. Sources of thorium active deposit.

Sources of thorium active deposit were collected on conducting discs exposed in a radiothorium pot.

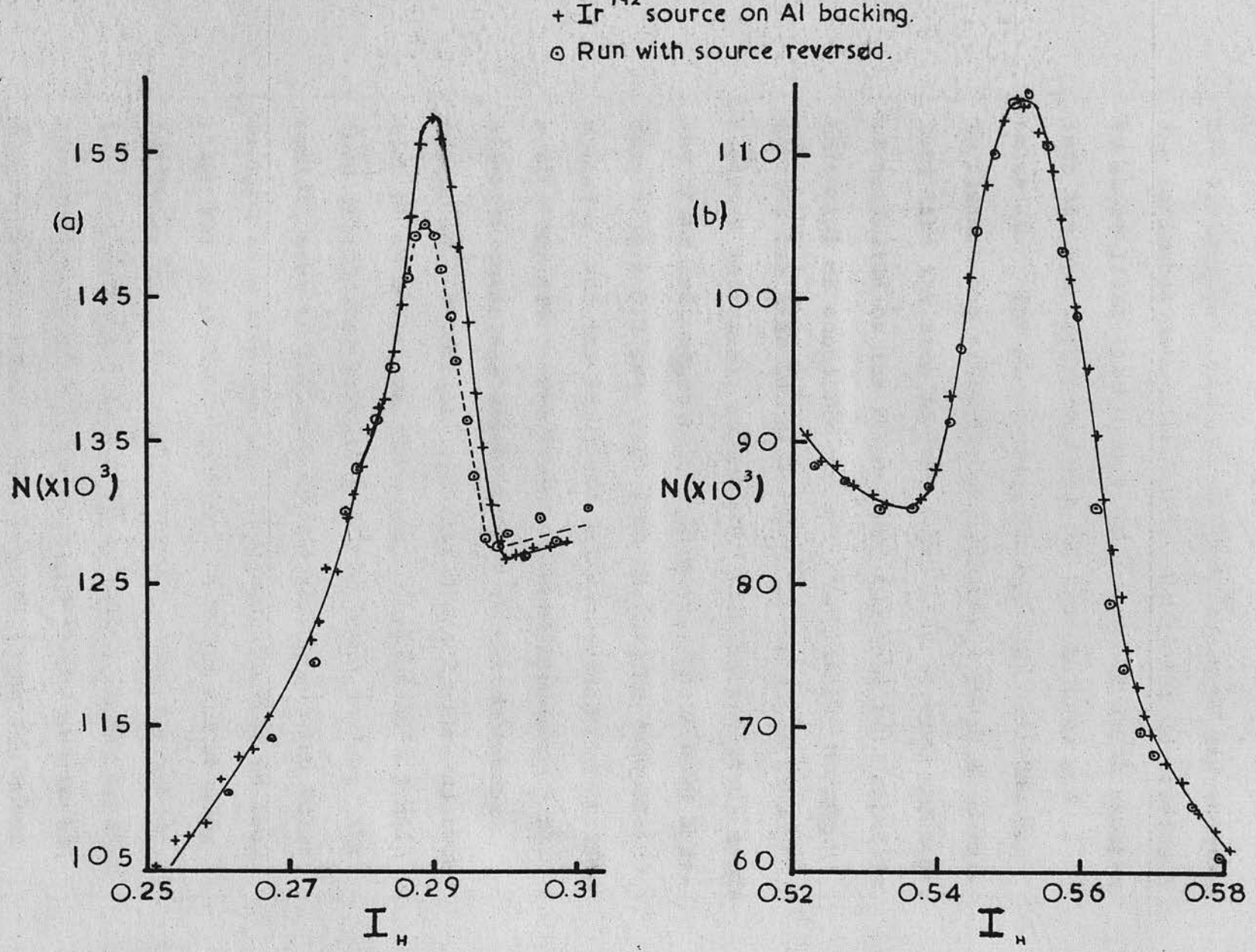

Figure 10. The effect of absorption in Al. on the K-conversion lines of gamma transitions in Ir^{192} of (a) 201-205 and (b) 468 kev.

The earthed pot contains an open source of dry emitting radiothorium salt which decays by way of thorium X to short-lived thoron emanation, some of which escapes into the pot before decaying to thorium A by α-emission. The α-particle is expected in principle to disturb the extra-nuclear electrons to such an extent that the atom is left positively charged and may be collected on the source disc which is at a negative potential of about 200 volts. In practice strong sources may also be collected with the plate at a positive potential, suggesting that the thorium A atoms are often left negatively charged. The thorium A decays with a 0.2 sec. half-life to thorium B by α-emission, and the resultant source is known as thorium active deposit. The sources are collected on 3 mm. diameter stainless steel buttons or on the central region of a thin film made conducting by the evaporation of an aluminium layer and supported by a 3 mm. long cylindrical brass ring, 7 mm. in diameter; the central area of the film is defined by a $\frac{1}{3}$ mm. hole drilled in a mica sheet. The steel buttons or brass rings are mounted at the end of a brass rod passing centrally through a bakelite plug. The sources obtained are carrier-free near monatomic layers of high specific activity. For calibrating the instrument $\frac{1}{3}$ mm. diameter sources were used in order to reduce

the experimental width of the conversion lines; a resolution of 1.7% was usually obtained.

4. The preparation of thin source backings.

The precise measurement of the shapes of continuous electron spectra requires thin sources mounted on thin backings. Considerable attention has been given to the production of suitable thin backing films. The requirements will vary with the method of source preparation, but adequate mechanical strength, and chemical resistance throughout the preparation are essential. For conversion line studies thicker backings may be used; 500 $\mu g/cm.^2$ layers of mica have very good chemical and mechanical properties while 200 $\mu g/cm.^2$ aluminium leaf is available commercially and has the advantage of being conducting, but this is offset by its lack of mechanical strength and moderate resistance to acids and alkalis.

Film thicknesses of much less than 100 $\mu g/cm.^2$ can be obtained by using several organic materials dissolved in suitable solvents. The films have low atomic number but are non-conducting while the mechanical and chemical properties vary. Two general techniques are used to produce the films. If the solvent used is volatile and immiscible with water and has a suitably low surface tension, then a few drops of solution are

put on the surface of a trough of water. The drops spread out over the surface under the surface tension forces and finally the solvent evaporates leaving behind a thin film of organic material which may be carefully lifted off the surface by a wire frame. The second method consists of dipping a scrupulously cleaned glass slide into a suitably dilute solution of the material, and slowly withdrawing it so that a thin film is formed on the surface which can be subsequently floated off in water. The first method is more direct and was used in the present work; it is necessary to use the second method if the solvent will not spread on water, even when hot solutions are used. The properties of the films made during the present work are summarised in Table 5.

Table 5.

Material	Solvent	Film thickness $\mu g/cm.^2$	Film properties
Collodion	amyl acetate	~ 20	weak with moderate acid resistance
Formvar	ethylene dichloride	~ 20	strong but with poor acid resistance
Nylon	isobutyl alcohol	~ 40	quite strong but with moderate acid resistance
V.Y.N.S. resin	cyclohexanone	1-10	strong films with excellent chemical resistance.

Ethylene dichloride does not spread very readily on water even with hot solutions and formvar films are better made by the second method described above. Grade CA nylon polymerised in the United States dissolves in isobutyl alcohol if heated in a double boiler at 60°C; the supersaturated solution spreads readily on hot water. British grade nylon chips were not found to be suitable. The increasing fragility at small thicknesses and the moderate resistance to acids of collodion, formvar and nylon films are disadvantages that are not found with V.Y.N.S. films, whose production by a special film spreading technique will be described in §5. Mention must here be made of three types of material, which show very high resistance to chemical reagents.

(1) Terylene has a very high resistance to most kinds of solvents and the resistance of a 1 mg/cm.^{2} sheet to concentrated hydrochloric acid was confirmed. Crouch (49) reports that under favourable conditions a terylene sheet may be thinned to 100 μ g/cm.^{2} by stretching. Terylene is reported to dissolve in orthochlorphenol with refluxing and the production of thinner films may be possible.

(2) Graphite films of less than 1 μ g/cm.^{2} with resistance to concentrated acids have been reported (50). Such conducting films are ideal for use in

β-spectroscopy but at present require supporting grids if areas greater than 1 mm. in diameter are used.

(3) Zapon nitro-cellulose lacquer has been much used in America to produce acid resistant films of a few $\mu g/cm.^2$, but these are very fragile.

In the present investigation nylon films have been used as backings when backscattering is relatively unimportant; V.Y.N.S. films have been used when very thin backings are required.

5. An improved source backing - V.Y.N.S. films.

5.1. The production of thin films of V.Y.N.S. resin.

The use of V.Y.N.S. resin (a polyvinylchloride-acetate co-polymer) for the production of very thin films was proposed by Pate and Yaffe (51). The films are produced on water in a Langmuir trough, or are spread by a similar method. A sample of V.Y.N.S. resin was kindly supplied by Bakelite Limited and after preliminary experiments a satisfactory procedure was evolved. The resin, supplied as a fine white powder, is dissolved in cyclohexanone by heating in a double boiler at 60°C until completely dissolved; a ~~constituency~~ mixture of one volume of resin to three volumes of solvent proving satisfactory. The films were produced on a water surface in a 17 in. long and 14 in. wide trough as follows. A plastic or perspex rod was

placed, half-submerged, against one end of the trough and several c.c.'s of V.Y.N.S. solution were spread evenly in the V-shaped intersection of the rod and the trough. The rod was then displaced along the surface by 2-3 cm., when the solution spreads over the surface to form a rectangular strip bounded by the rod. The rod is lifted momentarily out of the water surface and the strip starts to expand along the trough. The rod is then lowered to touch the film, which adheres to it, and is then moved along the trough at constant speed, slightly above and parallel to the surface to avoid the production of waves. A sheet of thin film feeds out of the original strip attached at one end to the fast moving rod and floats on the water surface. The technique is easily mastered after some experience provided care is taken to spread the solution evenly and in good contact with the rod and the end of the trough; a constant speed of about 30 cm./sec. is used in pulling out the film. The films are removed on a metal frame which is lowered beneath the water before the film is produced and then raised into contact with the film, which adheres to the metal surface; a brush dipped in cyclohexanone is used to free the frame from the rest of the sheet of film. The films are lifted off the water with a rolling motion which separates one edge first; the frame is nearly perpendicular to

the surface when the second edge separates keeping the surface tension forces acting principally in the plane of the film. The metal frames are normally 50 cm.^{2} in area and the films are later transferred to the source rings. Alternatively a 20 cm. square sheet of V.Y.N.S. film was removed, supported on a metal sheet containing sixteen 4 cm. diameter circular holes. This second frame is more difficult to remove from the shallow trough without film breakage but is worthwhile if a large number of films are required. Pate and Yaffe (51) have measured the superficial film densities for various thicknesses of film by a beta radiation absorption method and have correlated the film thickness with its colour; their results are shown in Table 6.

Table 6.

Superficial density $\mu g/cm.^2$	Film thickness $m\mu$	Colour observed
1	7	dark grey
5	36	light grey
10	70	white
20	140	light yellow

The V.Y.N.S. films used as source mountings in the present work are light or dark grey in colour and are thus 1-5 $\mu g/cm.^2$ superficial density. They are remarkably strong and endure the mechanical shocks of normal source preparation. Their resistance to acids and alkalis is very high, 6N hydrochloric acid has been evaporated to dryness under infra red irradiation without film breakage. A further advantage over normal thin films is that the film is not under tension so that small holes do not spread to the rest of the film. The films are hydrophobic so that drops containing dissolved source material do not spread and may be evaporated to dryness over a localised area. The complete drops can be moved small distances across the film by a fine air jet directed under one edge; the same technique applied round the whole circumference can be used to reduce the area on which a large evaporating drop deposits its solid content. The small source sizes required in the present work were easily obtained using a syringe or finely drawn out glass tube to produce small drops.

6. Evaporation of gold on to thin films.

For use as source backings in β-ray spectroscopy thin films must be rendered conducting and, if this is done by an evaporation procedure, films must be chosen

that can stand the vacuum deposition of a thin metallic layer. V.Y.N.S. films withstand the slow deposition of gold up to a thickness when the purple colour of the film, seen by reflected light, becomes metallic. At this thickness, certainly greater than 10 μ g/cm.^{2}, the films tend to sag and become fragile. Pate and Yaffe (51) have made spectrophotometric measurements on gold layers of known thickness deposited on V.Y.N.S. film; they report that the first purplish coloration appears at 0.4 μ g/cm.^{2} of gold and deepens until a rich red-purple is obtained with a 5 μ g/cm.^{2} layer. By transmitted light the films appear a progressively deeper blue. On this basis it is estimated that most of the present V.Y.N.S. films used as source backings supported a gold layer 1-3 μ g/cm.^{2} thick; the probable total source backing is about 5 μ g/cm.^{2}. Gold is preferred to aluminium with the V.Y.N.S. films on account of its greater chemical resistance.

The gold evaporation was done from a tungsten ribbon filament with the thin films mounted on a frame about 8 in. above. The evaporation was performed under a bell jar evacuated down to a pressure of 10^{-4}-10^{-5} mm. of mercury by a two-stage pump. A metal sheet was interposed between the films and the filament before the gold started distilling when a slow deposition rate was maintained until the correct film coloration was reached.

Chapter 5.

THE DETERMINATION OF THE DETECTION EFFICIENCY USING THE β-SPECTRUM OF SULPHUR-35.

1. The efficiency of the scintillation counter detector.

1.1. The limitation set by the photomultiplier noise level.

The detector is an anthracene crystal whose scintillations pass down a 20 in. light guide to a photomultiplier-cathode follower system. Electrons selected by the slit system enter the anthracene crystal, the number of photons emitted being proportional to the electron energy; the efficiency with which these photons are detected by the photocathode of the photomultiplier is arranged to be as high as possible. A polished aluminium disc reduces the loss of light from one end of the disc crystal; the light passes through the opposite face into the light guide, and is transmitted by internal reflection to the photocathode of the electron multiplier. The light guide is highly polished and good optical joints are made with white vaseline; some losses in the crystal and light guide are inevitable while there is a further loss due to the quantum detection efficiency of the photocathode. Random noise pulses are produced by the thermionic emission of the cathode so that the

final signal to noise ratio is largely determined by the ratio between the pulse height from the photocathode due to the photons emitted by the scintillator, and that due to thermionic emission. The latter is reduced if the tube is cooled but this introduces further difficulties. The noise pulse height is comparable with that produced by 10-20 kev electrons in anthracene (52); with the reduced efficiency of the crystal light-guide system the noise level is probably equivalent to electrons of nearly 100 kev. The gain of the photomultiplier for this type of noise will be equal to that for genuine pulses and must be chosen such that, after amplification, most of the noise spectrum is below the discriminator bias level of the scaler; this means that pulses from low energy electrons in anthracene may also be biased out. A noise level giving a background of a few hundred counts a minute on the scaler may be tolerated, provided it is very stable.

The photomultiplier tube has been selected to give a high gain with low dark current and the noise level at the 5v discriminator bias setting is normally very stable at 100-400 counts per minute for an average inter-stage voltage of 150-160v. The tube is carefully cleaned with carbon tetrachloride and dried with methyl alcohol so as to reduce conducting paths in the

glass which may contribute to the noise; where possible the tube is handled in reduced light to minimise the excitation of metastable states in the Cs Sb photocathode surface.

1.2. The variation of efficiency with electron energy.

The voltage pulses in the photomultiplier output circuit, corresponding to mono-energetic electrons selected by the spectrometer, show a statistical spread about a mean value of pulse height; if they were constant in voltage a pulse height analyser could be used to select only genuine pulses, rejecting the wide noise band. The pulse height per Mev produced in anthracene is linear, at any rate above 100 kev, and the mean pulse height of the genuine counts will increase as the spectrometer focuses higher energy electrons. The electrons are counted with 100% efficiency when the complete range in height of genuine pulses lies, after amplification, above the bias level of the scaler. As the pulse height is decreased by the selection of lower energy electrons, an increasing proportion of the genuine pulses fall below the bias level and are not counted; an increasing reduction in detector efficiency results. The detection efficiency under normal conditions begins to decrease below 100 kev falling to zero by 10 kev.

The most direct method of determining the

variation of detection efficiency with energy is by the measurement, with a very thin source and backing, of a spectrum whose shape is very well known; S^{35} on a gold coated V.Y.N.S. film was chosen.

2. The β-spectrum of Sulphur-35.

2.1. Introduction.

The simplest spectral shape is that corresponding to a single allowed β-transition between the ground states of parent and daughter nuclei. The total energy, E_o, released by the nucleus is divided between the electron, E, and the neutrino $(E_o - E)$. The observed electron energy distribution reflects the relative probabilities of the way in which the energy is shared. The Fermi theory of β-decay allows those variable factors which have an extra-nuclear origin to be removed from the distribution so that there remain only truly nuclear features of the disintegration.

The observed momentum distribution $N(\eta)d\eta$ is given by:-

$$N(\eta)d\eta = \eta^2(\varepsilon_o - \varepsilon)^2 F(Z,\eta)\, d\eta,$$

where the electron momentum η is expressed in units of $m_o c$, the product of the electron mass and the velocity of light; the energy ε is in units of $m_o c^2$ and includes the rest mass energy $m_o c^2$. The function $F(Z,\eta)$ represents the effect on the electrons of the

electrostatic field near the nucleus together with that of the outer screening electrons. Tables of $f(Z,\eta) = \eta^2 F(Z,\eta)$ have been published (53). The graph of $(N/f)^{\frac{1}{2}}$ against ε is a straight line meeting the energy axis at the total disintegration energy ε_0 of the β-transition, the precise value is determined from such a Fermi plot by the least squares method. According to the Fermi theory the plot is linear down to zero energy for allowed transitions and in the case of most first forbidden transitions.

The decay of S^{35} is by a single allowed β-transition between the ground states of the parent and daughter nuclei. No conversion lines appear in the spectrum and the linearity of the Fermi plot has been the subject of several investigations. The end-point energy of 167 kev is sufficiently high for present purposes.

2.2. <u>The linearity of the Fermi plot of S^{35}</u>.

The first measurements of the shape of the β-spectrum of S^{35} were made by Cook et al. (54) with a high resolution spectrometer and Geiger counter detector. Below 80 kev an excess of low energy electrons was found over that expected from the allowed shape predicted by Fermi theory; this was apparently unaffected by varying the source or backing thickness. Confirmation of these results was claimed by Cockcroft

and Insch (55) using a gaseous source in a proportional counter. Bergrenn and Osborne (56), using a lens spectrometer, found a spectrum shape in agreement with a $\Delta I = 1$ (yes) first forbidden transition.

The reported disagreement with Fermi theory prompted a series of investigations in which careful attention was given to the effect of source and backing thickness on the spectral shape. Albert and Wu (48) using 1-5 μ g/cm.^{2} sources mounted on 3 μ g/cm.^{2} collodion obtained a straight line Fermi plot down to 16 kev with 1 and 2 μ g/cm.^{2} sources; they report that 10 μ g/cm.^{2} additional backing noticeably distorted the low energy region. Langer et al. (57) re-measured the spectrum with 10 and 50 μ g/cm.^{2} sources finding a linear Fermi plot to below 50 kev provided the source was uniformly deposited. The region of linearity was further extended by Moljk and Curran (58), using a gaseous source in a proportional counter, down to 5 kev. The 6-25 kev region was investigated by Gross and Hamilton (59) by a retarding potential method and showed no serious departure from the theoretical shape. Heller and Sturcken (60) corrected carefully for the effect of Geiger counter window thickness and found the resultant Fermi plot linear to 32 kev. The β-transition may be taken to be allowed with $\Delta I = 0$ (no) with a linear Fermi plot to at least 5 kev.

Table 7.

Worker	Method	End-point energy (kev)	Source thickness ($\mu g/cm.^2$)	Backing thickness ($\mu g/cm.^2$)	Nature of the Fermi plot
Cook et al.	Magnetic spectrometer	169.1 ± 0.5	Relatively thin	30,500	linear to 80 kev
Cockcroft and Insch	Proportional counter	168	Gaseous source	-	linear to 80 kev
Bergrenn and Osborne	Magnetic spectrometer	169 ± 3	50	20	I = 1 (yes) shape
Albert and Wu	Magnetic spectrometer	166	1, 2 & 5	3	linear to 16 kev
Langer et al.	Magnetic spectrometer	167.0 ± 0.5	10, 50		linear to 50 kev
Moljk and Curran	Proportional counter		Gaseous source	-	Corrected plot linear to 5 kev
Gross and Hamilton	Retarding potential	168.3 ± 4	0.4	5	6-25 kev region has theoretical shape
Heller and Sturcken	Magnetic spectrometer	167	10	10	linear to 32 kev (with window correction).

The precise value for the high energy end-point of the spectrum is at present more in doubt than the linearity of the Fermi plot; the values reported are given in Table 7 together with the source and backing thicknesses and the degree of linearity of the Fermi plot. The calibration of the present instrument is known with some precision and the experiment to determine the low energy detection efficiency of the scintillation counter from the linearity of the Fermi plot has been extended to include the measurement of the end-point energy of the S^{35} β-spectrum.

2.3. Measurements of the β-spectrum of S^{35} with the spheroidal field spectrometer (63).

"Carrier free" S^{35} was obtained from the Radiochemical Centre, Amersham in the form of about 1 c.c. of neutral solution.

The sources were deposited on a 3 mm. diameter disc by the evaporation of several drops of solution. The source backings available at this time were 40 μ g/cm.^{2} nylon films made conducting by the evaporation of a comparatively thick aluminium layer. The nylon film was supported by a 7 mm. diameter 3 mm. long cylindrical brass ring. This ring was mounted in a brass recess in the source holder which is mounted in the slide passing through the door of the vacuum box. Three runs were made on the β-spectrum and, after

Fermi analysis, all gave a value for the end-point of about 162 kev. The discrepancy between this value and the previously reported end-point values is serious and can be attributed to two causes.

The S^{35} normally supplied as a "carrier free" solution has a solid content of up to 1 mg per mℓ and the source used is estimated to have been up to 1 mg/cm.^{2} thick. It is clear from the work of Albert and Wu (48) that considerable distortion of the spectrum results from the use of both sources and backings of this thickness; in addition the close proximity of the brass block in which the sources are mounted is undesirable. The system of source mounting was altered so that a 3 cm. diameter thin film is supported on an aluminium ring fitting into an aluminium source holder. A 5 μg/cm.^{2} V.Y.N.S. film with a 5 μg/cm.^{2} conducting gold layer was used as backing for a thinner source of the same S^{35} solution and with this source the end-point energy for two runs on the spectrum was 166 kev, in better agreement with the values reported by other workers. With the arrival of a specially prepared carrier free supply of S^{35} a further source was prepared about 5 μg/cm.^{2} thick and mounted on a V.Y.N.S. film similar to that used previously. This source appeared as a white stain on the blue gold layer and appeared to be very uniformly deposited.

Three runs were made of the β-spectrum and the straight portion of the Fermi plots gave the end-point values of Table 8, determined by the method of least squares. A typical plot is shown in Fig. 11.

Table 8.

Run	End-point energy	
	($m_o c^2$)	(kev)
1	1.3278	167.5
2	1.3270	167.1
3	1.3280	167.6

Mean energy : 167.4 ± 0.2 kev

The mean value of the end-point energy agrees quite well with that of 167.0 ± 0.5 kev by Langer et al.; these workers mention the use of the thorium B conversion lines for the calibration of their spectrometer and it seems likely that they used the 148 kev thorium F-line, whose $B\rho$ value has subsequently been redetermined (47). If the quoted value of the end-point is revised on the assumption that the calibration was in terms of the $B\rho$ value of Ellis (61) for the F-line, then the value of 167.0 kev given by Langer et al. should be 167.5 kev, agreeing almost exactly with the present work.

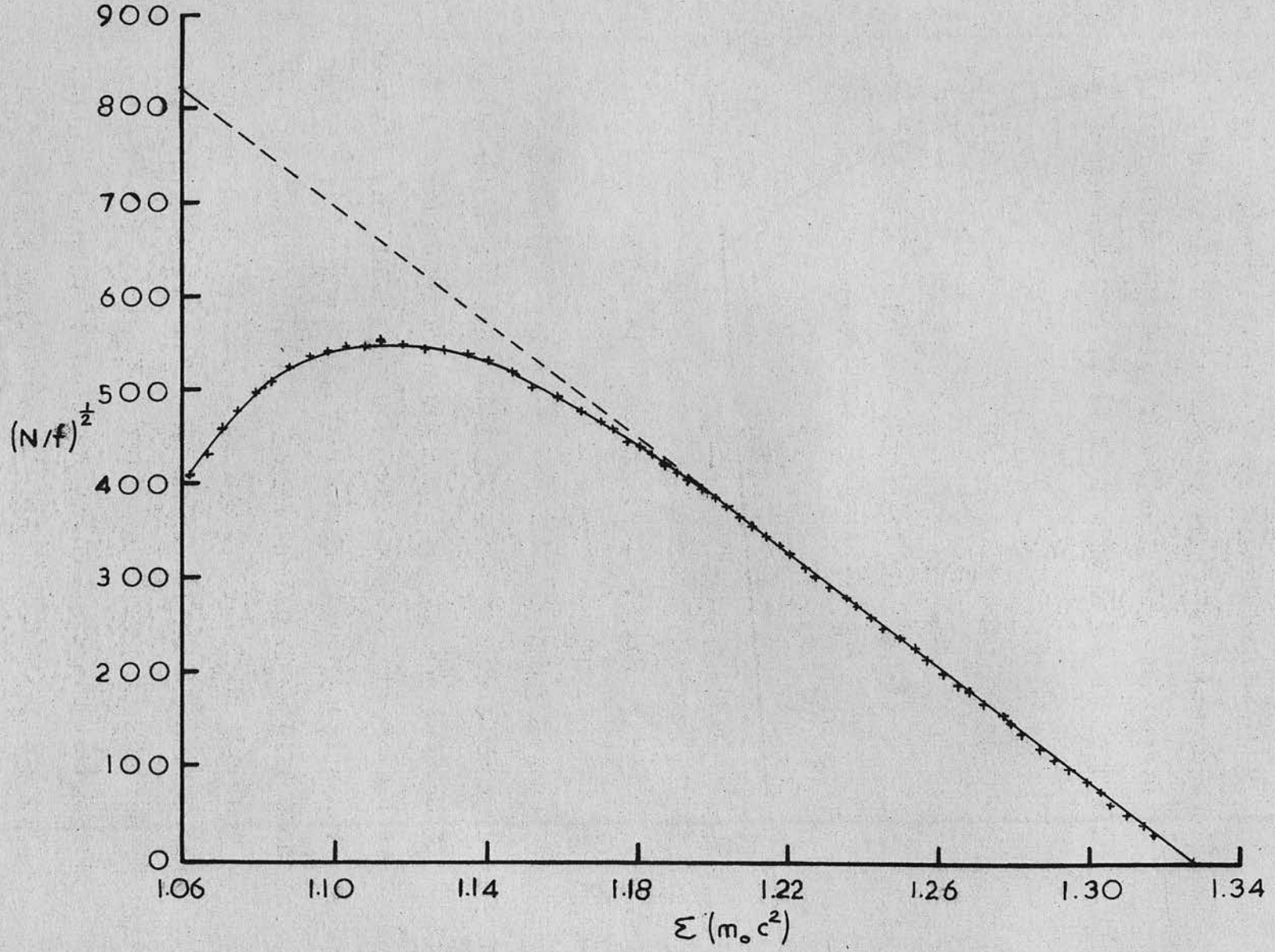

Figure 11. Fermi plot of the beta spectrum of S^{35}.

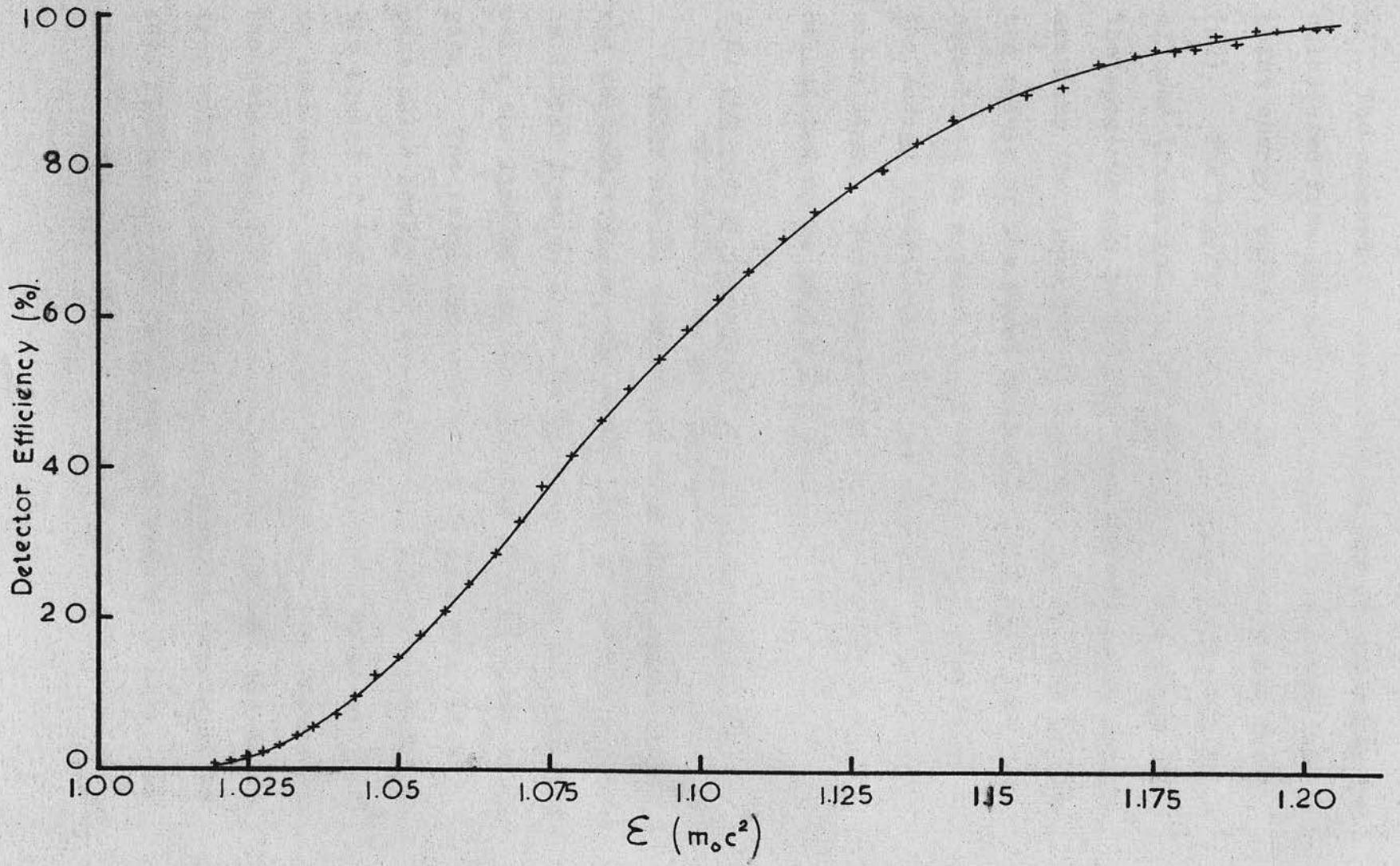

Figure 12. The variation of detector efficiency with electron energy.

The comparative half-life or log ft value may be calculated from the 87.1 day half-life and the end-point energy, using the graphs of Feenberg and Trigg (62). The log ft value is 5.01 consistent with an allowed transition for S^{35} β-decay. The shape of the spectrum can be deduced from the end-point energy, assuming the linearity of the Fermi plot; the tabulated values of the Fermi function $f(\eta)$ (53) were re-normalised as a function of energy $f(\varepsilon)$ from which the energy distribution of the electron spectrum was calculated. The mean energy of the electrons was calculated to be 48.8 ± 0.2 kev.

2.4. The energy dependence of detection efficiency as determined experimentally.

Under normal conditions, with 1800v supplied to the photomultiplier, the Fermi plot of the S^{35} spectrum is linear down to about 95 kev, but falls increasingly below the line of the extrapolated plot at lower energies. The Fermi function $f(\varepsilon)$ is constant for a particular energy so the efficiency of the detector is the square of the ratio of the observed value of $(N/f)^{\frac{1}{2}}$ to that on the extrapolated Fermi plot, see Figure 11. The detection efficiency is plotted against the electron energy in Fig. 12; full efficiency ceases at 95 kev, falling to 50% at 50 kev and zero at 8 kev. If the S^{35} source is assumed to be of negligible thickness

then any β-spectrum taken under the same conditions may be corrected for loss of detector efficiency by the curve of Fig. 12.

Chapter 6.

THE β-SPECTRUM OF IRIDIUM-192.

1. Introduction.

The principal object of the present investigation of Ir^{192} β-decay is the re-determination of the high energy end-points and relative intensities of the components of the continuous β-spectrum, see Chapter 2 Table 1; in particular the existence or non-existence of the high energy components reported by Kyles and Campbell (13) is in question. The low specific activity of Ir^{192} necessitated the use of comparatively thick sources in order to provide adequate source activities. The investigation has been in two parts.

(1) A series of runs ~~were~~ was made with very strong and relatively thick sources to examine the high energy region. End-point energies and relative intensities of the high energy β-feeds were deduced by Fermi analysis. An experimental correction for the effects of source and backing thickness was applied, and the spectrum was re-analysed; the absolute intensities of the stronger conversion lines were deduced.

(2) The β-spectrum was re-determined using thinner source material and the end-point energies again calculated. The effect of source thickness is reduced, but not negligible.

2. Measurements with a thick source.

2.1. The preparation of the sources.

Pure natural iridium was sputtered uniformly on 0.2 mg/cm.^{2} aluminium foil to a thickness of 0.45 mg/cm.^{2} by Messrs. Barr and Stroud Limited. Small discs 1 and 2 mm. in diameter were cut from the iridium coated foil and irradiated with neutrons at A.E.R.E., Harwell. The source discs were mounted on 40 μg/cm.^{2} nylon film and an aquadag earthing strip across the film connected the source to the small brass supporting ring. The initial source activities were 50 and 200 μc respectively. The 19 hour Ir^{194} was allowed to die out completely before the sources were used.

2.2. The measurement of the high energy region of the β-spectrum.

The region above 700 kev was examined carefully, with the 2 mm. diameter source, for any sign of a high energy tail to the β-spectrum. The photomultiplier volts were set at 1600v reducing the background noise to a very low level that showed high stability over a period of several days. The K and L conversion lines of the 885 kev γ-ray are just beyond the end-point of the 700 kev β-transition; the lines are shown in Fig. 13 together with the end of the β-feed plotted on the same scale and a part of the higher energy region of the spectrum. The background level that has

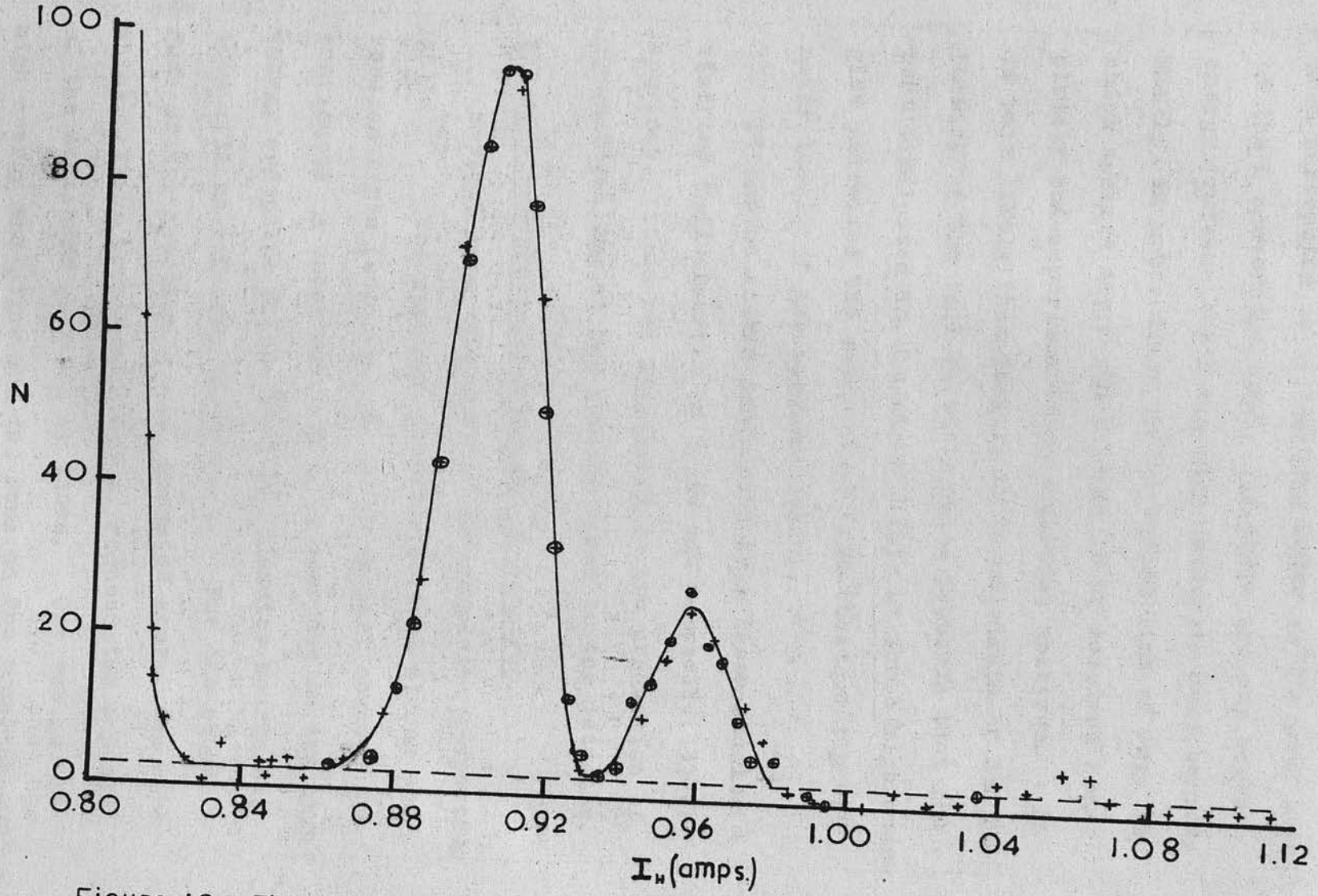

Figure 13. The high energy region of the Ir^{192} beta spectrum showing the end-point of the 690kev component together with the conversion lines of the 885kev gamma ray and the possible high energy tail (shown dashed).

been subtracted is of the same order as the peak height of the L conversion line. If there are any higher energy β-feeds their combined intensity must be very small; an upper limit is the dashed line of Fig. 13 which assumes the K and L lines to be resolved completely but superimposed on a partial spectrum. It is very likely that this is an overestimate of the intensity of the tail as it is quite probable that the heat dissipated in the magnet coils at these high energies increased the temperature, and consequently the noise level, of the photomultiplier.

It can be stated definitely from these results that the tail observed by Kyles and Campbell (13) is spurious; it is now attributed to the production of bremsstrahlung at the shutter close to the detector.

2.3. The uncorrected continuous β-spectrum.

Several runs were made of the complete β-spectrum of Ir^{192}. The spectrum contains several strong conversion lines (see Fig. 16) which in part obscure the continuous β-spectrum. One run was done on the high energy end-point using the 2 mm. diameter source and this will be referred to as run 1. For the other runs on the spectrum a 1 mm. diameter source was used which, giving better resolution, reduced the portion of the continuum obscured by lines. One run on the high energy end-point and two runs on the complete con-

tinuous spectrum have been analysed by the Fermi method; the end-point energies and relative intensities of the partial β-components are shown in Table 9. Only points which are clear of the known conversion lines have been used.

Table 9.

	First partial kev	Second partial kev	Ratio of intensities (1st:2nd)
Run 1	688.3 ± 2	-	
Run 2	693.5 ± 2	-	
Run 3	688.7 ± 2	553.2 ± 2	1:1.15
Run 4	691.7 ± 2	554.0 ± 2	1.40:1

It can be seen that the end-points agree quite well within themselves. The value of the first partial end-point agrees with Kyles (13) rather than Bashilov (12) who was supported by earlier workers, (see Chapter 2 Table 1). The energy difference between the first and second end-points is very close to that of the 136 kev γ-ray between the corresponding levels in Pt^{192}, but there is only fair agreement as to the relative intensities of these two partial spectra. When the third partial was looked for it was found that the points on the Fermi plot fell below the extrapolated line of the second partial, showing

that the effects of source thickness are appreciable below 300 kev. An experimentally determined correction was applied to the spectrum, to allow for the effects of source thickness.

2.4. An experimental source thickness correction.

The effects of source thickness in a layer of 0.45 m g/cm.^{2} iridium was investigated in the following manner. A thin source of thorium active deposit was obtained in a 1 mm. diameter disc on a 0.2 mg/cm.^{2} gold foil, the source then being covered by a similar gold foil. Since gold is close in atomic number to iridium this source simulates the case of a central active layer of iridium in a 0.4 mg/cm.^{2} thick disc. The continuous spectrum of electrons from this sandwich source was recorded with the spectrometer up to 1.5 Mev. The actual thorium deposit spectrum has been very carefully determined by Flammersfeld (64) using thin sources and backings and a thin window Geiger counter as detector. Flammersfeld's published spectrum was normalised, in the high energy region, to the spectrum obtained with the present spectrometer. The ratio of the curves gives a correction for the effects of source thickness and the loss of efficiency at low energies in the scintillation counter detector, see Fig. 14.

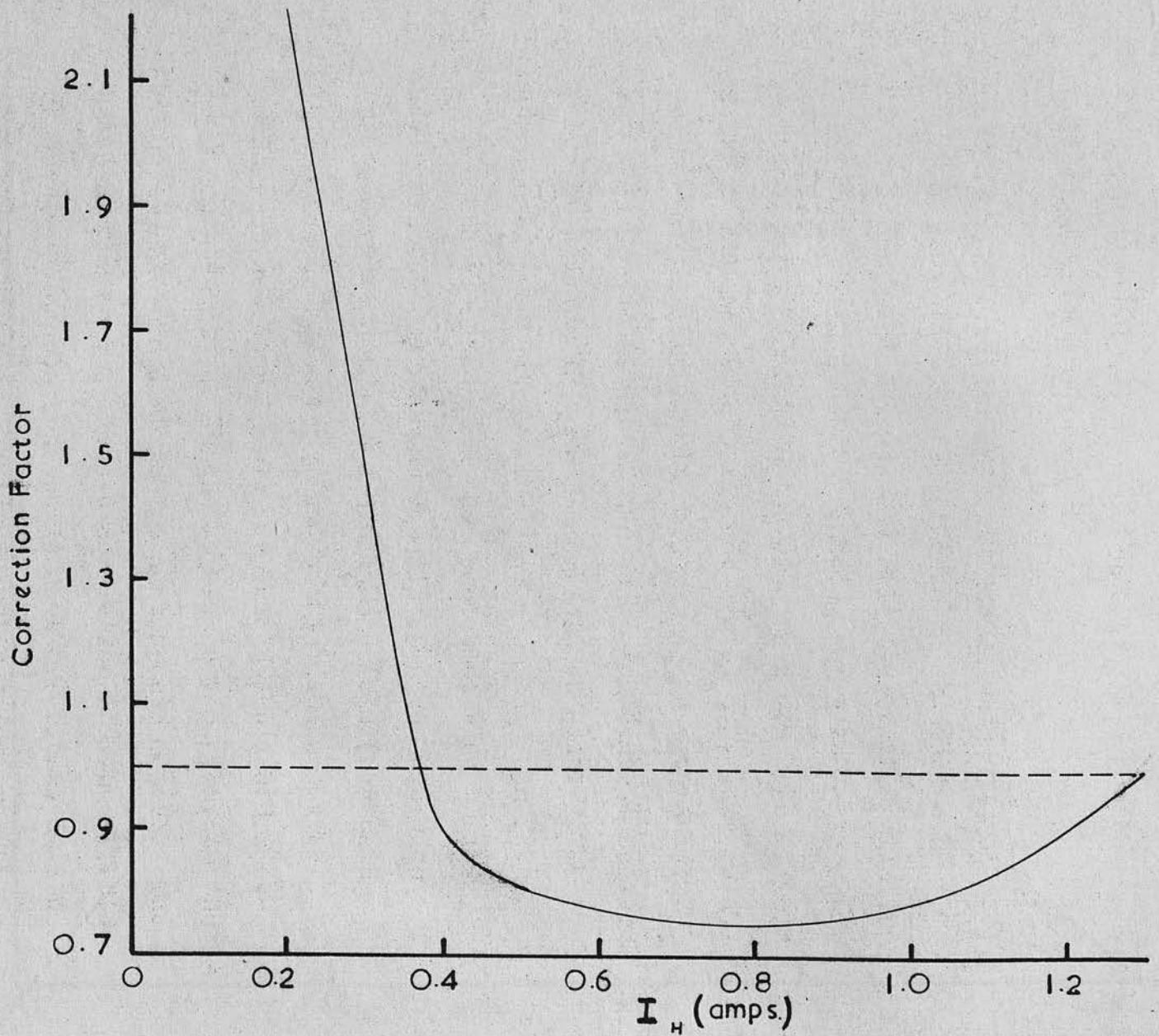

Figure 14. Correction to the observed Ir^{192} spectrum for the effects of source and backing thickness.

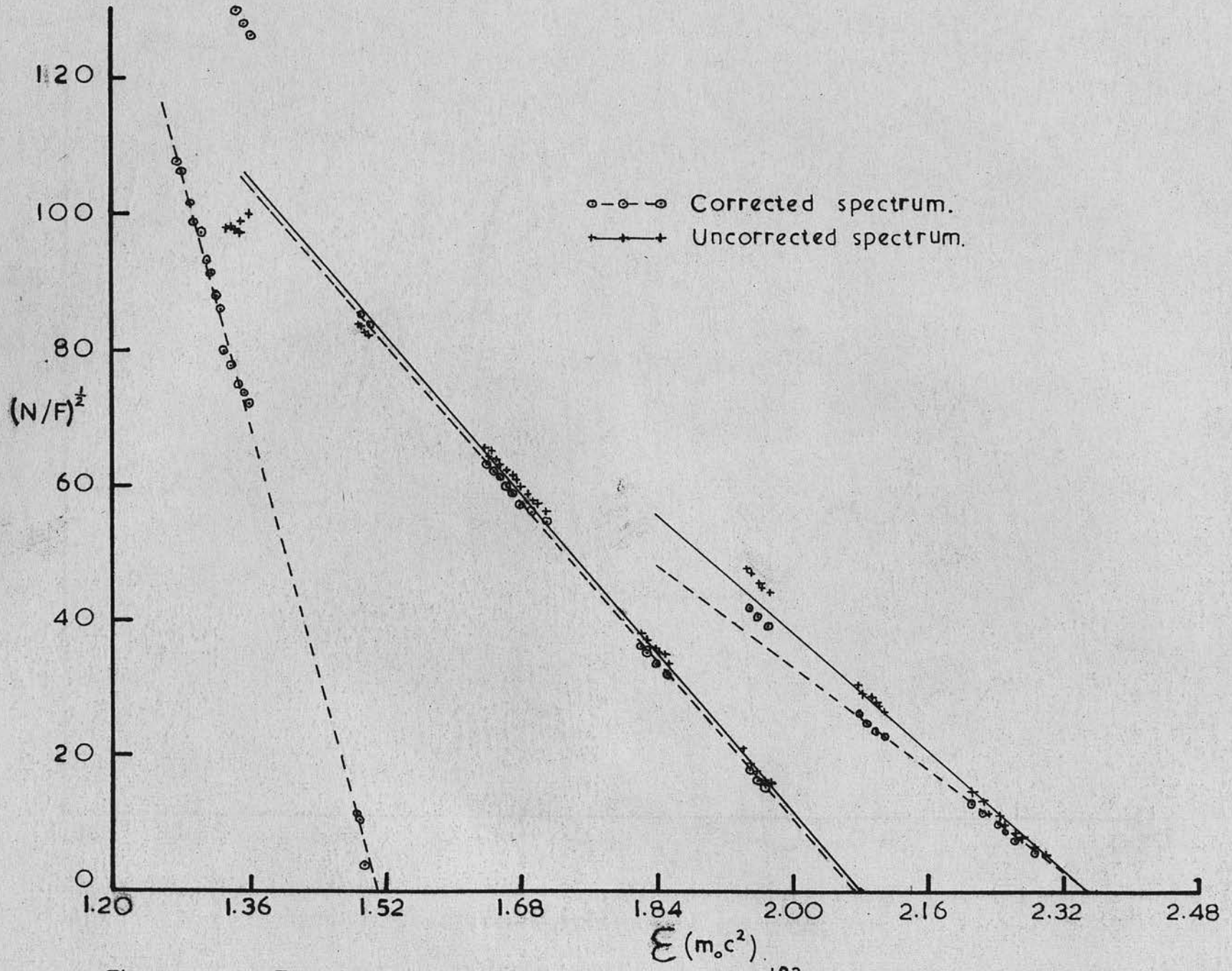

Figure 15. Fermi plot of the beta spectrum of Ir^{192}

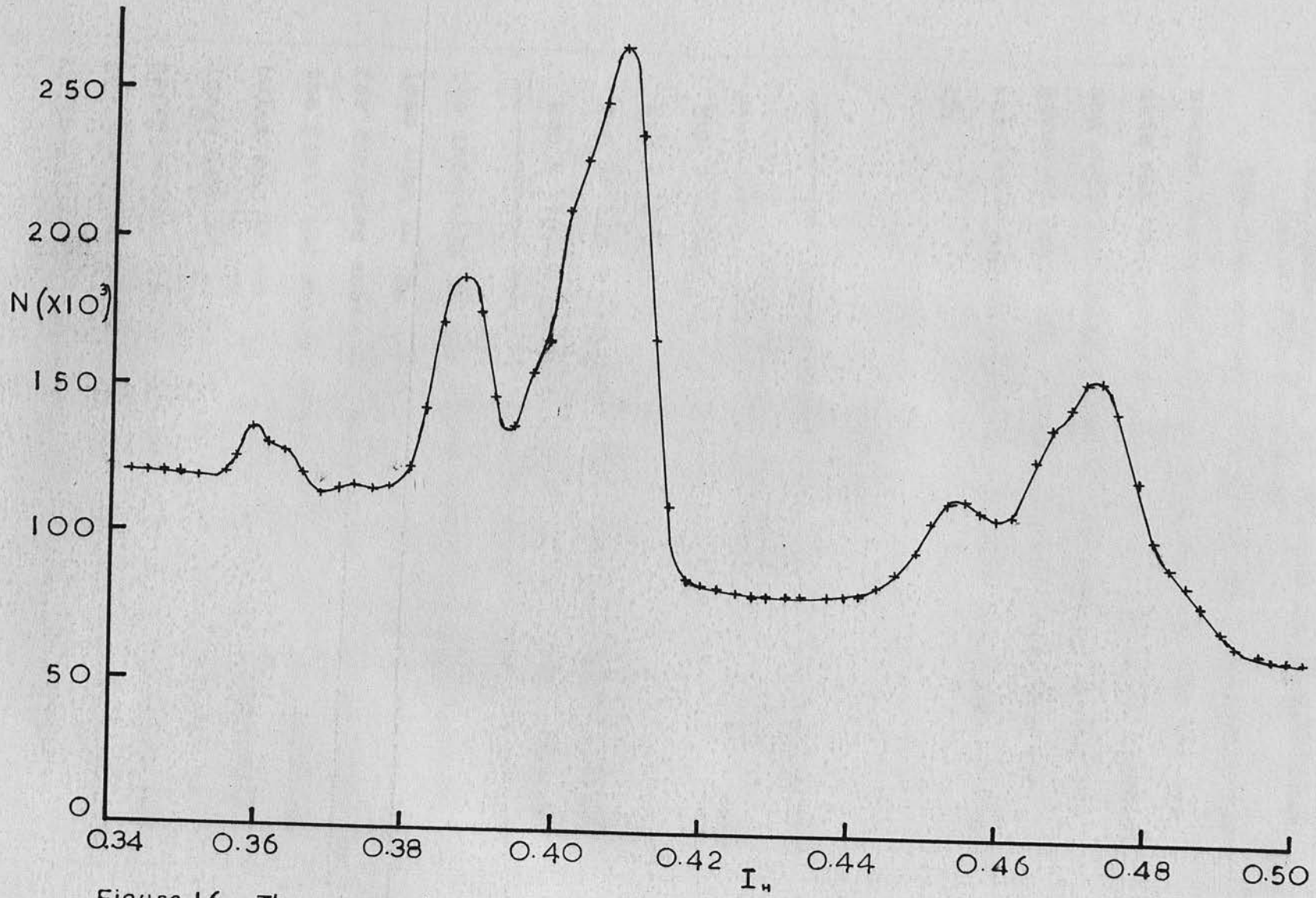

Figure 16. The conversion lines of the 296, 308 and 316 kev γ-rays and the underlying corrected continuous spectrum.

2.5. The continuous β-spectrum of Ir^{192} corrected for source thickness.

The runs on the β-spectrum were corrected for source thickness effects using Fig. 14 and the new data was re-analysed to yield the end-point energies and relative intensities of the partial β-spectra given in Table 10. Typical Fermi plots for the corrected and uncorrected spectrum are shown in Fig. 15.

Table 10.

	First partial kev	Second partial kev	Third partial kev
Run 1	688.0	-	-
Run 2	693.1	-	-
Run 3	688.9 (38.8%)	548.3 (42.8%)	263 (18.4%)
Run 4	691.0 (43.1%)	550.2 (35.9%)	271 (21.0%)

The intensity of any higher energy partial spectrum is less than 10^{-4}%. The experimental correction is small for energies above 230 kev and has little influence on the first and second beta end-points. For energies below 230 kev the correction factor is increasingly large and the corrected spectrum may be subject to appreciable error. However, for energies above 100 kev the corrected β-spectrum agrees well with that of Kyles (13), who has shown that above 130 kev his

spectrum shape was not affected by increasing the effective source thickness from 0.45 to 0.63 mg/cm.^{2}. The shape of the corrected spectrum was found to show some deviation from theory in the region below 200 kev, due to the approximate nature of the source correction. When the first and second partial momentum spectra are subtracted from the complete corrected β-spectrum the remaining spectrum is attributed to a third partial component. It was found that the shape of this third partial spectrum gives a linear Fermi plot in the region from 150-250 kev. The plot was extrapolated linearly to zero energy and the shape of the 0-150 kev region was calculated; it was found that the calculated area for the 0-150 kev region of the momentum spectrum is greater than that available for the third partial in this region of the corrected spectrum. The intensity quoted for the third partial (see Table 10) corresponds to the area remaining when the first and second partial spectra have been subtracted from the complete corrected spectrum.

2.6. <u>The conversion lines</u>.

The Bρ values of the Ir^{192} conversion lines calculated from the values of the γ-ray energies as given by Muller (15) were found to be in good agreement with the calibration.

The absolute intensities of several of the

conversion lines were measured and are given in Table 11. In some cases the lines were not resolved and the total intensity of the group is given. The chief source of inaccuracy for the stronger lines is in the measurement of the area under the continuous spectrum. The intensities are given in terms of the corrected continuum, which is 1.41 times the area of the uncorrected continuum. The values of run 5 were obtained with a thinner source, see § 3.

Table 11.

γ-ray energy kev	Absolute electron intensity					
	K (x 10^{-3})			L + M + ... (x 10^{-3})		
	Run 3	Run 4	Run 5	Run 3	Run 4	Run 5
201	6.1		7.3	4		4.8
205						
296	64.8	63.5	61.7	39.5	39.0	36.2
308						
316						
468	8.5	8.5	9.2	2.7	3.1	2.7
484	0.4		0.25			
588	1.8		1.6	0.4		0.3
604						
613						
885	1.2 x 10^{-2}		1.3 x 10^{-2}	3 x 10^{-3}		3 x 10^{-3}

3. Measurements on the β-spectrum of Ir^{192} using thinner source material.

3.1. Source preparation.

Pure iridium was sputtered on to two 0.2 mg/cm.^{2} aluminium foils to thicknesses of 40 and 100 μg/cm.^{2} respectively. Discs 2 and 3 mm. in diameter were activated by neutron irradiation at A.E.R.E., Harwell. The 3 mm. diameter 40 μg/cm.^{2} thick iridium discs were of similar total activity to the 1 mm. diameter 450 μg/cm.^{2} thick discs used previously. Some loss in resolution is introduced by the increased source diameter.

The 40 μg/cm.^{2} source discs were supported by a 3 cm. diameter V.Y.N.S. film less than 5 μg/cm.^{2} thick made conducting by a layer of gold a few μg/cm.^{2} thick; the 100 μg/cm.^{2} source discs were supported by a 40 μg/cm.^{2} nylon film earthed by a conducting strip of aquadag between the source and the aluminium source holder.

3.2. Re-measurement of the β-spectrum with thinner source material.

A run was made (run 5) over the complete β-spectrum of Ir^{192} with a 40 μg/cm.^{2} source; a further run was made on the high energy region (run 6). The spectrum was also measured using a 100 μg/cm.^{2} source (run 7). Fermi analysis yielded the end-points and relative intensities for the components of the

β-spectrum shown in Table 12.

Table 12.

	First partial kev	Second partial kev	Ratio of intensities (1st:2nd)
Run 5	691.1	553.8	1.28:1
Run 6	690.8	-	-
Run 7	689.1	551.9	1.23:1

The end-point values confirm those found previously with a 0.45 m g/cm.^{2} iridium source, see Tables 9 and 10. The region beyond the high energy end-point was again examined with no sign of a high energy tail; the position of the K and L conversion lines of the 885 kev γ-ray again confirmed the momentum calibration.

The effect of reversing the source was investigated and has been described in Chapter 4 (see Fig. 10). It is concluded that there is no effect on the shape of the continuous spectrum above 100 kev due to backscattering in the aluminium foil; there is the same amount of backscattering and absorption in the iridium layer irrespective of whether the source is reversed or not.

The continuous spectrum begins to fall below the corrected spectrum, obtained with the thicker source,

at an energy of about 300 kev. The large angle of emission selected by the spectrometer means an effective source thickness of 150 $\mu g/cm.^2$ of iridium for the 40 $\mu g/cm.^2$ source; the combined effects of backscattering, source absorption and loss of detector efficiency account for the observed spectrum shape. The continuous spectrum is so reduced at 200 kev that the points chosen for Fermi analysis fall a little below the extrapolated line of the second partial plot; the end-point and relative intensity of the third partial component cannot be deduced from the uncorrected spectrum shape.

Chapter 7.

THE DISINTEGRATION SCHEME OF IRIDIUM-192.

1. The end-points and intensities of the β-transitions.

The present investigation has shown the high energy tail observed by Kyles and Campbell (13) to be spurious. Kyles has corrected his data empirically for the amputation of the tail and his revised values are given in Table 13, together with the mean values of the present work and the results of Bashilov (12).

Table 13.

Observer	First partial kev	Δ kev	Second partial kev	Δ kev	Third partial kev
Bashilov et al.	670 (44%)	130	540 (40%)	300	240 (16%)
Kyles and Campbell	697 (38%)	128	569 (41%)	288	281 (21%)
Present work	690.3 ± 0.6 (42½%)	139	551 ± 1 (37½%)	284	267 (20%)

The contribution of the third partial was taken to be 20%, see Table 10, and the relative intensities of the remaining partials were calculated from the results of Tables 10 and 12. The ratio of the

intensities of the first and second partials confirms the results of Bashilov rather than those of Kyles; the precise value of the intensity of the third partial is not definitely established by the present work but the value of 20% is in fair agreement with the results of Kyles and Bashilov. The differences between the end-point energies of 139 and 284 kev agree quite well with the corresponding γ-transition energies of 136 and 280 kev; the log ft values are 8.6, 8.3 and 7.6 for the first, second and third partials respectively. The value of 690.3 kev for the beta end-point to the 784.5 level of Pt^{192} yields a mass difference for the Ir^{192}-Pt^{192} nuclei of 1475 kev. This is in good agreement with the value of 1490 $\pm$ 20 reported by Pringle et al. (14).

The end-point values of Kyles may be affected slightly by the empirical removal of the high energy tail but confirm that the high energy end-point is considerably greater than the 670 kev reported by Bashilov and previous workers.

2. The conversion lines.

2.1. The absolute intensities of the lines.

The absolute intensities of the conversion lines were given in Table 11. In Table 14 the values quoted previously for groups of unresolved lines have

been split up into the contributions estimated for the individual lines. This has been done by calculating the relative intensity ratios for the lines of a group from the results of previous workers; in the table their results are compared with the mean values of the present work. There may be considerable error in the distribution of the intensity between the lines of low intensity groups such as the weaker L-lines.

Table 14.

γ-ray energy	Absolute intensities of conversion lines K(x 10^{-3})				L + M + ... (x 10^{-3})			
	1.	2.	3.	4.†	1.	2.	3.	4.†
201	2.3	2.1	0.65	0.87	0.7	5.2	5.2	0.55
205	4.4	4.0	4.3	3.9	3.7			2.87
396	15.6	17.5	16	14.7	9.0	7.5	8.7	7.0
308	14.7	14.9	15	15.2	9.0	7.2	8.0	7.9
316	33.1	34.2	34	34	20.2	15.8	20.6	15.1
468	8.7	11.0	7.7	8.9	2.8	2.6	2.84	2.5
484	0.3	0.8	0.5	0.54	-	-	-	-
588	0.34	0.4	0.45	0.5	0.08		0.07	0.14
604	0.95	1.2	1.4	1.4	0.19	0.5	0.25	0.27
613	0.43	0.7	0.56	0.58	0.08		0.10	0.12
885	0.012	0.015	0.0044	0.022	0.003	-	0.0016	

1. Present work.
2. Kyles and Campbell (13).
3. Bashilov et al. (12).
4. Baggerly et al. (17).

† Normalised to $K_{316} = 34$.

2.2. Experimental and theoretical K:L ratios.

The K:L ratios have been calculated from the results of Table 14, ~~the individual runs~~ assuming that the M + N + ... :L ratio is 0.3 as reported for most types of transitions by Newton (38). The mean values of the K:L ratios are compared with those of other workers in Table 15. Only the strong 300 kev group of lines is here split up into its components.

Table 15.

γ-ray energy kev	Experimental K:L ratios				
	Present work	Kyles & Campbell	Bashilov et al.	Baggerly et al.	Kelman et al.
201	2.0	1.6	1.1	1.6	1.85
205				1.4	1.83
296	2.2	2.6	2.2	2.1	2.35
308	2.1	2.4	2.2	1.9	2.38
316	2.1	2.4	1.9	2.2	2.22
468	4.0	4.2	3.5	3.6	3.0
588	4.8	4.6	6.4	3.6	-
604			5.6	5.2	4.7
613			5.6	4.8	-
885	5.5		4.0		

In Table 16 the K:L ratios of the present work are compared with the theoretical values for E1, M1

and M2 transitions, determined graphically by logarithmic interpolation from the results of Rose (66). In the case of E2 transitions values of Sliv (67) and Rose have been used which take into account the finite size of the nucleus; they show little deviation from the uncorrected values of Rose. The calculation of the K:L ratio is more liable to error in the case of high energy transitions and the ratio becomes less sensitive to the nature of the transition so that definite assignments cannot always be made.

Table 16.

Transition energy kev	K:L ratios					Transition assignment	M1 admixture
	expt.	theoretical E2	M2	E1	M1		
201	2.0	1.1	3.6	6.1	6.1	E2	(15%)
205		1.2					
296	2.2	2.0	4.3	6.2	6.2	E2	4%
308	2.1	2.2	4.3	6.2	6.2	E2	none ~~2%~~
316	2.1	2.2	4.4	6.2	6.2	E2	none
468	4.0	3.2	4.8	6.5	6.2	E2	35%
588	4.8	4.0	5.2	6.6	6.2	E2 (or M2)	(40%)
604							
613							
885	5.5	5.0	5.6	6.7	6.3	E2 (or M2)	(40%)

The comparison of the experiments and theoretical K:L ratios of Table 16 leads to the assignment of E2 for the 296, 308 and 316 kev transitions; the dipole admixture is very low. The results for the 200 and 600 kev groups of lines may lead to an incorrect assignment if the component lines are not all of the same multipolarity. The 200 kev group is apparently E2 with some M1 admixture while the 600 kev group is probably similar; the possible error in the values for the 600 kev group is such that an M2 assignment cannot be excluded. The 468 kev transition is E2 with some dipole admixture and the 885 kev transition is probably similar but could also be M2.

Recent work by Kelman et al. (65) on the $L_I:L_{II}:L_{III}$ ratios is in agreement with the assignments of Table 16, but indicates that the 468 kev transition is pure E2.

3. The γ-transitions in Pt^{192}.

3.1. The absolute intensities of the γ-transitions.

The relative intensities of the unconverted γ-rays of Ir^{192} decay have been measured by Johns and Nablo (11) and by Baggerly et al. (17); their intensities are given in Table 17 relative to the intensity of the 316 kev γ-ray. The intensity of 866×10^{-3} assigned to the 316 kev photons is chosen so that the

sum of the total intensities of the 316 and 613 kev γ-transitions is 1000. These ~~γ-rays~~ transitions populate the ground state of Pt^{192} in nearly all modes of Ir^{192} β^--decay so that the values of Table 17 are absolute intensities of the unconverted γ-transitions expressed as a fraction of the β-disintegration rate. Both sets of workers report that the intensities may be subject to errors of up to 20% but the two independent sets of results agree quite closely in most cases. The mean total intensities of the conversion lines are also given in Table 17, expressed in the same units.

The 201, 205, 283, 375, 485 and 1060 kev γ-rays are assigned to Os^{192} which is populated by K capture in Ir^{192} with 4.5% of the β-decay rate. The level scheme of Os^{192} is discussed by Baggerly and by Shiel et al. (68).

The absolute conversion coefficients of the γ-transitions may be calculated from Table 17. The total conversion coefficient is $\alpha = N_e/N_q$ while the K- and L-shell conversion coefficients may be calculated from the absolute intensities of the K and L conversion lines given in Table 14. The experimental K conversion coefficient α_K for the 316 kev transition is $\alpha_K = 0.039 \pm 0.008$. The 316 kev transition is known to be a pure E2 transition between the ground

Table 17.

Transition energy kev	Photon Intensity N_γ ($\times 10^{-3}$)			Total electron intensity Ne ($\times 10^{-3}$)	Transition intensity $N_e + N_\gamma$ ($\times 10^{-3}$)
	Baggerly	Johns	Mean		
136	1.6	29	15	-	15
173	-	9	(9)	-	9
201 (Os)	4	9	6	3.0	9
205 (Os)	34	39	36	8.1	44
283 (Os)	5	11	8	-	8
295	312	294	303	24.6	328
308	303	312	307	23.7	331
316	866	866	866	53.3	919
375 (Os)	16	5	10	-	10
417	14	-	(14)	-	14
440	-	5	(5)	-	5
468	554	641	598	11.5	610
485 (Os)	34	61	47	0.3	47
588	61	72	67	0.4	67
604	121	113	117	1.1	118
613	73	87	80	0.5	81
745	-	0.5	(0.5)	-	0.5
785	0.9	0.5	0.7	-	0.7
885	4	10	7	0.015	7
1060 (Os)	0.4	1.7	1	-	1
1157	-	0.9	(1)	-	1

and first excited states of an even-even nucleus (see Table 16); the theoretical K conversion coefficients for an E2 transition are $\alpha_K = 0.055$ and $\alpha_K = 0.054$ according to the values of Rose (66) and Sliv (67) respectively. It is concluded that the theoretical K conversion coefficients are 40% too high for this E2 transition. Such deviations from Rose's theoretical values are well known for M1 transitions but have not been reported previously for E2 transitions.

The total transition intensities may be calculated from the absolute electron intensities and the theoretical conversion coefficients. In the present case the sum of the 316 and 613 kev transition intensities, which populate the ground state, only accounts for 75% of the β-disintegration rate if the theoretical conversion coefficients are used. The unreliability of the theoretical coefficients leads to the choice of the sum of the experimental photon and electron intensities for the total transition intensities quoted in Table 17.

3.2. The detailed transition intensity balance at the energy levels of Pt^{192}.

The principal energy levels in Pt^{192} have been well established from the γ-ray energies and γ-γ coincidence measurements of previous investigations (11, 13, 14, 17). The simplified level scheme is

shown in Fig. 17 and the full scheme in Fig. 18.

The absolute intensities of the γ-transitions may be determined from the balance at each energy level of the absolute β- and relative γ-intensities of the principal transitions. The relative photon intensities reported for adjacent lines are unlikely to be so liable to error as the relative intensities for lines differing considerably in energy. The relative intensities for the lines comprising the 300 and 600 kev groups are deduced from the data of Baggerly and of Johns in terms of the 316 and 613 kev transitions which populate the ground state A with an absolute intensity of 1000. No β-transitions are observed to levels A, B and C so that the γ-transition intensities must balance at levels B and C. If the 885 kev transition is assumed to be comparatively weak then the absolute intensities of all the lines of the 300 and 600 kev groups follow. In principle the complete intensity scheme can be deduced for the stronger transitions since many of the γ-transitions are very weak. In practice the disagreements in the reported values of the relative photon intensities for the 296 and 308 kev transitions allow only approximate values of the absolute transition intensities to be calculated; these agree within the limits of the estimated error with the experimental β- and γ-transition intensities.

The balance of the experimental transition intensities is shown in Fig. 17 for the energy levels of Pt^{192}; the mean photon intensities of Baggerly and of Johns have been used. There are serious discrepancies in the intensity balance at the D and G levels.

(i) The 784.5 kev (D) level is populated almost entirely by the 550 kev β-transition whose absolute intensity has been determined as 425 ($\times 10^{-3}$), see Table 13. The level is de-excited by two γ-rays one of which, the 172 kev, is definitely very weak. The principal de-excitation mode is the 468 kev γ-transition for which an intensity value of 653 or 566 may be deduced from the results of ~~Baggerly~~ Johns and ~~Johns~~ Baggerly respectively. Neither of the reported 468 kev photon intensities is consistent with the measured β-transition intensity which is the mean of several values; even if the 270 kev β-transition is halved in intensity the resultant population rate is only 470. It may be further seen that the incoming intensity at level B, populated by the 468 kev transition, is greater than the single outgoing 316 kev transition. The intensity of the 316 kev transition follows directly from the ratio of the observed relative intensity of the 613 and 316 kev γ-rays; the difference in the values reported for the ratio does not affect the intensity assigned to the 316 kev transition to any great extent.

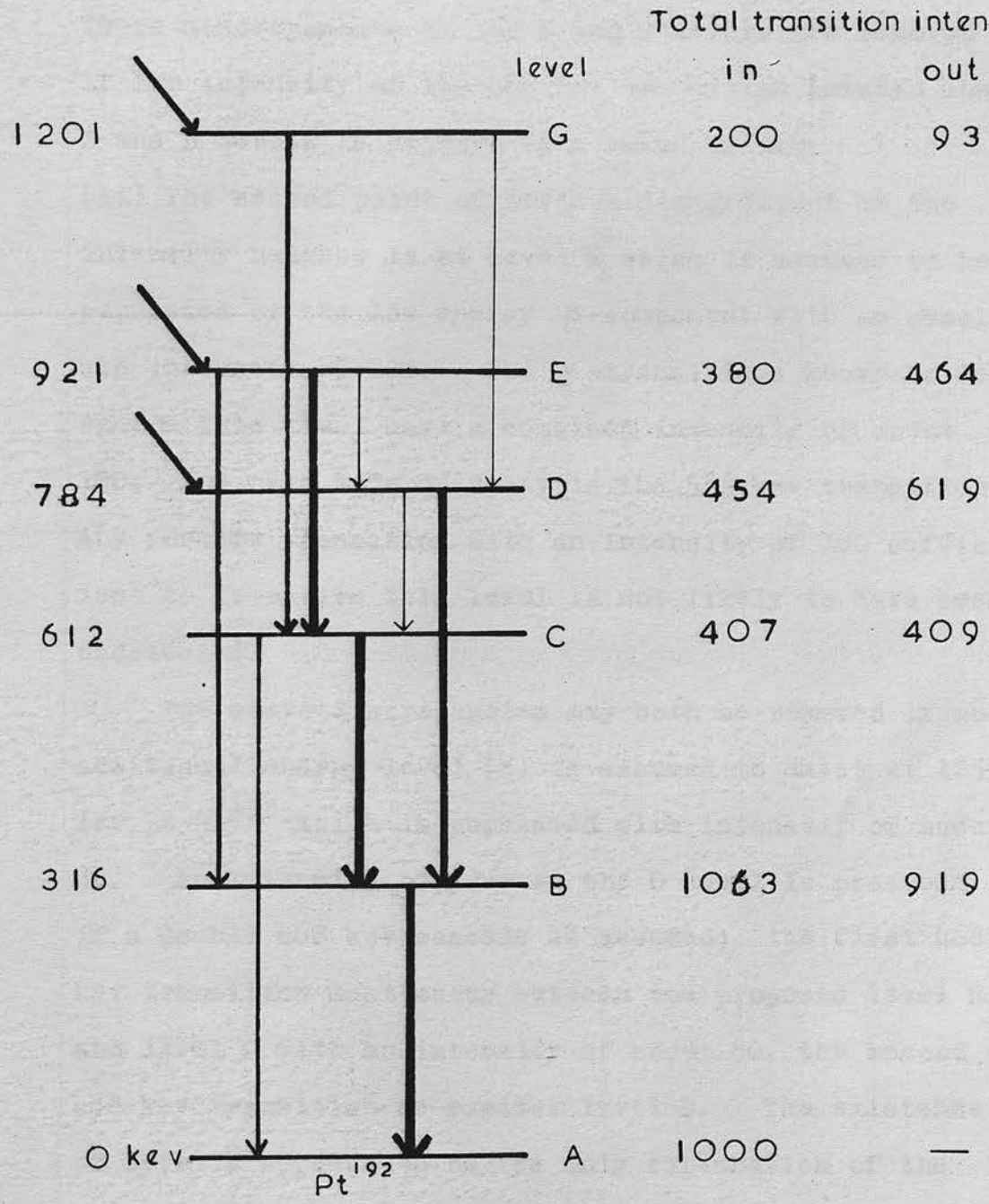

Figure 17. Simplified Pt^{192} level scheme showing the balance of the β-and γ-transitions at the levels.

These discrepancies at the B and D levels are removed if the intensity of the 468 kev transition between the B and D levels is reduced by a value of 160.

(ii) The second point of serious disagreement in the intensity balance is at level $\overset{G}{\chi}$ which is assumed to be populated by the low energy β-component with an absolute intensity of 200. The γ-transitions known to de-excite this level have a combined intensity of about 100; the main mode of decay is the 588 kev transition. Any further transition with an intensity of 100 sufficient to de-excite this level is not likely to have been undetected.

The above discrepancies may both be removed if an additional energy level (H) is assumed to exist at 1253 kev in Pt^{192} which is populated with intensity of about 80. An intensity balance at the D level is possible if a double 468 kev cascade is assumed; the first 468 kev transition must occur between the proposed level H and level D with an intensity of about 80, the second 468 kev transition de-excites level D. The existence of level H appears to be the only explanation of the reported β- and γ-transition intensities but can only be tentatively proposed at present.

A conclusive re-determination of the β-spectrum with the spectrometer requires much thinner, and therefore weaker, sources than have been used in the present

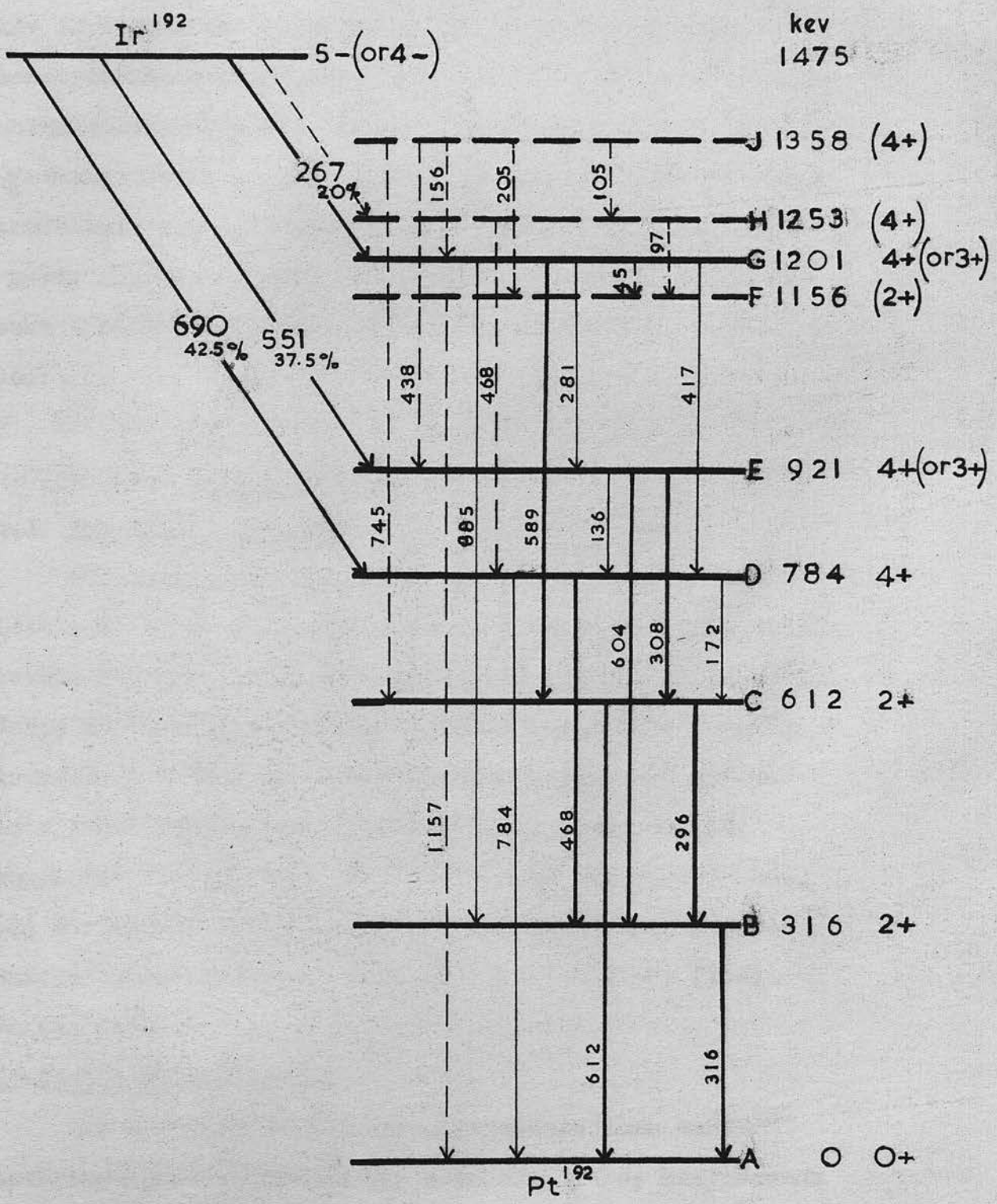

Figure 18. Proposed β-disintegration scheme of Ir^{192}.

investigation. Alternatively the existence of the 1253 kev level may be investigated by β-γ coincidence measurements on the spectrum. The existence of genuine coincidences between conversion electrons of the 468 kev γ-transition with photons of the same transition energy would establish the existence of level H and the double γ-ray cascade. The conversion of the spectrometer for such a coincidence experiment is described in Chapter 10.

4. The level scheme of Pt^{192}.

4.1. The energy levels.

The proposed level scheme is shown in Fig. 18. Levels A, B, C, D, E and G are well established while levels F and J have been proposed by Pringle et al. (14), Johns and Nablo (11) and Baggerly et al. (17); the existence of a 1456 kev level has been suggested by Huq in a recent paper (69). The present work, see §3, suggests the existence of a previously unreported level (H) at 1253 kev; the evidence for this level is discussed below, together with that for the other levels in the scheme.

Levels B, C, D, E and G.

The energies of the stronger transitions in Pt^{192} have been deduced accurately from the γ-ray measurements of Muller et al. (15), Ryde and Andersson (16) and Johns

and Nablo (11) and confirm the results of early workers, notably Cork (18) who proposed the level scheme of Fig. 17. Muller showed that the measured energy differences allow only two possible schemes and Roulston and Pringle (14) showed that Cork's scheme was correct by γ-γ coincidence measurements; this has been confirmed by later workers. The β- and γ-intensity measurements are largely in agreement with this scheme with the possible exception of the 468 kev γ-transition as discussed in §3.2. The spins and parities of the levels will be discussed in § 4.2.

Level J.

The 1358 kev level was tentatively proposed by Roulston and Pringle on the basis of coincidences observed between the 885 and 156 kev γ-rays and the report of weak 156 and 438 kev γ-rays by Cork. The assignment of the latter γ-rays to Pt^{192} is confirmed by their detection by Ewan and Thompson (20), and more recently by Huq (69), in the electron capture decay of Au^{192} to Pt^{192}. Johns and Nablo have observed 440 and 745 kev γ-transitions which correspond to the JE and JC energy differences.

Level F.

The 1156 kev level was proposed by Johns and Nablo who observed the weak cross-over transition to the ground state; it is also present in Au^{192} decay (20,68)

together with the 205 kev γ-ray, which is also assigned to Os^{192} but is here interpreted as the JF transition.

Level H.

The existence of level H is suggested by the strong intensities of the 468 kev γ-transition and the low energy β-transition. If the 468 kev γ-ray is in coincidence with itself then it must originate at a 1253 kev level which is assumed to be populated by part of the low energy β-component. Additional evidence for the existence of this level is provided by measurements on the conversion lines of Pt^{192} observed by Huq (69) in Au^{192} electron capture decay using an 180^{o} magnetic spectrograph. Huq finds γ-rays of 45, 97, 105 and 167 kev which find no place in the published decay schemes and cannot be attributed to Auger electrons. The 45 kev transition is probably between levels G and F; a level near 1456 kev is suggested by Huq but cannot account for both the 97 and 105 kev transitions. These transitions fit into the present scheme as HF and JF. No place is found for the 167 kev γ-ray unless it corresponds to the transition DC that is not otherwise observed by Huq.

4.2. The spins and parities of the energy levels.

Level A.

Pt^{192} is an even-even nucleus and the spin of the ground state is assumed to be 0, with even parity.

Level B.

Level B decays to the ground by the 316 kev transition which is pure electric quadrupole (E2), see Table 16. The assignment is unambiguously 2 +, as expected for the first excited state of an even-even nucleus.

Level C.

The K:L ratio shows the 600 kev group to be principally E2. The 612 kev transition, CA, to a state of spin 0 can have no admixture and is assumed to be pure E2; it follows that level C is 2 +. The transition CB between these 2 + levels has very little M1 admixture.

Level D.

The spin of this level must be greater than 2 since it is fed by the strongest β-component while there are no β-transitions to the lower levels with spins 0 and 2. Taylor and Pringle (21) report that in order to give the observed γ-γ angular correlation the 3 + assignment requires a 94% M1 admixture for the 468 kev transition, which is not consistent with the present conversion electron data; their alternative assignment of 4 + is confirmed by the work of Baggerly et al. (17) and of Kelly and Wiedenbeck (70). Johns and Nablo (11) claim to have detected the 784 kev cross-over to the ground state which can only be an E4 transition.

Level E.

The β-transitions to level D and level E are both of the same type, first forbidden, so that these levels are expected to have spins which differ by no more than one unit. Johns and Nablo have failed to observe the 921 kev cross-over transition, EA, so the spin of level E must be at least 3 while the E2 nature of the 308 kev transition to the 2 + level C limits the spin of level E to 4 + or less. Several workers have performed angular correlation experiments in order to decide between the possible 3 + and 4 + assignments but the presence of interfering cascades involves corrections which assume the intensity values for the γ-rays. Taylor and Pringle assumed only the intensities of the 300 kev group and report that only a spin of 4 is consistent with their results. Shiel et al. (68) disagree with this assignment on the basis of angular correlations of the 604-316 cascade which, after corrections for the interference of other cascades, are only consistent with a spin of 3; a similar experiment by Mraz(71) confirms the earlier value of 4.

Level G.

The principal transition from this level is to level C, which is known to have a spin of 2. The 588 kev γ-ray is E2, with possibly some M1 admixture, leading to the assignment of 4 + (or 3 +) for level G.

Contrary assignments are proposed by Baggerly (spin 4) and Shiel (spin 3) from angular correlations of the 588-613 kev cascade. Level G is populated by a first forbidden β-transition as are levels D and E which have been assigned a spin of 4 +; thus G is restricted to 3 +, 4 + or 5 +, with 4 + the most probable value.

The ground state spin of Ir^{192}.

Before considering the levels F, H and J the ground state of Ir^{192} will be discussed.

The spin and parity of Ir^{192} are only known from the nature of the β-transitions. There are no transitions to the lower 0 + and 2 + levels in Pt^{192} while those to levels D and E, assigned as 4 +, have log ft values of 8.6 and 8.3 respectively. The values for first forbidden transitions are usually in the range 6-8 so that the choice of first forbidden $\Delta I = 1$ (yes) is preferred to the alternative first forbidden $\Delta I = 0$ (yes), which is expected to have a lower log ft value; it follows that the ground state spin of Ir^{192} is 5 -, or possibly 4 -.

Ir^{192} lies outside the closed-shell region and if the nuclear shape is deformed there is the possibility of additional K-selection rules operating to hinder some of the transitions, cf. Chapter 2 §2. The K-values of the ground states are equal to their respective spins while for other levels K may be less than

or equal to the spin value; the degree of K-forbiddenness of a transition is K - L, where L is the multipolarity. If the spin of Ir^{192} is 5 then the β-transitions to levels D and E are forbidden by the K selection rules, which would account for the high log ft values. A ground state spin of 4 is also possible with transitions to levels D and E that are K-forbidden if their K-values are less than 4. The extent to which K is a good quantum number in this region of the periodic table is uncertain but the absence of rotational levels in the Pt^{192} nucleus suggests that the influence of the K selection rules should be small; the choice of 5 - for Ir^{192} is therefore preferred.

Levels F, J and H.

The γ-rays associated with these levels are of low intensity, with the possible exception of the transition HD. The multipole orders of some of the γ-transitions are not definitely established so that only tentative assignments can be made of the spins and parities of these levels.

There is no β-transition to level F which implies a spin of less than 4 for this level if the spin of Ir^{192} is 5. The only γ-transition observed from this level is the cross-over FA to the 0 + ground state which was detected by Johns and Nablo requiring a spin of 2 (or 1) for level F.

Part of the low energy β-component is assumed to populate level H, suggesting a spin of 4 or 5 since the transition is first forbidden. The level is excited by the E2 (+ M1) transition HD to a 4 + level so that H must have even parity; if Huq's assignment of E2 with possible M1 admixture is correct for HF then level H is 4 +, level F is 2 +, the transition HF being pure E2.

In the present decay scheme level J is de-excited by three weak γ-rays. The β-transition to this level must be at least first forbidden, a population rate of $1\frac{1}{2}\%$ corresponding to a log ft value of 7.5; this level is therefore taken to be 4 +. The 205 kev transition JF is pure E2 while the 156 kev transition JG is M1 both consistent with the assignment of Huq but his assignments of M3 for transition GF and M2 for JH are not consistent with the present scheme.

Chapter 8.

THE β-SPECTRUM OF NEPTUNIUM-239.

1. Introduction.

The purpose of the present investigation of the β-spectrum of Np^{239} is to utilise the high collecting power of the spectrometer in the careful determination of the partial end-points of the continuous spectrum. The intensities reported for the higher energy end-points cannot be explained by the Bohr-Mottelson nuclear model if the measured values of the ground state spins are accepted, while the reported existence of an intense low energy β-component involves theoretical difficulties and finds no confirmation from γ-ray studies.

The work has been carried out using sources of high specific activity and low solid content mounted on very thin source backings. A correction has been determined for the loss of efficiency of the detector below 100 kev. In view of the short half-life of 2.3 days for Np^{239} the observations of the spectrum were taken, where possible, continuously 'round the clock'.

2. The preparation of the sources.

The Np^{239} source material was prepared by A.W.R.E., Aldermaston by ion exchange following the neutron

irradiation of U^{238}. It was supplied in the form of 0.2 mℓ of active solution containing about 5 mc of active Np^{239} with a total solid content of less than 10 μg. Sources were prepared by evaporating drops of active solution to dryness on a supporting film of V.Y.N.S. resin of 2 $\mu g/cm.^2$ thickness on to which a conducting gold film of similar thickness had previously been evaporated. The active regions of these sources were barely visible against the supporting film. The radiochemical purity of the source material was confirmed by following the decay of each supply of material for seven half-lives. No sign of longer-lived radiations was found and the mean value found for the half-life was 2.34 ± 0.02 days, in good agreement with the recent determination of 2.346 days by Wish (72).

3. Preliminary measurements of the β-spectrum.

Two thin sources were prepared from the first supply of Np^{239} source material; the first, 2 mm. in diameter, was used for examining the low energy region and the second, 3 mm. in diameter, was used for runs on the high energy end-points. The weaker source was first used for a detailed run on the spectrum which below 300 kev has a large number of conversion lines superimposed on the continuum. The source was found

to be too weak for observations to be made on the high energy region above 500 kev where the genuine electron counting rate fell below that due to the photomultiplier noise. A second run on the low energy region was interrupted by the partial failure of the scaler and amplifier in the detector system. Subsequently two runs were made over the high energy region with the 3 mm. diameter source. The noise level was reduced by decreasing the photomultiplier volts so that only the higher energy electrons were on the plateau and recorded with full efficiency. The source activity was found to be rather low, two half-lives having elapsed since its preparation, and detailed observations were not made on these two runs. They were however subjected to Fermi analysis and the results, which are no more than approximate, are shown in Table 18.

Table 18.

Run	First partial kev	Second partial kev	Third partial kev	Fourth partial kev	Ratio of intensities
1	722 ± 10	660 ± 10	437 ± 10	405	7:13:100:30
2	723 ± 10	661 ± 10	441 ± 10	-	9:13:100:-

There is considerable uncertainty as to the correct separation of the first partial because only a few of

the observed points could definitely be assigned to it; any error in the end-point and relative intensity of the first partial will introduce some error in the values found for the second partial but may be lessened in the case of the third partial by reason of its greater intensity.

4. The continuous β-spectrum of Np^{239}.

The high energy region of the β-spectrum was recorded with a 3 mm. diameter source of strength about 200 μc prepared from a second supply of active solution. The region above 290 kev contains no observable conversion lines so that the reduced resolution of the instrument was not very important. Two careful runs were made and by Fermi analysis of the data five partial β-components were identified. The values of the end-points and the corresponding relative intensities are given in Table 19. The Fermi plots for one of these runs (run 4) are shown in Figures 19a and 19b.

Table 19.

Run	First partial kev	Second partial kev	Third partial kev	Fourth partial kev	Fifth partial kev
3	713.4 (6.1%)	653.8 (4.4%)	436.4 (46.5%)	396.6 (12.4%)	330.9 (30.6%)
4	712.1 (7.0%)	653.5 (3.5%)	437.1 (49.7%)	390.2 (14.5%)	333.3 (25.3%)

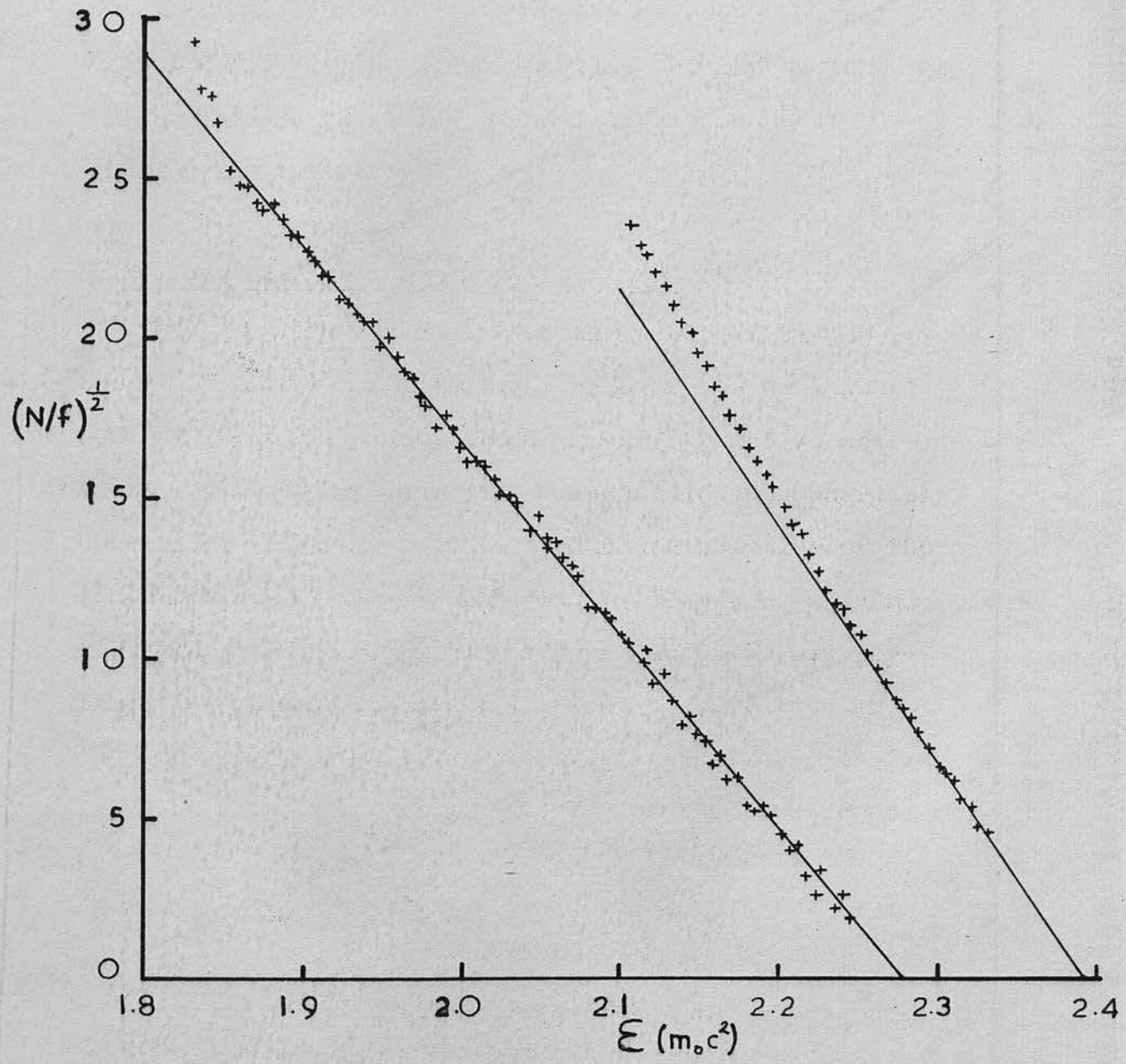

Figure 19a. Fermi plot of Np^{239} decay (first and second partials).

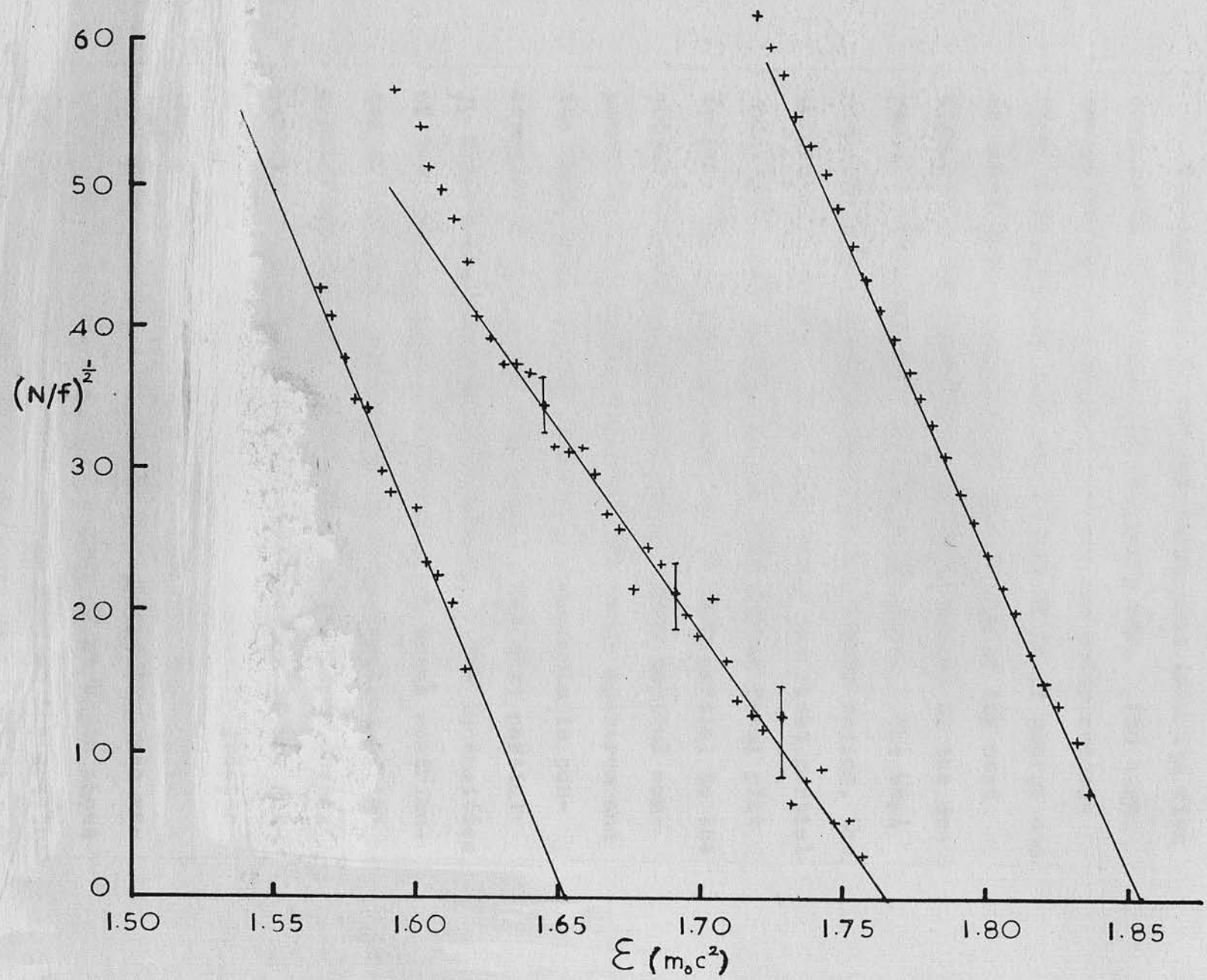

Figure 19b. Fermi plot of Np^{239} decay (third fourth and fifth partials).

The analysis of the raw Fermi plot into its five components is done in the following way. The high energy region of the plot is free fom contributions from β-components with end-points of lower energy and is therefore linear down to the energy of the next highest partial end-point, which is marked by the departure from linearity of the Fermi plot. The best straight line is calculated for the linear region, the intercept with the energy axis being the first partial end-point. By extrapolating this linear Fermi plot to zero energy the contribution of this partial to the complete spectrum is calculated. This partial component is then subtracted from the whole spectrum and the Fermi plot for the remaining components is constructed from the new continuum. The next partial β-component is separated similarly. The intensities of the β-components are the relative areas contributed to the whole continuous momentum spectrum by the partial components. The errors in the lower energy partial components, after the subtraction of the contributions of other partials, are relatively greater than in the higher energy partials.

The low energy region of the β-spectrum was recorded with a 2 mm. diameter source of strength about 100 μc. The low and high energy runs on the spectrum were normalised on to each other and it was found that

the abundance of low energy conversion lines obscured the continuum except in the region of 110 kev. The continuous spectrum corresponding to the five partial β-components was subtracted from the spectrum and showed that the resolution of the spectrometer had not been good enough to separate most of the conversion lines. It is possible to obtain a moderately linear Fermi plot from points at 15, 60 and 70 kev which appeared to be clear of conversion lines. Such a partial spectrum would have a high energy end-point at 90 kev and an intensity of about 25% of the whole spectrum. If the low energy region observed in the preliminary measurements of the spectrum is used (see §3) an upper limit is set to this low energy partial of 18% of the complete continuum.

In the region below 100 kev there are intense Auger lines as well as the conversion lines of five γ-rays with energies in the narrow range of 44-68 kev. It is therefore doubtful if the true level of the continuum was observed at all below 100 kev. It seems probable that there is no low energy β-component of appreciable intensity, the observed electrons belonging to unresolved conversion lines and Auger lines. The difference in the estimated intensities of such a component may be due to differences in the detector efficiency corrections applied over this region in the

two cases.

5. The conversion lines of the β-spectrum.

The energies of the conversion lines are in good agreement with those found by other workers (32, 33).

The absolute intensities of those strong conversion lines with electron energies greater than 70 kev were measured and are given in Table 20. The lines were not completely resolved and the base observed to the lines is not the true one, being raised above the level of the continuum. The groups of lines were split up empirically to give component lines with the correct line profile whose addition gives the observed line-shape. In the case of the L and M conversion lines of the 210 and 228 kev γ-rays this was not sufficient. The 228L and 210M lines are coincident and the relative contributions to the observed line intensity were calculated on the following assumption. Newton (38) has shown that the M + N:L conversion ratio for most types of transitions is about 0.3, as in confirmed by the intensities of the 278 kev conversion lines. The intensities of the 210L and 228(M + N) conversion lines were calculated from the observed intensities of the 210(M + N) and 228L lines so as to be as far as possible consistent with the expected ratio.

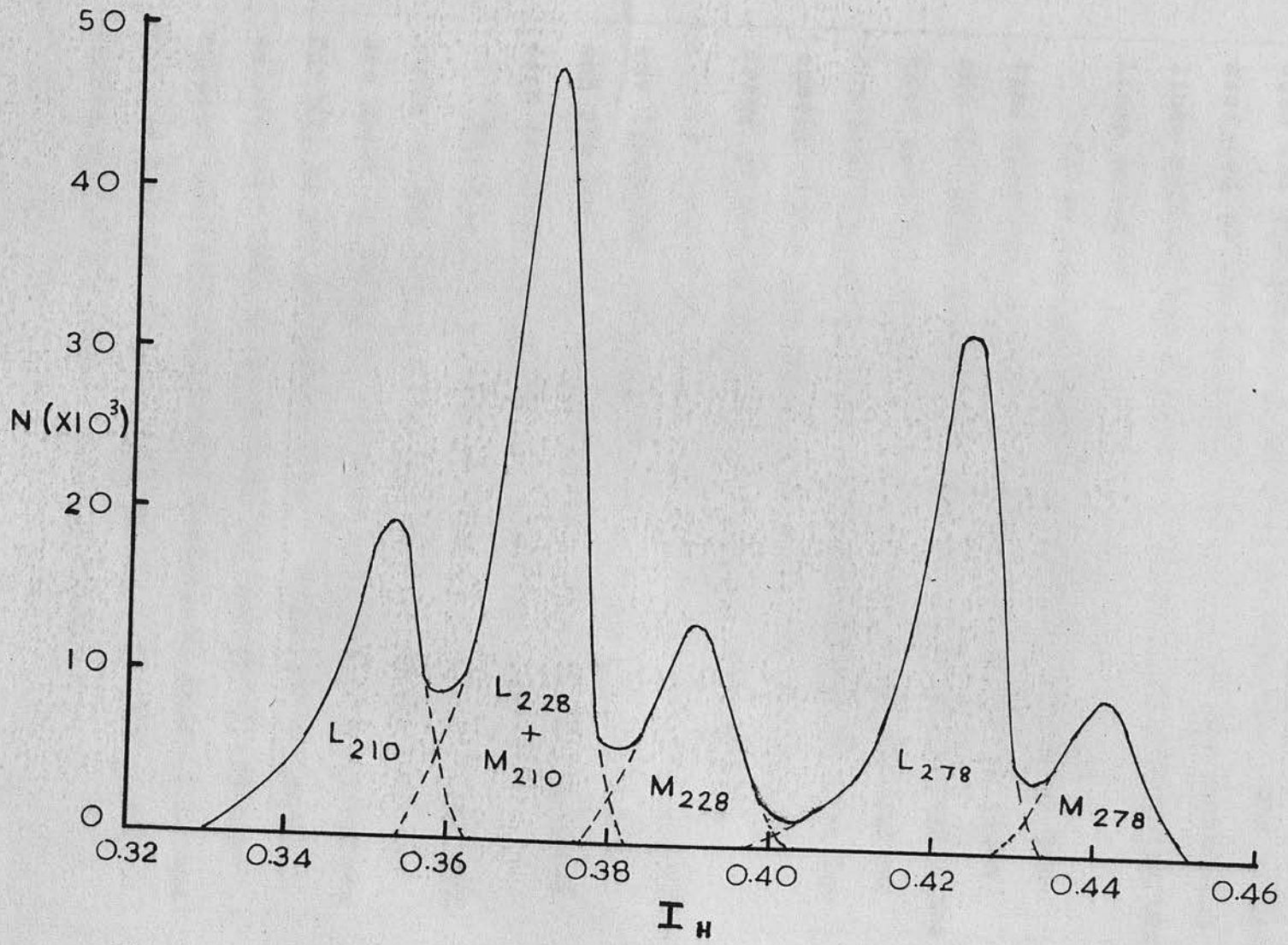

Figure 20. The L and M conversion lines of the 210, 228 and 278 kev γ-rays in Np^{239} decay.

The composite profile for this group of lines is shown, with the continuum subtracted, in Fig. 20. The errors assigned to the absolute intensities of the conversion lines reflect the relative uncertainties with which the lines could be separated.

It is assumed that the possible low energy partial spectrum is due to unresolved conversion lines and the intensities of groups of these low energy lines have been calculated on this basis. The correction for detector efficiency increases rapidly in this low energy region and may be the cause of considerable error in the intensities quoted for these groups.

It should be noted that the very weak 226 and 273 kev lines are included in the intensities of the 228 and 278 kev lines respectively. No conversion lines were observed in the region above 300 kev.

The K:L ratios were calculated for the conversion lines of the 278, 228 and 210 kev γ-transitions and are shown in Table 21 together with theoretical values for M1, E1 and E2 transitions. These theoretical values have been derived from the values of the conversion coefficients for the K-shell of Sliv (67), and for the L-shell of Rose (66) and in both cases are corrected for the finite nuclear size.

Table 20.

Assignment of conversion line		Absolute intensity %
Transition energy kev	Conversion shell	
300	-	< 0.1
278	M + N	1.3 ± 0.2
278	L	4.4 ± 0.3
228	M + N	1.8 ± 0.3
228	L	5.1 calc. } 5.9 ± 0.6
210	M + N	0.8 calc. }
210	L	2.4 ± 0.3
278	K	16.8 ± 0.2
228	K	17.3 ± 2
106	M + N	2.4 ± 2
210	K	7.5 ± 2
106	L	4.8 ± 2
44	L	} 13.4
49	$L_{I,II}$	}
49	L_{III}	} 14.1
57	$L_{I,II}$	}
49	M + N	} 16.4
57	L_{III} + M + N	}
61	L + M + N	}
68	L + M + N	}

Table 21.

Transition energy kev	K:L ratio (expt.)	Theoretical K:L ratio			E2 admixture for M1 assignment
		E1	M1	E2	
210	3.1 ± 1	4.8	4.1	0.32	25%
228	3.4 ± 0.6	4.8	4.1	0.43	20%
278	3.8 ± 0.3	4.8	4.1	0.66	10%

The K:L ratios, with the measured lifetime of 1.1×10^{-9} sec. (26) for the 286 kev level from which these γ-rays originate, lead to the assignment of magnetic dipole for these γ-rays, with some electric quadrupole admixture. This confirms the results of several previous workers (32, 33 and 37). The internal conversion coefficients of these three γ-rays have recently been studied in detail with a momentum resolution of 0.35% by Ewan et al. (73), and it is concluded from the observed $L_I + L_{II}:L_{III}$ ratios that a limit of 10% should be placed on the E2 admixture for these radiations. The larger admixtures found here for two of the γ-rays are no doubt due to the inaccuracies in separating the overlapping conversion lines.

Chapter 9.

THE DISINTEGRATION SCHEME OF Np^{239}.

1. The end-points and intensities of the partial β-spectra.

The two runs over the complete continuous spectrum which were analysed fully (see Table 19) gave values of the end-points and intensities of the β-components which are in close agreement. The mean values for these runs is shown in Table 22 together with the corresponding log ft values calculated from the graphs of Feenberg and Trigg (62).

Table 22.

Partial spectrum	End-point energy kev	Δ kev	Relative intensity %	log ft
1	713	59 } 276	6½	8.4
2	654	217 }	4	8.4
3	437	44	48	6.8
4	393	61	13½	7.2
5	332		28	6.7

The preliminary end-point energies quoted in Table 18 agree approximately with those above; the relative intensities of the sum of the first and second partials to the third and fourth partials show very good

Table 23.

	First partial kev	Second partial kev	Third partial kev	Fourth partial kev	Fifth partial kev	Sixth partial kev
Graham and Bell	705 (7%)		435 (46%)		301 (47%)	
Tomlinson et al.	715	654	440		330 (38%)	
Freedman et al.	715 (4.8%)	655 (1.7%)	441 (31%)	380 (10%)	329 (52%)	
Baranov and Shlyagin	(723 +	655)(7%)	439 (21%)	382 (27%)	327 (45%)	
Hollander et al.	650 (5%)		440 (45%)		330 (45%)	212 (5%)
Present work	713 (6.5%)	654 (4%)	437 (48%)	393 (13.5%)	332 (28%)	

agreement. In Table 23 the results of the present work are compared with those of other investigators. The values quoted by Hollander et al. (33) are estimated from the γ-transition intensities calculated from conversion electron data. The intensity attributed to Tomlinson et al. (27) for the 330 kev β-partial is quoted by Engelkemeir and Magnusson (30).

It can be seen that the differences between the end-points of the present work agree well with the accurate energy values of the γ-transitions between the corresponding levels of the decay scheme of Fig. 3 proposed by Hollander et al. (33). The end-points quoted by other workers do not show such close agreement which suggests that the relative intensities found in the present work may be more accurate than previous determinations, for they will be sensitive to the faulty separation of partial components when the end-point energy differences involved are small. The intensities of the β-transitions are discussed below in terms of the energy levels of Pu^{239} proposed by Hollander et al. (33); the evidence for these levels is given in §3.

<u>The 332 kev β-transition.</u>

The present value of 0.28 for the fraction of disintegrations populating the 392 kev level in Pu^{239} is significantly lower than the intensities of 0.38,

0.52 and 0.45 reported by previous workers (see Table 23). Additional evidence as to the intensity of this β-component is provided by the results of Engelkemeir and Magnusson (30) who measured the 193 mμsec. lifetime of the 392 kev level. They deduced the rate of population of this level by β-decay in two ways.
(1) Conversion electron data of Fulbright was combined with the measured γ-ray and X-ray intensities to yield values for the total L conversion coefficients of 0.65 ± 0.25 and 0.23 for the 61 and 105 kev E1 transitions respectively. These compare only moderately well with the theoretical values 0.34 and 0.08 of Rose (66), corrected for finite nuclear size. From scintillation studies and the rate of growth of Pu^{239} α-activity it was deduced that the combined intensities of the 105 kev γ-ray and K X-rays is 0.89 per β-disintegration. This figure combined with their previous measurements yields a value of ca. 0.5 per disintegration for the population rate of the 392 kev level. The principal de-excitation mode is the 105 kev γ-transition for which the experimental and theoretical L conversion coefficients differ considerably. If the theoretical coefficient is used the population rate is reduced to ca. 0.4 per disintegration.
(2) A direct comparison of the delayed and prompt coincidence rates associated with the193 mμsec. level

leads to the value of 0.29 for the fraction of β-disintegrations populating this state. Correction for the estimated efficiencies lowers this result to ca. 0.2.

The first estimate of the population rate is in agreement with the values of other authors but appears more likely to be subject to error than the second value which is confirmed by the present work.

The 393 kev β-transition.

The β-component to the 330 kev level in Pu^{239} has been previously reported by Freedman et al. (28) and by Baranov and Shlyagin (32) with values of 10% and 27% respectively for the relative intensity; the end-point energies of 380 and 382 kev are not in good agreement with those expected from the energy differences in the level scheme. Hollander et al. find a rough balance of the estimated total γ-transition intensities at the 330 kev level so it is probable that the intensity of the β-transition is small. The present value of 13.5% confirms that of Freedman et al. and would appear to establish definitely the existence of this transition.

The 437 kev β-transition.

There is general agreement that $\sim$ 90% of the β-transitions have energies in the range 330-440 kev. The present work assigns an intensity of 48% for the

transition to the 1 mμsec. level at 286 kev in Pu^{239}. This is significantly more than that reported by Freedman and by Baranov and Shlyagin but is consistent with the work of Hollander et al. If the intensity of the 332 kev partial has been correctly assigned as 28% then the present assignment for the 437 kev partial is very probably also correct.

The 654 and 713 kev β-transitions.

The combined beta end-point energies have been used in conjunction with the precise values of the energy levels of Pu^{239} reported by Hollander to determine the levels populated by these transitions. The total disintegration energy Q_{β^-} of Np^{239} decay is the sum of the β- and γ-transition energies involved in the cascade to the ground state of Pu^{239} for each mode of β-decay. The mean value of Q_{β^-} is 719 $\pm$ 3 kev if the high energy β-transitions populate the 57 kev and ground states of Pu^{239}, see fig. 21. If the transitions are to the 76 and 8 kev levels the corresponding value is Q_{β^-} = 724 $\pm$ 1.5 kev. The reduced standard deviation leads to the choice of the latter mode of decay and determines the total disintegration energy value for Np^{239}. The β-component showing the greatest deviation from the end-point energy calculated for it from the γ-ray and Q_{β^-} energy values is the 654 kev feed which is expected to be 649 kev. It is

possible that there is some population of the lower 57 kev level separated by only 18 kev from the 75 kev level which receives most of this β-component.

The relative intensity found for these high energy transitions is somewhat greater than that reported by other workers, who used instruments of lower collecting power.

Possible low energy β-components.

The possibility of lower energy β-components was first mentioned by Tomlinson et al. (27) and the existence of a 70 kev β-component was tentatively reported by Baranov and Shlyagin (32). The latter workers assigned an intensity of 22% to this component from their measurements with thinner sources, an increased intensity being found for both the 70 and 327 kev feeds with thicker sources. Their proposed decay scheme, Fig. 22, shows this β-feed populating a 656 kev level in Pu^{239}. Such a β-transition would have a log ft value of 4.4 which is rather low for an allowed transition in this region of the periodic table. In the present work the possibility of a 90 kev transition could not be excluded owing to the masking of this region of the continuum by conversion lines; the possible intensity of up to 20% would give rise to quite strong γ-rays and conversion electron lines which are not observed. The total absolute

intensity of all lines in the region 17.5-67 kev reported by Hollander et al. and by Baranov and Shlyagin, has been compared with the intensity for the corresponding region in the present work, which is to be divided between conversion lines and the possible low energy partial. The three values agree closely provided the contribution of Baranov and Shlyagin's low energy partial is ignored; there is rather poor agreement as to the detailed distribution of electrons in the region. Recent work by Connor (74) using a spectrometer with a 0.05% ~~resolving power~~ resolution has confirmed the multiplicity of the conversion lines in this region. There seems to be no definite evidence for the existence of a β-spectrum in addition.

2. The intensities of the 210, 228 and 278 kev γ-transitions.

The absolute intensities of the better resolved conversion lines have been presented in Table 20. The magnetic dipole nature of the 210, 228 and 278 kev γ-transitions is well established (see Table 21) and the total transition intensities have been calculated assuming the M1 nature of these radiations; the results are given in Table 24.

Table 24.

Transition energy kev	Total electron intensity N_e %	Total conversion coefficient K + L + M (M1)	Transition intensity $N_e + N_q$ (%)
210	10.7 ± 2.6	3.70	13.6 ± 3
228	24.2 ± 0.6	3.24	31.7 ± 4
278	22.5 ± 0.7	1.74	35.4 ± 1

The conversion coefficients are the theoretical values of Sliv (66) and Rose (67) for M1 transitions and are corrected for the finite size of the nucleus. The presence of some E2 admixture would increase the transition intensities. It will be observed that the three transitions, together with the two highest energy β-transitions populate the low lying band of levels in Pu^{239} with an intensity of 91 ± 8% of all β-disintegrations of Np^{239}. This is in good agreement with the low intensity (< 0.1%) of the conversion lines corresponding to higher energy γ-transitions.

3. The energy levels of Pu^{239}.

The decay scheme of Fulbright, see Chapter 2 Fig. 2, accommodates the principal γ-rays of Np^{239} decay. It is consistent with the observed beta end-points and with delayed coincidence measurements on the two

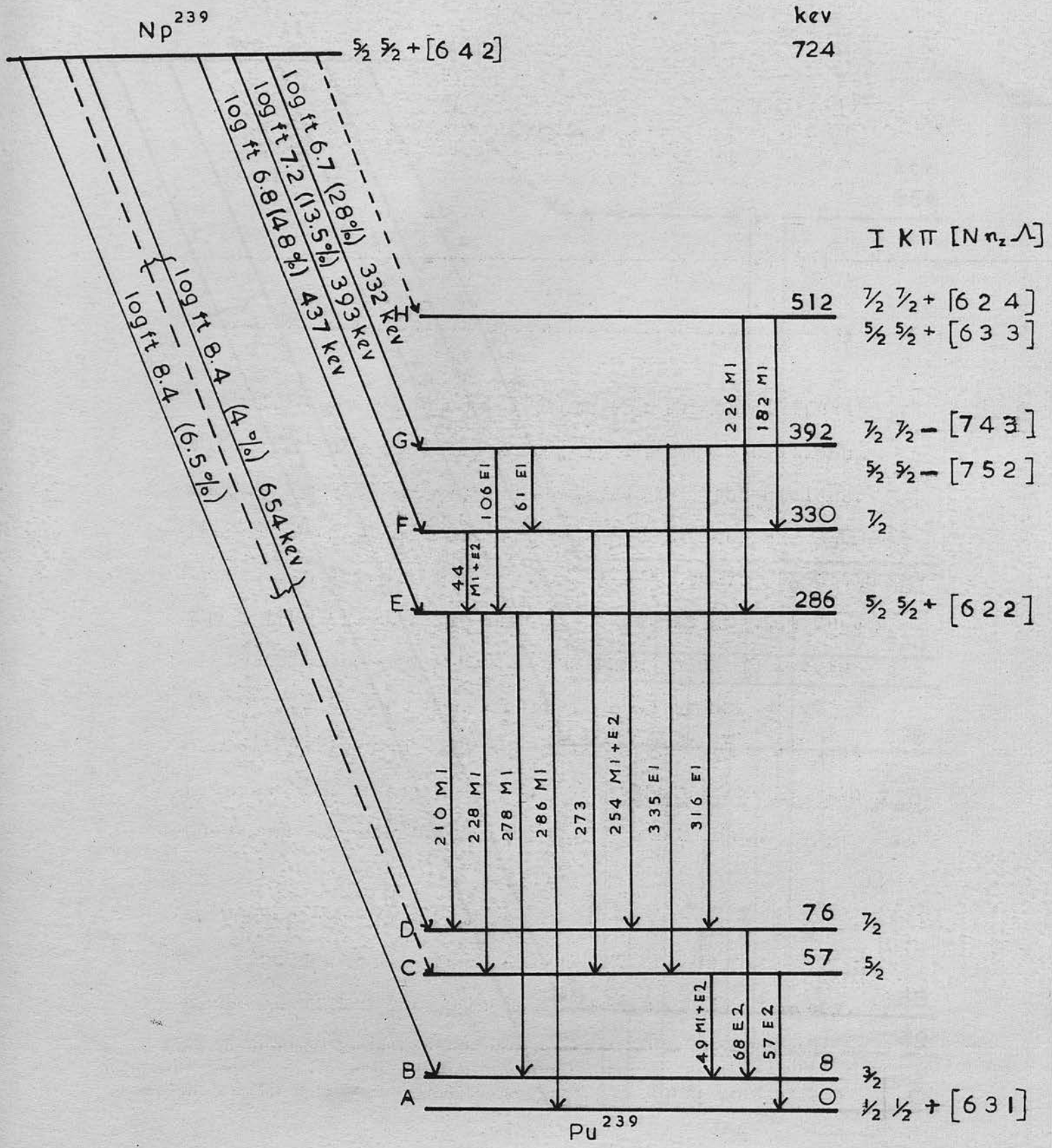

Figure 21. Disintegration scheme for Np^{239}

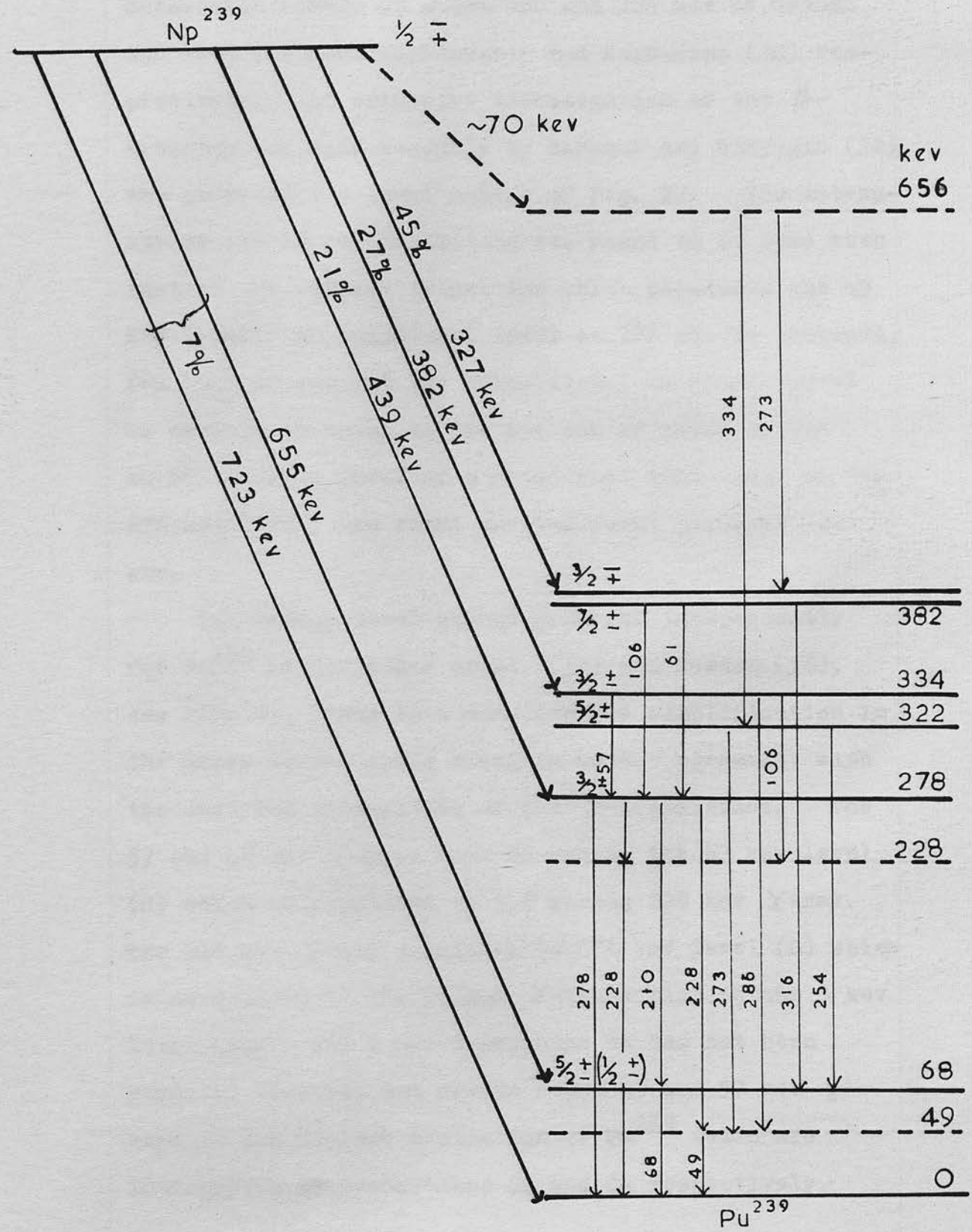

Figure 22. Decay scheme for Np^{239} by Baranov and Shlyagin.

metastable levels at about 280 and 385 kev by Graham and Bell (26) and Engelkemeir and Magnusson (30) respectively. An extensive investigation of the β-spectrum was made recently by Baranov and Shlyagin (32) who proposed the level scheme of Fig. 22. The intensity of the 49 kev transition was found to be less than that of the 228 kev transition which populates the 49 kev level; an additional level at 228 kev is proposed, fed by a second 106 kev transition. A double level is assumed to exist at 384 kev one of which is the second excited level of a rotational band based on the 278 kev level, the first excited level being at 322 kev.

The energy level scheme proposed independently for Pu^{239} by Hollander et al. (33) and Newton (38), see Fig. 21, leads to a considerable simplification in the decay scheme while being in better agreement with the observed intensities of the γ-transitions. The 57 and 49 kev γ-rays both de-excite the 57 kev level (C) which is populated by the strong 228 kev γ-ray. The 210 kev γ-ray populates the 76 kev level (D) which is de-excited by the 68 kev γ-transition to the 8 kev level (B). The 8 kev transition BA has not been directly observed but Newton found 49 and 57 kev γ-rays in the Coulomb excitation of Pu^{239} which are interpreted as transitions CB and CA respectively.

The energies of levels A, B, C and D are consistent with their being members of a rotational band based on the ground state, see § 3.2.

Hollander et al. (33, 39) have deduced precise energy values for the γ-transitions from conversion electron data. The observed γ-rays fit well into a scheme having only four levels in addition to the ground state band discussed above. The 1.1 m μsec. level (E) of Graham and Bell (26) is at 286 kev; the 286 kev cross-over transition EA has been observed by Hollander and the strong 278, 228 and 210 kev γ-rays originate at this level. Level E is populated by the 437 kev β-transition and by 44 and 106 kev γ-transitions from levels F and G at 330 and 392 kev respectively. These levels are fed by the 393 kev and 332 kev β-transitions. The 392 kev level (G) is the 193 m μsec. of Engelkemeir and Magnusson (30) who observed the 106 and 61 kev transitions GE and GF. Two weak γ-rays of energies 182 and 226 kev were observed by Hollander and were shown by coincidence measurements to originate at a level (H) at 512 kev. Weak 440 and 490 kev γ-rays reported by Lefevre et al. (82) are probably the transitions HC and HB. Hollander et al. have determined the population rate of level H to be about one tenth that of level G; since the feed to level G is 28% that to level H is about

3% and was not observed due to the many conversion lines in this region.

The level scheme proposed by Hollander is based on the assumption of an unobserved level (B) at 8 kev. Nevertheless it explains the γ-ray energies very well and is in general agreement with the observed γ-ray intensities. The apparent disagreement with the β-transition intensities is discussed in § 4.

4. The spins and parities of the energy levels.

4.1. The ground state rotational band.

Hollander (33) and Newton (38) have proposed that levels A, B, C and D form a rotational band. The ground state spin of Pu^{239} has been measured by Bleaney et al. (34) and by van den Berg et al. (75) and found to be $\frac{1}{2}$. The 8 kev transition BA has not been observed but the 57 kev transition CA has been classified as E2 with very little M1 admixture by both Hollander and by Baranov and Shlyagin (32); level C is therefore $\frac{5}{2}$, or just possibly $\frac{3}{2}$, with the same parity as A. The transition CB is reported to be an M1-E2 admixture so that level B is probably $\frac{3}{2}$ with the same parity as C and A. The 68 kev transition DB is predominantly E2 so that a spin of $\frac{3}{2}$ for level B is consistent with spin $\frac{7}{2}$ for D. This spin sequence may be compared with that expected for this level spacing according to

the Bohr-Mottelson theory (35).

The ground state spin of an odd A nucleus has $I = K = \Lambda$, with the notation of Chapter 2 §2. The energies of the levels forming a rotational band are normally $E = \frac{\hbar^2}{2J} I(I + 1)$ where J is the effective moment of inertia. When $\Lambda = \frac{1}{2}$ the spin of the last odd particle is partially decoupled from the rotational motion and the energies of the levels are anomalous. They are given by

$$E = \frac{\hbar^2}{2J} \left[I(I + 1) + a(-1)^{I + \frac{1}{2}} (I + \tfrac{1}{2}) \right]$$

where 'a' is the decoupling parameter. The level sequence 0, 8 and 57 kev with spins $\frac{1}{2}$, $\frac{3}{2}$ and $\frac{5}{2}$ respectively, with the same parity, leads to a value of $a = -0.584$; the next level of the band is expected to be at 76 kev with spin $\frac{7}{2}$. This precise agreement with the theory provides strong evidence for the correctness of Hollander's level scheme.

4.2. The spin of Np^{239}.

The value of spin $\frac{1}{2}$ for the ground state of Np^{239}, reported by Conway and McLaughlin (36) and recently confirmed by Abraham et al., (41) and the values of the spins assigned to the rotational band are not consistent with the observed intensities of the partial β-spectra. No β-transition is observed to the ground state of Pu^{239} whereas such a transition should

be allowed or at most first forbidden; if the ground spins of Np^{239} and Pu^{239} are the same there is no possibility of explaining the retardation by invoking K selection rules. Furthermore the spin of level E follows as $\frac{5}{2}$, with the same parity as the ground state, from the M1 nature of the ED, EC and EB transitions, see Table 21. The β-transition to level E has a log ft value of 6.8 characteristic of an allowed hindered or first forbidden unhindered transition; if the spin of Np^{239} is $\frac{1}{2}$ this transition should be first forbidden with spin change 2 and a log ft value of at least 9. Similar difficulties arise in the assignment of spins and parities to levels F and G. Any attempt to alter the level scheme so as to be consistent with the reported spin of Np^{239} created as many difficulties as it removed; it was therefore concluded that both measurements of the Np^{239} are in error.

Since the close of the present investigation a new determination of the spin of Np^{239} has been reported by Hubbs and Marrus (76). The results of these workers are consistent, to an accuracy of one part in a thousand, with a value of $\frac{5}{2}$ for the ground state spin of Np^{239}, in agreement with the value proposed by Hollander et al.; there can be little doubt as to its correctness.

The β-transitions to the ground state rotational

band may now be explained by the normal, and K, selection rules; transitions are K-forbidden if $\Delta K > L$. The transition to level A is now second forbidden and has not been observed in the present work. The levels B and D are populated by allowed but K-forbidden transitions; there is some evidence, see §1, that the transition assigned to level D in part populates level C but this normally allowed transition is twice K-forbidden. Transitions to higher levels of the rotational band at 165 and 193 kev, with spins $\frac{9}{2}$ and $\frac{11}{2}$ respectively, are at least second forbidden and are not observed but there is evidence of weak feeds to them in the α-decay of Cm^{243} reported recently by Asaro et al. (77).

4.3. Other levels in Pu^{239}.

Level E has been assigned a spin of $\frac{5}{2}$, with even parity with respect to the ground state, on the basis of the M1 transitions to the $\frac{3}{2}$, $\frac{5}{2}$ and $\frac{7}{2}$ levels of the rotational band. The lifetime of this level has been measured as 1.1 mμsec. so that the partial lifetimes of the 210, 228 and 278 kev transitions are somewhat less than 10^{-8} sec. in each case. The single particle estimates for the lifetimes of M1 and E2 transitions of this energy are $\sim 10^{-12}$ and 10^{-9} sec. respectively (78); the predominantly M1 transitions from level E are therefore retarded by a factor of $\sim 10^{4}$. This may be explained as due to the

violation of the K selection rules if level E is the basic state of a rotational band with $K = \frac{5}{2}$.

Level F is mainly de-excited by the 44 kev transition to level E which is assigned as principally M1 by Hollander and by Baranov and Shlyagin; the spin of level F is thus $\frac{3}{2}$, $\frac{5}{2}$ or $\frac{7}{2}$. If the spin is $\frac{7}{2}$ then level F may be the first excited state of a normal rotational band based on level E. The energy difference of the E and F levels yields a value of $\frac{\hbar^2}{2J} = 6.38$ kev for the splitting constant which is quite close to the value of 6.25 for the ground state band. The second excited state for the $K = \frac{5}{2}$ band is expected to be at 388 kev. There is a level (G) conveniently situated at 392 kev but it is populated by a β-transition which is allowed or at most first forbidden ($\Delta I = 0$ or 1) while the transition to the 388 kev level is first or second forbidden ($\Delta I = 2$). Asaro et al. (77) report weak α-transitions to both the 388 and 392 kev levels which confirms the existence of the rotational band and the assignment of spin $\frac{7}{2}$ for the level F; the parity is again even with respect to level A.

The state at 392 kev, found by Engelkemeir and Magnusson (30) to have a mean lifetime of 193 mμsec., is level G; the 61 and 106 kev transitions to levels F and E are identified as E1 by their L conversion coefficients so that level G has spin $\frac{5}{2}$ or $\frac{7}{2}$ with odd

parity. Both of these E1 transitions are retarded by $\sim 10^5$ from the single neutron estimate and, since $\Delta K \leq L$, this cannot be explained as due to the violation of the K selection rules; a similar retardation for E1 transitions in Np^{237} is discussed by Strominger and Rasmussen (79) in terms of the asymptotic selection rules. The weak transitions GD and GC are K-forbidden and retarded by $\sim 10^9$. Asaro et al. (77) find a weak α-transition to a level at 434 kev which it is possible to interpret as the first state of a rotational band based on level G; the splitting constant for such a band would be 6.0 or 4.7 kev according as the spin of level G is $\frac{5}{2}$ or $\frac{7}{2}$. The higher spin cannot be excluded as a reduction of $\frac{\hbar^2}{2J}$ is associated with a change of parity in Th^{228}, Ra^{224} and Ra^{226}.

The 182 and 226 kev transitions from level H to levels F and E have been studied by Smith et al. (39) in the electron capture of Am^{239}. They are assigned as M1, with E2 admixture, so that the spin of level H is $\frac{5}{2}$ or $\frac{7}{2}$, with even parity.

5. <u>The interpretation of the observed log ft values by the asymptotic selection rules</u>.

The assignment of $\frac{5}{2}$ for the spin of Np^{239} removes the more serious discrepancies between the observed log ft values and the level assignments of §4 but certain anomalies remain. The retardation of the allowed transitions to the ground state rotational band is expected, owing to the violation of the K selection

rules, but log ft values of 8.4 are still rather high. Although β-transitions observed to the higher levels in Pu^{239} are not K-forbidden nevertheless the log ft values of the two allowed transitions are greater than that of the nearby first forbidden transition. Hollander (40) has pointed out that considerable progress can be made in the interpretation of the log ft values by the use of the asymptotic selection rules and the Nilsson diagram (80); the relevant portion of the diagram is published by Hollander (40).

In the case of strongly deformed nuclei the nuclear motion may be separated into collective and intrinsic modes. The binding states are described by the quantum numbers N, n_z, Λ and Ω_Λ (see page 16) where N is the principal quantum number of the oscillator and n_z and Λ are respectively the components of N and the particle's orbital angular momentum (ℓ) along the symmetry axis. The order of the symbols assigned to the levels on Fig. 22 is $I\ K\ \pi\ [N\ n_z\ \Lambda]$ where I and K have the usual meaning and π is the parity. Selection rules for transitions between the levels have been given by Alaga (81); transitions are "unhindered" if they satisfy the following rules:-

Allowed transitions ($\Delta I = 0, \pm 1$ no)

$\Delta N = 0 \qquad \Delta n_z = 0 \qquad \Delta\Lambda = 0$

First forbidden transitions ($\Delta I = 0, \pm 1$ yes)

$\Delta N = 1 \quad \Delta n_z = 1 \quad \Delta \Lambda = 0$

$\Delta N = 1 \quad \Delta n_z = 0 \quad \Delta \Lambda = 1$

First forbidden transitions ($\Delta I = 2$, yes)

$\Delta N = 1 \quad \Delta n_z = 0 \quad \Delta \Lambda = 1$

In the Nilsson diagram (40, 80) the intrinsic energy levels are plotted as a function of the prolate deformation, which is taken to be $\eta = +5$ for Pu^{239} by comparison with the value for Np^{237} deduced from the quadrupole moment measured by Newton (38). In the region of 19 neutrons above the 126 neutron shell, counting two particles per level, there is only one state with spin $\frac{1}{2}$ which can represent the ground state of Pu^{239}; the state is characterised by $\frac{1}{2}\ \frac{1}{2}+\ [6\ 3\ 1]$ and indicates that the levels of Pu^{239} have even parity except for level G. The nearby even parity state $\frac{5}{2}\ \frac{5}{2}+\ [6\ 2\ 2]$ is probably the next intrinsic level at 286 kev. Counting up to 13 protons above the 82 proton shell gives a state for Np^{239} characterised by $\frac{5}{2}\ \frac{5}{2}+\ 6\ 4\ 2$ which agrees with the measured spin; the state $\frac{5}{2}\ \frac{5}{2}-\ [5\ 2\ 3]$ lies close by and must be considered as an alternative choice. Both of these $\frac{5}{2}$ states are able to explain the log ft values corresponding to the β-transitions to the levels A-H, in conjunction with the asymptotic selection rules, but two considerations

indicate that the $\frac{5}{2}\frac{5}{2}+\ [6\ 4\ 2]$ state is the correct choice for the ground state of Np^{239}. The ground state of Np^{237} has been shown by Hollander, Smith and Rasmussen (82) to be $\frac{5}{2}+$ which suggests that Np^{239} has a similar assignment; the alternative odd parity state is probably the ground state of Am^{239}. If the odd parity state is adopted then an anomaly arises in the case of the $\frac{9}{2}+$ level at 388 kev in Pu^{239}. β-transitions to this rotational level would be first forbidden ($\Delta I = 2$ yes) and unhindered by the asymptotic rules so that, according to Alaga (81), the log ft value would be about 8.2. The level would then be appreciably populated by β-transitions, which would however not be resolved from those to the 392 kev level G. No γ-transitions are observed from the 388 kev level which is therefore unpopulated in Np^{239} decay so that the choice of the $\frac{5}{2}+$ state as the ground state of Np^{239} is preferred.

It follows from the assignment of the $\frac{5}{2}\frac{5}{2}+\ [6\ 4\ 2]$ state to Np^{239} that the β-transitions to levels B, C and D of the ground state band are allowed, K-forbidden and hindered, with $\Delta n_z \neq 0$, $\Delta \Lambda \neq 0$ and $\Delta K > \Delta I$. Mottelson and Nilsson (82) report that for allowed hindered transitions $6.0 < \log ft < 7.5$ and as in the present case the transitions are also forbidden by the strong K selection rules the observed values of log ft

= 8.4 are quite reasonable. The transition to level A is second forbidden. If this level had been identified by the alternative negative parity configuration transitions to levels B, C and D would have been first forbidden, hindered and K-forbidden with a log ft value of about 9.

The next intrinsic level in Pu^{239} is at 286 kev and has been assigned the state $\frac{5}{2}\frac{5}{2}+ [6\ 2\ 2]$. The β-transitions to this, and the associated rotational level at 330 kev are allowed and hindered, with $\Delta n_z \neq 0$, but are not K-forbidden; the observed log ft values of 6.8 and 7.2 are in good agreement with the predicted value.

Level G at 392 kev is the next intrinsic level with spin $\frac{5}{2}$ or $\frac{7}{2}$ and odd parity. Suitably placed states in the diagram are $\frac{5}{2}\frac{5}{2}- [7\ 5\ 2]$ and $\frac{7}{2}\frac{7}{2}- [7\ 4\ 3]$ although the former is rather lower than expected. Transitions to the levels E and F from either of these states would violate the asymptotic rules explaining in part the heavy retardation of the transitions from this level. In neither case are the rules broken for the β-transition which is, therefore, first forbidden unhindered and K-allowed consistent with the observed log ft value of 6.7.

The fourth intrinsic level is at 512 kev and has spin $\frac{5}{2}$ or $\frac{7}{2}$ with even parity. The states $\frac{5}{2}\frac{5}{2}+ [6\ 3\ 3]$

and $\frac{7}{2}\frac{7}{2}+$ [6 2 4] are available and in both cases the β-transitions are allowed and hindered in agreement with the log ft value of 7.1 calculated from the estimated intensity of 3% for this β-feed.

Chapter 10.

THE ADAPTATION OF THE SPECTROMETER FOR COINCIDENCE MEASUREMENTS.

1. Introduction.

The formulation of the complete disintegration scheme of a radio-element together with a full description of the energy levels of the product nucleus requires a variety of information. β - or γ-ray spectrometer measurements can elucidate the basic features of the decay but are not always sufficient to determine the full scheme unambiguously. This can usually be done by coincidence measurements to establish which pairs of transitions are in cascade and which are in parallel with each other. Three types of measurements can be made, they are γ-γ , β - β and β-γ correlations. The first employs two γ-ray detectors while in the second a double β-spectrometer is used; the present β-spectrometer has been adapted for the third type of experiment. The block diagram of the electronic units is shown in Fig. 23. Coincidence experiments in which one channel detects a narrow range of electron energies and the second channel selects a γ-ray have certain advantages over the more usual type using two photon detectors. The photon spectrum recorded by a scintillation counter

suffers from one serious defect - poor energy resolution of the γ-ray peaks. The resolution is usually expressed as the relative line width observed for the Cs^{137} 662 kev γ-ray which is usually only about 8.5%; lower energy peaks are not so well resolved. If the present β-spectrometer is used to provide the energy selection in one channel a momentum resolution of 2% will be possible in this channel. The coincidence of γ-rays with either the continuous electron spectrum or the conversion lines of a γ-ray may be examined. In the former case we can determine the end-points of the partial β-spectra which are followed by the selected γ-ray while in the latter case the comparatively good resolution of the β-detector reduces the interference of neighbouring cascades.

The effective solid angle for coincidence measurements is the product of the solid angles of each detector and if this is too small the time taken to achieve the necessary statistical accuracy may be impractically long. In the present case the β-spectrometer has a large solid angle of about $\frac{1}{20}$ so that it is well suited for coincidence work. It is essential, however, that the sodium iodide crystal used to detect the photons be placed as near the source as possible; the position of the crystal with respect to the source is shown in Fig. 24.

The proposed coincidence experiment is that suggested in Chapter 7 §3. Measurements will be made of that part of the β-spectrum of Ir^{192} which is in coincidence with 468 kev photons. The experiment is not feasible unless the 468 kev photon peak is resolved from the intense group at 300 kev by the γ-ray channel.

2. The scintillation counter detectors.

The electron detection system has been outlined in Chapter 3 . The phosphor is an anthracene crystal coupled to an E.M.I. 6097B photomultiplier by a long perspex light guide. The associated photomultiplier and cathode follower is shown in Fig. 8.

The most suitable phosphor for the detection of γ-rays is thallium activated sodium iodide. In NaI(Tℓ) photoelectrons are produced from the heavy iodine atoms and the associated iodine K X-ray of about 28 kev is fairly readily absorbed by the crystal so that the total energy of the γ-ray is available for the photon pulse. Some of the γ-rays suffer Compton scattering and are either lost from the crystal or undergo further scattering, or perhaps photoelectron absorption processes; above 1.02 Mev pair production is a further absorption process. Those γ-rays that are not completely absorbed in the crystal form a background Compton distribution of γ-rays in the spectrum

having energies less than that of the corresponding photoelectron peak. The number of photoelectric absorption and pair production processes compared to Compton processes increases rapidly with the atomic number of the atoms in the crystal and in NaI(Tℓ) the iodine atoms are responsible for the high absorption efficiency for γ-rays; the pulse height per Mev is twice that of anthracene and is constant above 10-15 kev. The thallium activator shifts the photon emission band to 4100 A, which is in the region of the maximum spectral sensitivity of the photomultiplier, while the decay constant is 0.25 μ sec. For the present work a 1 in. diameter 2 in. long Harshaw NaI(Tℓ) crystal was obtained through Nuclear Enterprises Ltd. Sodium iodide is hygroscopic and the crystal is sealed in an aluminium can, the crystal being coated with alumina to reduce light losses at the walls; there is a glass window at one end of the crystal.

The NaI(Tℓ) crystal detector is located on the axis behind the source; its position is shown in Fig. 24. The crystal can has an outside diameter of $1\frac{1}{4}$ in. and is $2\frac{9}{16}$ in. long. The 1 in. diameter iron bar that passed through the core and was screwed into the pole-piece was removed, see Fig. 7. The pole-piece was drilled out to a diameter of $1\frac{1}{8}$ in. so as to receive a light guide while the 3 in. of the pole-piece in which the

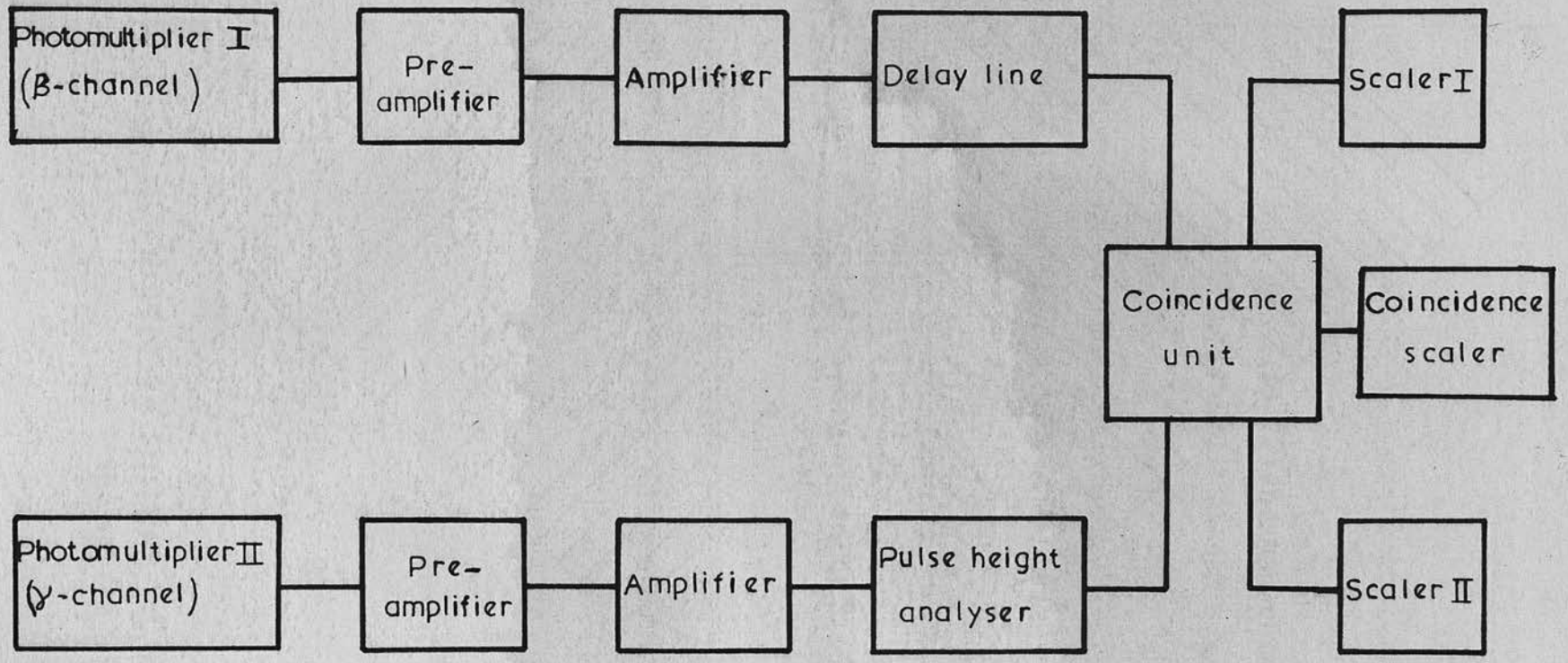

Figure 23. Block diagram of the electronic circuits.

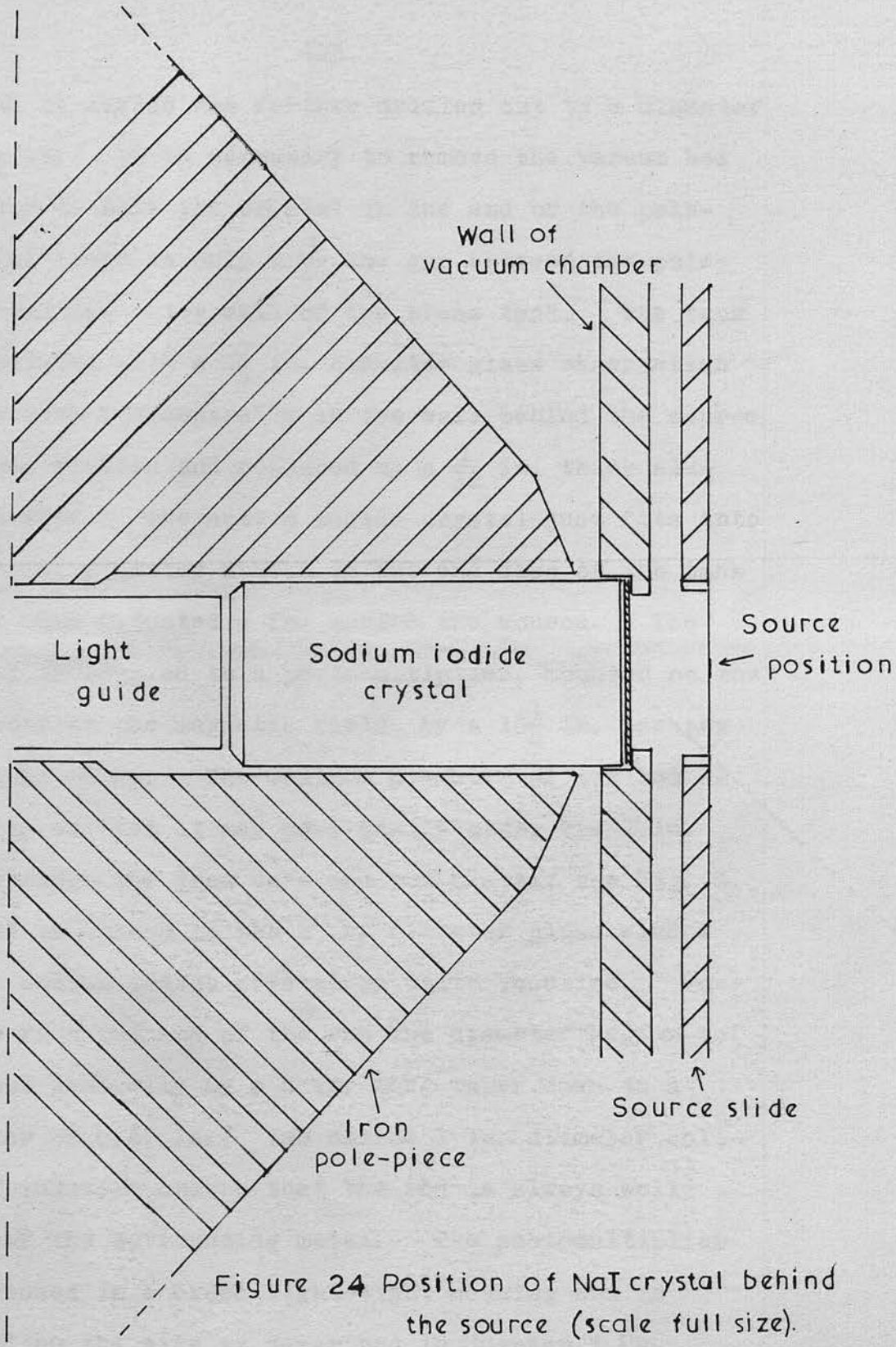

Figure 24 Position of NaI crystal behind the source (scale full size).

crystal is seated was further drilled out to a diameter of $1\frac{9}{32}$ in. It is necessary to remove the vacuum box in order to seat the crystal in the end of the pole-piece as there is only a $\frac{3}{16}$ in. gap between the pole-piece and the outer wall of the brass tank. The tank was designed with a $1\frac{1}{4}$ in. diameter glass observation window situated centrally in the wall behind the source; this was removed and replaced by a $\frac{1}{32}$ in. thick aluminium disc. The sodium iodide crystal just fits into the $1\frac{1}{4}$ in. diameter recess in the end disc of the tank and is then situated $\frac{1}{2}$ in. behind the source. The crystal is coupled to a photomultiplier, mounted on the axis outside the magnetic field, by a $18\frac{1}{4}$ in. perspex rod light guide. The maximum diameter of the rod is 0.99 in. so that it may pass easily along the 1 in. hole through the iron core and end plates, see Fig. 7. The rod is joined to the 1 in. diameter glass window of the sodium iodide crystal by white vaseline. Four inches from the end of the rod the diameter begins to decrease gradually by a 4 in. long taper down to a diameter of 0.87 in.; two narrow 1 in. diameter collars of selotape ensure that the rod is always well clear of the surrounding metal. The photomultiplier is enclosed in a brass light-tight housing and is mounted on the axis as described in Chapter 3 §4.

The photomultiplier is an eleven stage E.M.I.

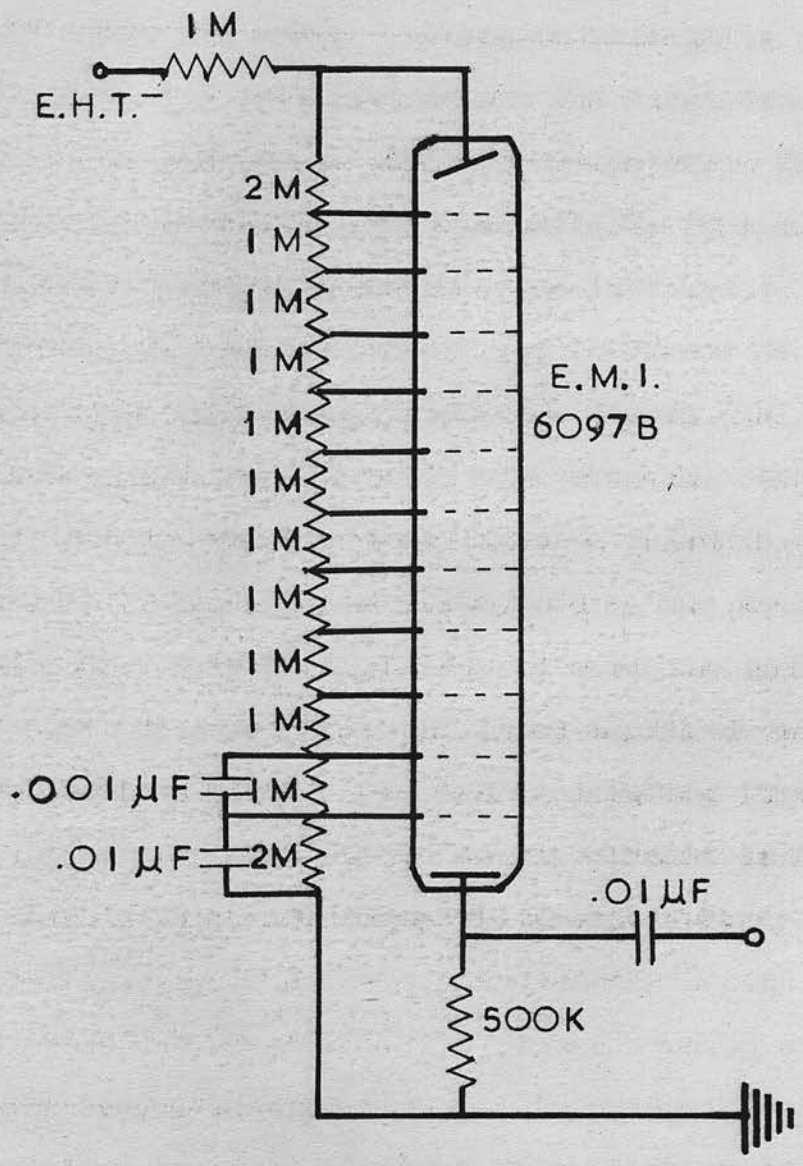

Figure 25 Circuit for the photomultiplier used with the sodium iodide crystal detector.

6097B tube and the associated circuit is shown in Fig. 25. The H.T. voltage is supplied by a Type 200 power unit to the resistance chain with an average interstage voltage of about 130 volts. A higher voltage is applied between the photocathode and the first dynode and between the last dynode and the collector. The former reduces the statistical fluctuations in the current pulse while the latter ensures that space charge limitation does not affect the linearity of the multiplier; the decoupling condensers across the last few dynodes ensure that there is no electrical feedback to earlier stages from the large current pulse in the output stages. The pre-amplifier unit is the Nuclear Enterprises Ltd. type NE 5202A and is essentially a White cathode follower having an input impedance of 10 megohms shunted by 6 pf. The differentiating time constant of the photomultiplier output circuit is 2-3 μsec. which is about ten times the phosphor decay constant.

3. <u>The coincidence system</u>.

The output from the electron scintillation counter is fed into a Dynatron 1049 amplifier and the 1 μsec. output pulse is passed to the channel 1 input of the Harwell type 1036A coincidence unit. The counting rate of this channel is recorded by an I.D.L. 500 and

501 scaler and prescaler combination capable of counting up to 10^5 counts per second efficiently. The momentum selection of electrons takes place in the spheroidal field spectrometer.

The γ-ray spectrum recorded by the photon scintillation counter passes from the pre-amplifier to an NE 5202 non-overloading linear pulse amplifier. This amplifier has been designed by Fairstein (84) for use with sodium iodide crystal detectors. It employs double delay line differentiation with a clipping time of 1.2 μsec. to give a 2.4 μsec. sine wave output pulse with zero D.C. component from a White cathode follower. The maximum gain is 50,000 with a possible attenuation of 1200 to 1. The pulse height analyser is the NE 5102 designed by Fairstein (85) for use with the above amplifier and has a discriminator range of 3 to 100 volts with a gate width of 0 to 10 volts. The output pulses from this analyser are fed into channel 2 of the coincidence unit, the single channel counting rate being recorded by a Dynatron 1009B scaler. Coincidences between channels 1 and 2 are registered by a 1009A scaler.

The coincidence mixer for channels 1 and 2 of the coincidence unit has a resolving time variable between 0.1 and 2 μsec. The delays between the crystal detectors and the coincidence unit may be equalised by

delaying the faster channel until coincidences are observed; the available delay is up to 1 μ sec. on each channel. The delay necessary was found by means of a double pulse generator. Coincident pulses were fed into the output stages of the photomultiplier and hence into the coincidence unit. No coincidences were detected with the shorter resolving times as the available 1 μ sec. delay was not sufficient to equalise the delays of the two channels. The channels of the pulse generator may be delayed with respect to each other and it was found that if the pulses passing through the 1049 amplifier were delayed by 2 μ sec. coincidences were obtained. A delay of $\sim$ 1.5 μ sec. takes place in the NE 5202 amplifier and of $\sim$ 0.5 μ sec. in the pulse height selector. It is proposed to equalise the two channels by inserting an appropriate length of delay line cable after the 1049 amplifier.

The γ-ray channel has been tested and found to perform satisfactorily, as discussed in §4, but it has not been possible to undertake the proposed coincidence experiment to date. There have been two failures in the insulation of one of the magnet coils. The repair of the coil involves the removal of the vacuum tank, magnet pole-piece and the copper cooling jacket. It is then necessary to line up the tank with respect to the field and to re-calibrate the spectrometer. The

magnet coils were originally chosen for their availability and the only cooling is by means of a copper water cooling jacket which is not really adequate. The earthed copper jacket surrounding the offending coil has been removed and a forced draught cooling system devised and fitted. Air is drawn over the coil by an iron free fan installed directly above the coil at the top of a wooden chimney. In addition a neon tube has been connected in parallel with the coils to suppress high voltage surges when the circuit is broken.

4. The γ-ray spectrum of Ir^{192}.

The main features of the Ir^{192} γ-ray spectrum are shown in Fig. 26. The sodium iodide crystal was mounted directly on top of the photomultiplier which was placed in the centre of the room to minimise back-scattering from the walls; the Ir^{192} source was placed about $2\frac{1}{2}$ in. above the crystal. The resolution of the Cs^{137} 662 kev γ-ray observed under the same conditions was only 10% so that the 600 and 300 kev groups in Ir^{192} are not resolved into their individual lines, nevertheless the 468 kev γ-ray is fully separated from these groups. The spectrum is shown in more detail in Fig. 27 which was obtained with a 1 in. diameter 1 in. deep Harshaw crystal, loaned by Nuclear Enterprises Ltd. This crystal was found to have a

resolution of 7½% for the Cs^{137} 662 kev line which indicates that the higher value obtained with the present crystal is inherent in the crystal itself and not due to the photomultiplier tube. In Fig. 26 the 136 and 200 kev photon peaks may be clearly seen together with the high energy side of the K X-ray of about 75 kev. There is no sign of the comparatively weak 885 kev γ-ray.

When the sodium iodide crystal is placed in the end of the iron pole-piece the γ-ray spectrum observed is altered considerably. γ-rays are scattered into the crystal by Compton processes in the surrounding iron while many more are backscattered at the massive lead block in the centre of the vacuum chamber. The former process gives a large increase in the underlying Compton distribution while the latter leads to the appearance of a backscattered γ-ray peak at about 180 kev. There is in addition a loss of resolution due to the 18 in. light guide. The observed spectrum is given in Fig. 28 and shows considerable distortion from the γ-ray spectrum of Fig. 26 taken with the same crystal. A Dynatron N101 pulse height selector was used for this run. The worst distortion of the γ-ray spectrum occurs in the low energy region. It can be seen from Fig. 28 that although the 468 kev γ-ray is broadened nevertheless it is still resolved.

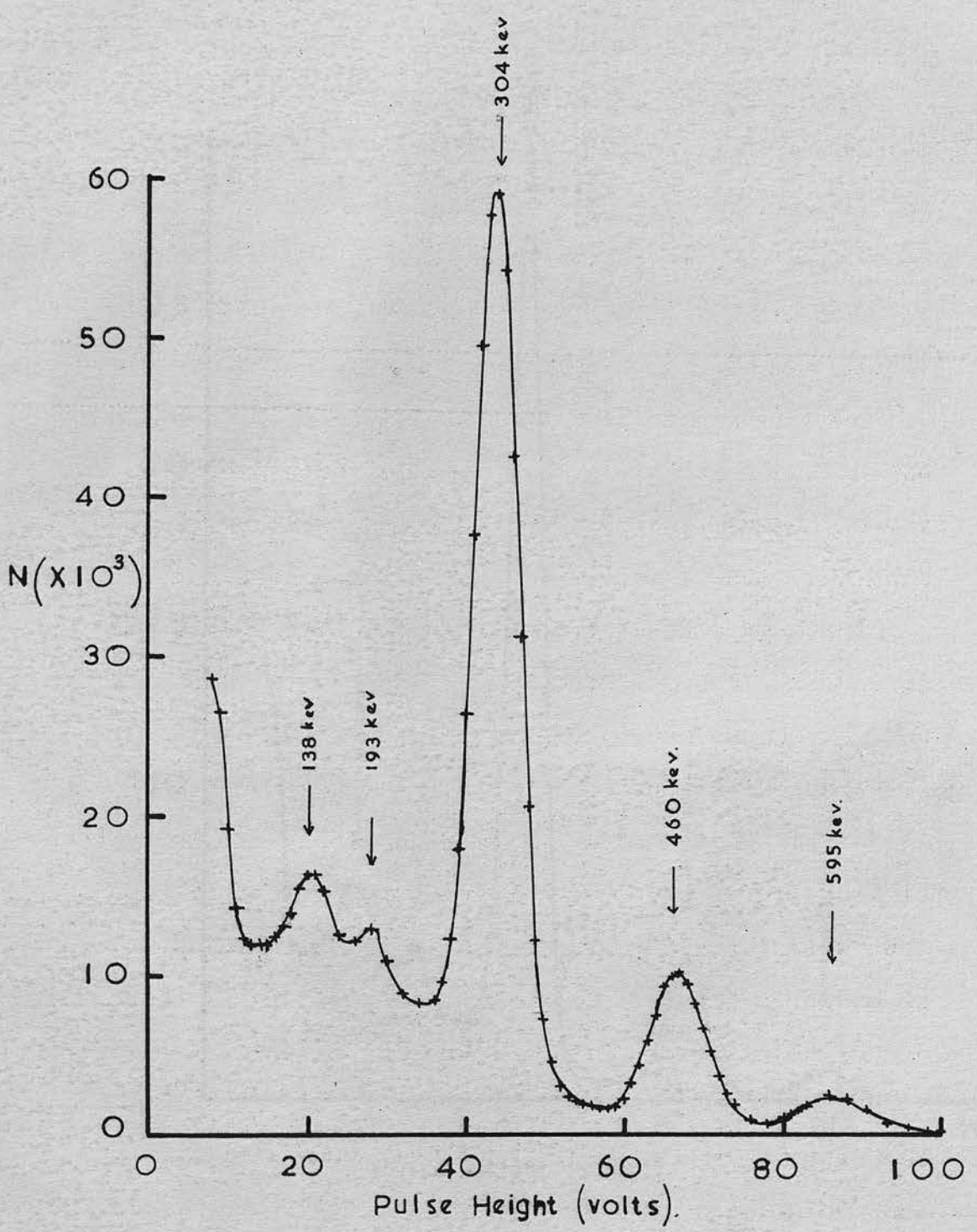

Figure 26. Gamma-ray spectrum of Ir^{192} (with 10% resolution).

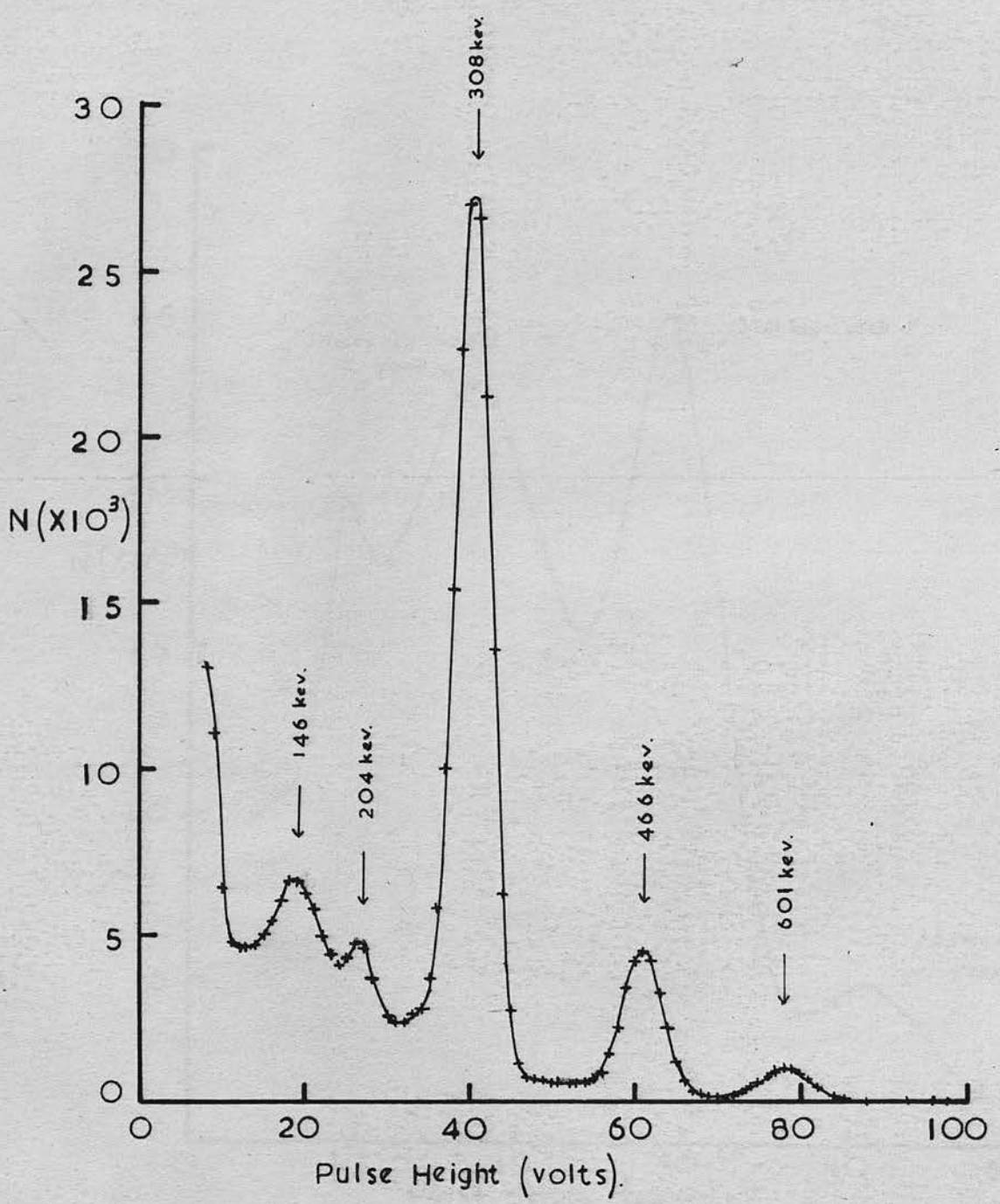

Figure 27. Gamma-ray spectrum of Ir^{192} (with 7.5% resolution).

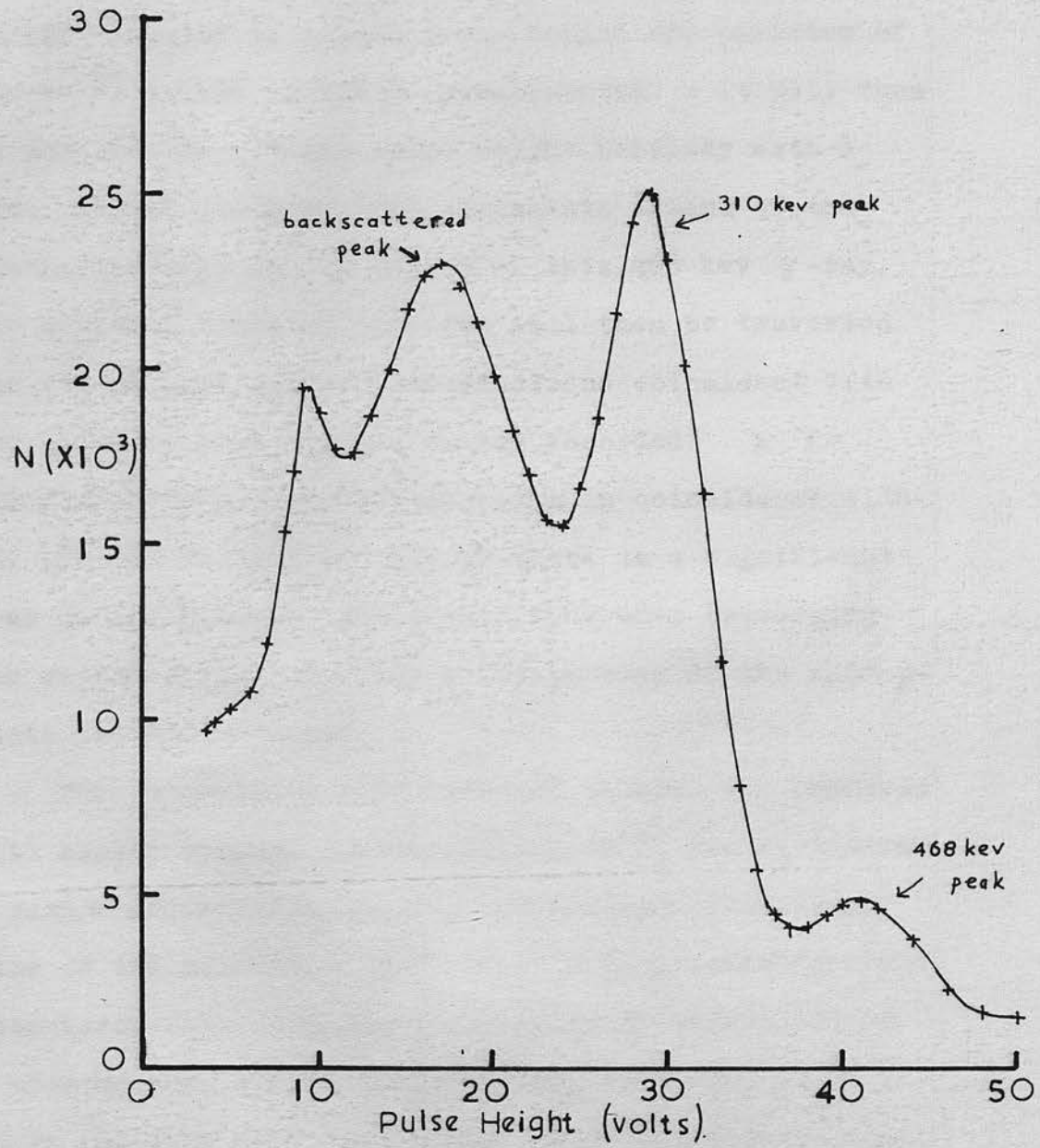

Figure 28. Gamma-ray spectrum of Ir^{192} with the sodium iodide crystal detector in the pole-piece.

5. The proposed coincidence experiment.

It has been noted above that the 468 kev γ-ray peak is resolved, despite being broadened, when the NaI(Tl) crystal is placed $\frac{1}{2}$ in. behind the position of the Ir^{192} source in the β-spectrometer. It will thus be possible to set the pulse height analyser with a wide channel width so that it selects a band of the energy spectrum in the region of this 468 kev γ-ray. The electron momentum spectrum will then be traversed and the partial spectrum of electrons coincident with the emission of a 468 kev γ-ray recorded. A γ-transition is established as being in coincidence with the 468 kev transition only if there is a significant peak in the genuine coincidence rate when traversing the region of the spectrum corresponding to the appropriate conversion lines.

The coincidence rate observed between two channels with single channel counting rates of N_1 and N_2 includes a random contribution due to the non-zero resolving time of the circuit. The use of scintillation counter detectors, with phosphor decay times of a fraction of a microsecond, allows the resolving time (τ) to be short and this will reduce the chance coincidence rate N_c which is given by $N_c = 2N_1N_2\tau$. In order to obtain the genuine coincidence rate it is necessary to subtract the contribution expected from chance coincidences.

In order to establish the existence or non-existence of a coincidence peak it is necessary to have a genuine coincidence rate that is significantly above the chance rate. The ratio of genuine to chance coincidences is greater for low counting rates so that a high source activity is of limited advantage in the detection of low coincidence counting rates.

In the present case we expect to find peaks in the coincidence spectrum from the 316 kev γ-ray conversion lines but no other strong peak is expected on the currently accepted decay scheme. If the present scheme is correct then there should be several additional low intensity coincidence peaks as well as quite strong coincidence peaks corresponding to the conversion lines of the 468 kev γ-ray. The interference of neighbouring cascades should be small as the 417 and 438 kev γ-transitions are very weak and the stronger 484 kev transition is assigned to Os^{192}. The detection of genuine coincidences corresponding to two γ-rays of about 468 kev would provide strong evidence for the existence of the proposed level at 1253 kev in Pt^{192}.

ACKNOWLEDGMENTS.

The author is indebted to Professor N. Feather, F.R.S., for extending the facilities of the Department of Natural Philosophy, and for his supervision of and continued interest in the investigation. Grateful thanks are due to Dr. R.D. Connor, late of this department and now Associate Professor of Physics at the University of Manitoba, for his participation in and supervision of much of the experimental work, and for his continued encouragement and advice. The many long and invariably valuable discussions with Mr. J. Kyles, M.A., have been greatly appreciated together with his constant advice and the communication of his unpublished results.

In addition thanks are extended to Dr. A.F. Brown for the use of his vacuum evaporation apparatus, and to Mr. A. Headridge and the technical staff for much valuable assistance and for the construction of apparatus. Thanks are due to Dr. R.G. Monk of A.W.R.E. for a supply of Np^{239} source material and to Dr. E.A.C. Crouch of A.E.R.E. for an introduction to V.Y.N.S. films. The provision of maintenance allowances by Lancashire County Council Education Committee and the Department of Scientific and Industrial Research is gratefully acknowledged.

REFERENCES.

1. Richardson, H.O.W., 1949, Phil. Mag., 40, 233.

2. Richardson, H.O.W., 1952, J. Sci. Inst., 29, 93.

3. Braid, T.H., and Richardson, H.O.W., 1951, Proc. Phys. Soc. A, 64, 163.

4. Danysz, J., 1912, Le Radium, 9, 1.

5. Braid, T.H., 1950, Ph.D. thesis, University of Edinburgh.

6. Mandeville, C.E., and Scherb, M.V., 1948, Phys. Rev., 73, 1434.

7. Goodman, L.J., and Pool, M.L., 1947, Phys. Rev., 71, 288.

8. Wiedenbeck, M.L., and Chu, K.Y., 1947, Phys. Rev., 72, 1164.

9. Levy, M., 1947, Phys. Rev., 72, 352.

10. Shpinel, V.S., and Forafontov, N.V., 1951, J. Exptl. Theoret. Phys. (U.S.S.R.), 21, 1376.

11. Johns, M.W., and Nablo, S.V., 1954, Phys. Rev., 96, 1599.

12. Bashilov, A.A., Anton'eva, N.M., and Dzhelepov, B.S., 1952, Izvest. Akad. Nauk S.S.S.R. Ser. Fiz., 16, 264.

13. Kyles, J., and Campbell, C.G., 1953, unpublished data, private communication from J. Kyles, University of Edinburgh.

14. Roulston, K.I., and Pringle, R.W., 1952, Phys. Rev., 87, 930.

Pringle, R.W., Turchinetz, W., and Taylor, H.W., 1954, Phys. Rev., 95, 115.

15. Muller, D.E., Hoyt, H.C., Klein, D.J., and DuMond, J.W.M., 1952, Phys. Rev., 88, 775.

16. Ryde, N., and Andersson, B., 1955, Proc. Phys. Soc. B, 68, 1117.

17. Baggerly, L.L., Marmier, P., Boehm, F., and DuMond, J.W.M., 1955, Phys. Rev., 100, 1364.

18. Cork, J.M., Le Blanc, J.M., Stoddard, A.E., Childs, W.J., Branyan, C.E., and Martin, D.W., 1951, Phys. Rev., 82, 258.

19. Grard, F., Danguy, L., and Franeau, J., 1955, J. Phys. Radium, 16, 839.

20. Ewan, G.T., and Thompson, A.L., 1953, Trans. Roy. Soc. Can., 47, 126.

21. Taylor, H.W., and Pringle, R.W., 1955, Phys. Rev., 99, 1345.

22. McMillan, E., and Abelson, P.H., 1940, Phys. Rev., 57, 1185.

23. Feather, N., 1941, British Atomic Energy Report, Br 46.

Feather, N., 1947, Nature, 160, 749.

24. Philipp, K., Riedhammer, J., and Wiedemann, M., 1944, Naturw., 32, 230.

25. Slätis, H., 1947, Arkiv. Mat., Astr. Fysik, 35A No. 3.

26. Graham, R.L., and Bell, R.E., 1951, Phys. Rev., 83, 222.

27. Tomlinson, E.P., Fulbright, H.W., and Howland, J.J., 1951, Phys. Rev., 83, 223.

28. Freedman, M.S., Wagner, F., Engelkemeir, D.W., Huizenga, J.R., and Magnusson, L.B., 1953, quoted by Hollander, J.M., Perlman, I., and Seaborg, G.T. in Rev. Mod. Phys., 25, 469.

29. Fulbright, H.W., 1952, quoted by Reference 30.

30. Engelkemeir, D., and Magnusson, L.B., 1955, Phys. Rev., 99, 135.

31. Asaro, F., Thompson, S.G., and Perlman, I., 1953, Phys. Rev., 92, 694.

32. Baranov, S.A., and Shlyagin, K.N., 1956, J. Nuclear Energy II, vol. 3, 132.

33. Hollander, J.M., Smith, W.G., and Mihelich, J.W., 1956, Phys. Rev., 102, 740.

34. Bleaney, B., Llewellyn, P.M., and Pryce, M.H.L., 1954, Phil. Mag., 45, 773, 991.

35. Bohr, A., and Mottelson, B.R., 1953, Dan. Mat. Fys. Medd., 27, No. 16.

Bohr, A., and Mottelson, B.R., 1955, Beta- and Gamma-ray Spectroscopy, ed. Siegbahn, K., (North-Holland), Chapter 17.

36. Conway, J.D., and McLaughlin, R.D., 1954, Phys. Rev., 96, 541.

37. Newton, J.O., Rose, B., and Milsted, J., 1956, Phil. Mag., 1, 981.

38. Newton, J.O., 1957, Nucl. Phys., 3, 345.

39. Smith, W.G., Gibson, W.M., and Hollander, J.M., 1957, Phys. Rev., 105, 1514.

40. Hollander, J.M., 1957, Phys. Rev., 105, 1518.

41. Abraham, M., Jeffries, C.D., Kedzie, R.W., and Wallman, J.C., 1957, Phys. Rev., 106, 1357.

42. Knight, J.C., 1953, Ph.D. thesis, University of Edinburgh.

43. Hedgran, A., Siegbahn, K., and Svartholm, N., 1950, Proc. Phys. Soc. A., 63, 960.

44. Curran, S.C., 1953, Luminescence and the scintillation counter (Butterworth), Chapter 10.

45. Lindström, G., 1951, Ark. f. Fysik, 4, Nr. 1.
Slätis, H., 1953, Ark. f. Fysik., 6, Nr. 41, 415.
Slätis, H., and Lindström, G., 1952, Phys. Rev., 88, 1429.

46. Lawson, J.L., and Tyler, A.W., 1940, Rev. Sci. Inst., 11, 6.

47. Beta- and Gamma-ray Spectroscopy, ed. Siegbahn, K., (North-Holland), Appendix 7.

48. Albert, R.D., and Wu, C.S., 1948, Phys. Rev., 74, 847.

49. Crouch, E.A.C., Chemistry Division, A.E.R.E., Harwell, private communication.

50. Bradley, D.E., 1954, Bri. J. Appl. Phys., 5, 65, and private communication.

51. Pate, B.O., and Yaffe, L., 1955, Canad. J. Chem., 33, 15.

52. Bell, P.R., 1955, Beta- and Gamma-ray Spectroscopy, ed. Siegbahn, K., (North-Holland), Chapter 5.

53. U.S. National Bureau of Standards, Applied Mathematics Series 13, Tables for the analysis of β-spectra.

54. Cook, C.S., Langer, L.M., and Price, H.J., Jr., 1948, Phys. Rev., 73, 1395.

55. Cockcroft, A.L., and Insch, G.M., 1949, Phil. Mag., 40, 1014.

56. Berggrenn, J.L., and Osborne, R.K., 1948, Phys. Rev., 74, 1240.

57. Langer, L.M., Motz, J.W., and Price, H.C., Jr., 1950, Phys. Rev., 77, 798.

58. Moljk, A., and Curran, S.C., 1954, Phys. Rev., 96, 395.

59. Gross, L., and Hamilton, D.R., 1950, Phys. Rev., 80, 484.

60. Heller, R.B., Sturcken, E.F., and Weber, A.H., 1951, Phys. Rev., 83, 848.

61. Ellis, C.D., 1932, Proc. Roy. Soc. A, 138, 18.

62. Feenberg, E., and Trigg, G., 1950, Rev. Mod. Phys., 22, 399.

63. Connor, R.D., and Fairweather, I.L., 1957, Proc. Phys. Soc. A, 70, 769.

64. Flammersfeld, A., 1939, Z. Physik, 114, 227.

65. Kelman, V.M., Metskhvarishvili, R. Ya., Romanov, V.A., and Tuchkevich, V.V., 1957, Nuclear Physics, 4, 240.

66. Rose, M.E., 1957, privately circulated tables of conversion coefficients.

67. Sliv, L.A., and Band, I.M., 1956, Coefficients of internal conversion of gamma radiation, Part 1: K-Shell, issued as Report 57 ICC K1 by University of Illinois.

68. Shiel, V., Wyly, L.D., and Braden, C.H., 1957, Phys. Rev., 105, 1521.

69. Huq, M.S., 1957, Nuovo Cim., 5, 1456.

70. Kelly, W.H., and Wiedenbeck, M.L., 1956, Phys. Rev., 102, 1130.

71. Mraz, J., 1957, Nuclear Physics 4, 457.

72. Wish, L., 1956, Nucleonics, 14, 102.

73. Ewan, G.T., Knowles, J.W., and MacKenzie, D.R., 1957, Phys. Rev., 108, 1308.

74. Connor, R.D., 1958, on leave to A.E.C.L., Chalk River, Canada, from University of Manitoba, private communication.

75. van den Berg, M., Klinkenburg, P.F., and Regnault, P., 1954, Physica, 20, 37.

76. Hubbs, J.C., and Marrus, R., 1958, Phys. Rev., 110, 287.

77. Asaro, F., Stephens, F.S., and Perlman, I., 1957, unpublished results quoted by Strominger, D., and Hollander, J.M., and Seaborg, G.T., 1958, Rev. Mod. Phys., 30, 828.

78. Moszkowski, S.A., 1955, Beta- and Gamma-ray Spectroscopy, ed. Siegbahn, K., (North-Holland), Chapter 13.

79. Strominger, D., and Rasmussen, J.O., 1957, Nuclear Physics, 3, 197.

80. Nilsson, S.G., 1955, Dan. Mat. Fys. Medd., 29, No. 16.

81. Alaga, G., 1955, Phys. Rev., 100, 432.

82. Mottelson, B.R., and Nilsson, S.G., 1958, Dan. Mat. Fys. Medd. (to be published).

83. Lefevre, H.W., Kinderman, E.M., and Van Tuyl, H.H., 1955, Phys. Rev., 100, 1374.

84. Fairstein, E., 1956, Rev. Sci. Instr., 27, 475.

85. Fairstein, E., 1956, Rev. Sci. Instr., 27, 549.